PHYSIOLOGICALLY BASED COMPUTATIONAL MODELING OF THE HYPOTHALAMIC – PITUITARY – GONADAL AXIS IN FATHEAD MINNOWS

By

Zhenhong Li

B.S., Microbiology, Anhui University, P.R. China, 2000

M.S., Environmental Science and Engineering, Shanghai Jiaotong University, P.R. China, 2003

Presented to the Division of Environmental & Biomolecular Systems within the Department of Science & Engineering and the Oregon Health & Science University School of Medicine in partial fulfillment of the requirements for the degree of

Doctor of Philosophy of Environmental Science & Engineering

June 2010

Department of Science & Engineering
School of Medicine
Oregon Health & Science University

CERTIFICATE OF APPROVAL

This is to certify that the Ph.D. dissertation of

Zhenhong Li

has been approved

Dr. Karen H. Watanabe, Thesis Advisor
Assistant Professor

Dr. Paul G. Tratnyek
Professor and Associate Division Head

Dr. Peter Zuber
Professor and Oral Defense Chair

Dr. Nancy D. Denslow
Professor, University of Florida

TABLE OF CONTENTS

LIST OF TABLES

LIST OF FIGURES

LIST OF ABBREVIATIONS

3β-HSD	3β-hydroxysteroid dehydrogenase
11β-HSD	11β-hydroxysteroid dehydrogenase
17α, 20β-DP	17α, 20β-dihydroxy-4-pregnen-3-one
17α-HDP	17α-hydroxy-progesterone
17β-HSD	17β-hydroxysteroid dehydrogenase
20β-HSD	20β-hydroxysteroid dehydrogenase
AR	androgen receptors
ARE	androgen response elements
BA	binding affinity
BW	body weight
CI	confidence interval
DES	diethylstilbestrol
DDT	dichloro-diphenyl-trichloroethane
DMF	N,N-dimethylformamide
E_1	estrone
E_2	17β-estradiol
EE_2	17α-ethynylestradiol
EDC	endocrine disrupting chemical
ELISA	enzyme-linked immunosorbent assay
EPA	environmental protection agency
ER	estrogen receptor
ERE	Estrogen response elements
FHM	fathead minnow
FSH	follicle-stimulating hormone
GM	geometric mean

GnRH	gonadotropin – releasing hormone
GSI	gonadosomatic index
GSD	geometric standard deviation
GtHs	gonadotropins
GTs	glucuronosyltransferases
GW	gonad weight
HPG axis	hypothalamic – pituitary – gonadal axis
HSI	hepatosomatic index
KT	11keto-testosterone
LH	luteinizing hormone
LW	liver weight
MCMC	Markov chain Monte Carlo
MH	Metropolis-Hastings
MIH	maturation-inducing hormone
MOA	modes of action
NMR	nuclear magnetic resonance
P450scc	P450 side chain cleavage enzyme
SBP	steroid binding protein
StAR	steroidogenic acute regulatory protein
STs	sulfotransferases
T	testosterone
TB	17β-trenbolone
VTG	vitellogenin
WWTP	wastewater treatment plant

ACKNOWLEDGEMENTS

I would like to acknowledge all the people who have helped, encouraged, and inspired me during my doctoral study. I especially thank my advisor Karen Watanabe for her tolerant and continuous directions during my research. Before I came to OGI School, I know nothing about computational modeling. Without Karen's direction, my dissertation is simply impossible.

I would like to thank my thesis committee, Paul Tratnyek, Peter Zuber, and Nancy Denslow for their insightful suggestions and comments on my research. Especially, I thank Paul Tratnyek for his guidance and encouragement throughout my study and research. I thank Peter Zuber for his interesting lectures and willing to be the chair of my oral defense at the last moment.

Special thanks to Bradley Tebo and our Division of Environmental and Biomolecular Systems at OHSU for financial support during the last two years of my Ph.D. study. Without the support, I could not continue education here, and my degree is simply impossible.

I would like to thank the OGI staff and friends who made my research and personal life so much easier. Especially, my thanks go to Nancy Christie who has assisted me with almost everything everyday, and Jim Mohan who has helped me to solve various IT problems.

My deepest gratitude goes to my family for their everlasting love and support throughout my life. I owe a big debt to my parents, Zhigang Li and Kaikuai Li. I owe my loving thanks to my husband, Jiabao Song. He was always there cheering me up, and helped me to overcome all the obstacles during the past decade. A special thank is given to my lovely baby son, Changze Song. He lightens and warms my life, and fills me with smiles and happiness everyday.

ABSTRACT

Physiologically Based Computational Modeling of the Hypothalamic – Pituitary - Gonadal Axis in Fathead Minnows

Zhenhong Li, M.S.
Doctor of Philosophy
Division of Environmental & Biomolecular Systems
Department of Science & Engineering
Oregon Health & Science University
School of Medicine

June 2010
Thesis Advisor: Karen H. Watanabe

Endocrine disrupting chemicals (EDCs) are known to affect reproduction through interacting with the hypothalamic-pituitary-gonadal (HPG) axis in fish. EDCs can mimic or block the functions of key elements (e.g. estrogen receptors and androgen receptors) of the HPG axis, and result in altered endocrine signals. The EDCs studied in this dissertation include estrogenic compounds such as 17β-estradiol (E_2) and 17α-ethynylestradiol (EE_2), and androgenic EDCs such as 17β-trenbolone (TB). E_2 is a predominant estrogen naturally present in females. EE_2 is a synthetic estrogen used in birth control pills. Both E_2 and EE_2 are discharged from wastewater treatment plants into water bodies throughout the United States. TB is a relatively stable metabolite of trenbolone acetate, a synthetic androgen used as a growth promoter for cattle. TB enters

the environment mainly through runoff from cattle feedlots. In the first part of this dissertation, a physiologically-based computational model was developed of the HPG axis in unexposed male fathead minnows (FHMs, *Pimephales promelas*) and male FHMs exposed to EE_2 and E_2. The second part of this dissertation describes a physiologically-based computational model of the HPG axis in unexposed female FHMs and female FHMs exposed to EE_2 and TB. For both models, apical reproductive endpoints include plasma concentrations of steroid hormones and vitellogenin. Using Markov chain Monte Carlo simulation, the models were calibrated with data from unexposed FHMs and FHMs exposed to the selected EDCs, respectively. Independent experimental data sets were used to evaluate model predictions. Good agreement was found between model predictions and a variety of measured reproductive endpoints. The conclusion is that the two models provide robust representations of the HPG axis in male and female FHMs, respectively. In the third part of this dissertation, a computational model of oocyte growth dynamics has been developed. The model provides a quantitative link between oocyte growth dynamics and biochemical processes in FHMs through the absorption of vitellogenin into oocytes, which contributes significantly to oocyte growth in fish. Model-predicted clutch sizes, spawning intervals, and average fecundity in unexposed FHMs and FHMs exposed to TB matched the experimental data well. The third model meets an urgent need in ecotoxicological studies to link the effects of endocrine disrupting chemicals at a biochemical level to adverse effects upon reproduction in individual fish and, subsequently, populations. Since oocyte growth and maturation are part of female reproduction, the third model could be integrated with the second one as a

future work. The models described in this dissertation can serve as a basis for government to develop cost-effective predictive tools to test and monitor EDCs.

CHAPTER 1

Introduction and Background

1.1 Introduction

Concern has arisen for the adverse effects of endocrine-disrupting chemicals (EDCs) in wildlife and humans (Colborn et al., 1993). According to a definition by the United States Environmental Protection Agency (EPA), EDCs are "*exogenous agents that interfere with the synthesis, secretion, transport, binding, action, or elimination of natural hormones in the body that are responsible for the maintenance of homeostasis, reproduction, development, and/or behavior*" (Crisp et al., 1998). EDCs can be either natural or synthetic compounds (Bretveld et al., 2006). In the early 1960s, scientists associated shell thinning in bird eggs with the rapid and unrestricted use of synthetic pesticides, such as dichloro-diphenyl-trichloroethane (DDT) (Carson, 1962; Markey et al., 2002). In the 1980s, scientists in Europe found intersex fish with ovo-testis downstream of the effluents from wastewater treatment plants (WWTPs) (Jobling et al., 1998; Purdom et al., 1994). Subsequently, it was found worldwide that fish exposed to WWTP effluents had altered hormone levels, increased plasma concentrations of vitellogenin (VTG, an egg yolk precursor protein), and decreased fecundity (Filby et al., 2007a; Jobling et al., 2002a; Jobling et al., 2002b; Liney et al., 2006; Orlando et al., 2004; Sumpter and Johnson, 2005; Vajda et al., 2008; Woodling et al., 2006). These adverse effects have been attributed to estrogenic compounds, such as estrone (E_1, a natural estrogen), 17β-estradiol (E_2, a natural estrogen), and 17α-ethynylestradiol (EE_2, a synthetic estrogen used in birth control pills) (Desbrow et al., 1998; Folmar et al., 2002; Jobling et al., 2002a; Kang et al., 2002; Orn et al., 2006; Parks et al., 1999; Purdom et al., 1994; Seki et al., 2002; Van den Belt et al., 2003; Versonnen and Janssen, 2004). Similar to estrogenic

compounds, androgenic compounds have been found in the aquatic environment and are known to affect fish reproduction. For example, 17β-trenbolone (TB) is a relatively stable metabolic product of trenbolone acetate, a synthetic androgen used as a growth promoter in livestock. It has been found in the aquatic environment outside of feedlots (Durhan et al., 2006; Schiffer et al., 2001). TB can masculinize female fish and alter plasma hormone and VTG concentrations in male and female fish (Ankley et al., 2003; Jensen et al., 2006; Orn et al., 2006; Schiffer et al., 2001; Seki et al., 2006; Sone et al., 2005). In humans, prenatal exposure to diethylstilbestrol (DES), a synthetic estrogen used to prevent spontaneous abortions in pregnant women, results in increased rates of reproductive organ dysfunction, abnormal pregnancies, and vaginal cancer in offspring (Giusti et al., 1995). Although there are few reports of EDC effects in humans, some diseases, such as breast cancer and reproductive disorders, are suspected to be associated with EDCs (Crain et al., 2008; Fenton, 2006; Safe, 2004).

In vertebrates, the target of EDCs is the endocrine system. The endocrine system comprises glands that produce and release hormones to regulate processes vital for growth, development, reproduction, metabolism, and behavior (Norris, 1997). As chemical messengers, hormones circulate throughout the bloodstream, transfer information from one set of tissues to another, and coordinate various functions dynamically. Within the endocrine system, a number of subsystems are conserved across vertebrates, which are referred as "axes." Each axis is composed of a group of glands that interact with each other in sequence through hormonal signaling. Being one of such subsystems, the hypothalamic-pituitary-gonadal (HPG) axis controls a complex set of interactions among hypothalamus, pituitary, and gonads (e.g., ovaries in females and testes in males). The key hormones of the HPG axis include, but are not limited to, gonadotropin-releasing hormone (GnRH), follicle-stimulating hormone (FSH), luteinizing hormone (LH), E_2, testosterone (T), and 11keto-testosterone (KT). These hormones regulate processes important for reproduction, such as vitellogenesis (the process to produce VTG in liver), oogenesis (the process of oocyte development and maturation), and spermatogenesis (the process of spermatocyte development and maturation). Similar to any other subsystem within the endocrine system, the HPG axis

is highly dynamic and particularly vulnerable to disruptions from EDCs. Any EDCs that interact with elements of the HPG axis (e.g., hormones, hormone receptors, and enzymes involved in producing hormones) may cause adverse reproductive effects.

The main goal of this dissertation research is to develop physiologically based computational models to simulate the HPG axis in unexposed and EDC-exposed fathead minnows (FHMs, *Pimephales promelas*). The modeling work is conducted using fish, the most widely used animal in EDC-related research, mainly because of the following reasons: (i) fish are the most diverse and numerous group of vertebrates (Schulz et al., 2010); (ii) fish can be exposed to EDCs in the aquatic environment throughout their lifetime, and a variety of wild fish species have been threatened by EDCs in the aquatic environment worldwide (Filby et al., 2007a; Jobling et al., 2002a; Jobling et al., 2002b; Liney et al., 2006; Orlando et al., 2004; Sumpter and Johnson, 2005; Vajda et al., 2008; Woodling et al., 2006); and (iii) the basic structure of the HPG axis is well conserved across vertebrates (Ankley and Johnson, 2004). The FHM is a small freshwater teleost fish species with a broad distribution across North America, and is arguably the most widely used small fish model for regulatory ecotoxicology in the USA (Ankley and Villeneuve, 2006). In the 1990s, the EPA initiated a program using FHMs to screen and test EDCs that affect the HPG axis (Ankley et al., 2009a). The program is still ongoing and generates experimental data (e.g., plasma E_2, T, KT, and VTG concentrations) from both unexposed FHMs and FHMs exposed to a variety of EDCs (e.g., EE_2 and TB). The data provided quantitative information about the HPG axis in FHMs and made it possible to develop physiologically based computational models.

In my doctoral research, I developed three physiologically based computational models to simulate the HPG axis and the EDC-HPG axis interactions based upon toxic modes of action (MOA) of selected EDCs. The first model simulates the HPG axis in unexposed male FHMs and male FHMs exposed to EE_2 and E_2. EE_2 and E_2 are estrogenic compounds, and their major MOA is to disrupt the HPG axis through binding to estrogen receptors (ERs). As a result, an ER-based model was built up. The second model simulates the HPG axis in unexposed female FHMs and female FHMs exposed to

EE_2 and TB. TB is an androgenic compound and its major MOA is to disrupt the HPG axis through binding to androgen receptors (ARs). The second model is advanced over the first one by adding in an AR-based modeling framework. The third model simulates oocyte growth and spawning in unexposed FHMs and FHMs exposed to TB. The model input is plasma VTG concentration, and the output is fecundity. Thus, the model connects the TB effects at a molecular level to TB effects at an individual level. Since oocyte growth and maturation are part of female reproduction, the third model could be integrated with the second one as a future work. The models were calibrated with experimental data to estimate parameters using Markov chain Monte Carlo simulation (MCMC). The estimated parameters were then used to simulate independent studies and to evaluate the models. All three models predict reproductive endpoint data (e.g., fecundity, and plasma concentrations of E_2, T, KT, and VTG) well.

This modeling research allows me to evaluate the prior knowledge of the MOA, to explore possible mechanisms responsible for observed adverse effects by different EDCs, and to generate hypotheses for future tests. In addition, the MOA-based models can be adapted to predict the effects of EDCs with the same MOA. For example, through defining chemical-specific parameters (e.g., binding affinity to ER or AR), the models can be adapted to predict the adverse effects of other EDCs that disrupt the HPG axis through binding to ER or AR. Therefore, the models can serve as a framework or basis for governments to develop cost-effective predictive tools to test and monitor EDCs. The tools can then be applied in ecological risk assessment. Thus, the models I developed during this dissertation research have a great value from a regulatory perspective.

1.2 Biological background of the FHM and the HPG axis

To develop the physiologically based computational models of the HPG axis in FHMs, I did a literature review to understand FHM reproductive biology and the molecular mechanisms of the HPG axis. In the following paragraphs, I describe the reproductive biology of the FHM and the principal components of the HPG axis. The information described below serves as the biological fundamentals for model development.

1.2.1 Reproductive biology of FHM

In oviparous fish, at least two distinct modes of spawning (synchronous and asynchronous) have been characterized. Synchronous-spawning females have oocytes all at the same stage of development and may spawn annually or only once in their life (e.g., Chinook salmon, *Oncorhynchus tshawytscha*). In contrast, asynchronous-spawning fish contain oocytes at different stages of development and may spawn many times during a prolonged breeding season (Nagahama et al., 1995; Wallace and Selman, 1981; Yaron et al., 2003). The FHMs are asynchronous spawners, and usually spawn successively during a three-month breeding period (Gale and Buynak, 1982).

Sexually mature FHMs are dimorphic (Figure 1.1). Adult males usually weigh three to five grams with large nuptial tubercles on the snout and an elongated dorsal pad extending from the nape to the dorsal fin (Ankley et al., 2001; Ankley and Villeneuve, 2006). Adult females usually weigh two to three grams, and have a fleshy ovipositor. The color of adult males is usually black on the sides with bright vertical bars, while the females have a lighter coloration (Ankley and Villeneuve, 2006; Jensen et al., 2001; Leino et al., 2005).

Sexually mature FHMs have bilateral elongated gonads (i.e., ovaries in females and testes in males) oriented longitudinally within their abdominal cavity, which contain gametocytes (i.e., oocytes in females and spermatocytes in males) at various developmental stages. Female FHMs usually start to form oocytes as early as three months after hatching, and start to spawn when they are four months old. Under favorable conditions, the clutch size (i.e., the number of eggs per spawn) is typically in a range of 50 to 100, and the spawning interval (i.e., the time between two successive spawnings) is usually three to four days (Jensen et al., 2001; Watanabe et al., 2007). After being fertilized, eggs hatch in approximately four to five days under ideal conditions (e.g., 25 °C). The new generation of the FHMs then grow and achieve reproductive maturity within four to five months after hatching (Ankley and Villeneuve, 2006).

Exposure to EDCs can cause morphological and reproductive changes in FHMs (Figure 1.2). For example, exposure to estrogenic compounds leads to feminization of male FHMs. Nuptial tubercles on the mouth of male FHMs disappear after an EE_2 exposure and their body weight decreases, which makes the males look like females (Kidd et al., 2007; Lattier et al., 2002). Exposure to androgenic compounds leads to masculinization of female FHMs. After exposure to TB, nuptial tubercles appear on female FHM mouths and their body weight increases, which makes the females look like males (Ankley et al., 2003). In addition, the fecundity of the FHMs exposed to EDCs can be changed significantly. For example, a seven-year, whole-lake experiment conducted in Canada (Kidd et al., 2007) showed that chronic exposure of FHM to 5 - 6 ng EE_2/L led to near-extinction of this species from the lake. Laboratory experiments (Ankley et al., 2003) showed that exposure to 0.5 µg TB/L stopped spawning in FHMs. These changes are associated with altered VTG production, decreased steroid hormone levels, and abnormal oocyte development and maturation (Ankley et al., 2003; Kidd et al., 2007; Lattier et al., 2002). All these processes and elements are linked with the HPG axis, which make it essential to understand the molecular mechanisms of the HPG axis.

1.2.2 The HPG axis in FHM

The molecular mechanisms of the HPG axis have been studied in synchronous spawners, such as Atlantic salmon (*Salmo salar)* (Lazier et al., 1985; Nagahama et al., 1995; So et al., 1985) and rainbow trout (*Oncorhynchus mykiss*) (Tyler et al., 1997; Tyler et al., 1996; Tyler et al., 1991; Tyler et al., 1990), but have not been studied as extensively in asynchronous spawners. Previous studies in FHMs mainly focused on fecundity, and apical reproductive endpoints such as plasma concentrations of E_2, T, KT, and VTG. In recent years, there has been more research on the HPG axis in FHMs. For example, there are reports on FHM gene expression data of GtHs (Villeneuve et al., 2007b), brain and ovary aromatase activity and mRNA transcripts (Halm et al., 2001; Villeneuve et al., 2006), VTG protein and gene isoforms (Lattier et al., 2002; Miracle et al., 2006; Parks et al., 1999), ARs (Wilson et al., 2007; Wilson et al., 2004), and ERs

(Denny et al., 2005; Filby and Tyler, 2005; Wilson et al., 2004). These studies provided valuable information and facilitated my model development.

In the following paragraphs, I describe the principal elements and molecular mechanisms of the HPG axis in fish. More detailed graphical models of the HPG axis in male and female teleosts have been published (Villeneuve et al., 2007a). The graphical models are based upon information from a variety of animal species including mammals, and many details cannot be supported quantitatively. When I developed the computational models, I reviewed the literature extensively, but simplified many biological processes. In the following paragraphs, I only focus on the biological processes that are associated with my model development.

1.2.2.1 GnRH

In teleost fish, such as the FHM, the HPG axis is hierarchically organized, and the hormonal signaling has a dynamic feature (Figure 1.3). The hormonal signaling of the HPG axis starts from GnRH, a peptide hormone produced in the hypothalamus. The production and release of GnRH is under the regulation of a variety of factors (Amano et al., 1997). For example, androgens have a negative feedback on the synthesis and release of GnRH (Villeneuve et al., 2007a) . In zebrafish (*Danio rerio*), a asynchronous-spawning small fish species closely related to the FHM, androgen response elements (AREs) have been found in the promoter regions of the GnRH genes (Zhenhong Li and Karen Watanabe, unpublished results, 2010). This indicates that the negative control of GnRH synthesis by androgens is associated with the AR regulation network.

1.2.2.2 GtHs

The released GnRH goes to the pituitary gland and binds to GnRH receptors to stimulate the synthesis of GtHs (i.e., FSH and LH) (Amano et al., 1997); however this is not the only mechanism regulating GtH production. For example, gene expression of LH is upregulated by estrogens, such as E_2 (Melamed et al., 1998; Yaron et al., 2003). Estrogen response elements (EREs) have been found in the promoter regions of the LH

genes (Yaron et al., 2003), which indicates that the positive control of LH gene expression by estrogens is associated with the ER-related regulatory network. In addition, aromatizable androgens such as T have a positive effect on LH gene expression, which is similar to E_2 (Antonopoulou et al., 1999; Melamed et al., 1998). However, non-aromatizable androgens such as KT do not have such an effect (Yaron et al., 2003). These imply that T may act via its aromatization to E_2 by brain aromatase.

GtHs play important roles in brain-gonad communication, and regulate steroidogenesis (i.e., steroid hormone production) and thus gametogenesis in males and females (Nagahama, 1994; Patino et al., 2001; Schulz et al., 2001). After being produced, GtHs are released into the bloodstream and circulate into the gonads. In males, GtHs bind to their receptors in testes, and regulate steroidogenesis and thus spermatogenesis. Similarly, in females GtHs bind to their receptors in ovaries, and regulate steroidogenesis and thus oogenesis.

1.2.2.3 Steroid hormone production

In males and females, steroid hormone production follows similar pathways. All steroid hormone production starts with cholesterol. Cholesterol is transported from the outer mitochondrial membrane into the inner membrane where it is processed to pregnenolone (Miller, 1988). The protein responsible for the cholesterol transport is named steroidogenic acute regulatory protein (StAR). It is generally believed that StAR-regulated cholesterol transport is a rate-limiting and hormonally regulated step (Arukwe, 2008). For example, GtHs induce StAR gene expression significantly in the Atlantic croaker (*Micropogonias undulatus*) (Nunez and Evans, 2007). In FHM testes, StAR gene expression level decreases significantly in response to an EE_2 exposure (Filby et al., 2007b; Garcia-Reyero et al., 2009). After being transported into the inner mitochondrial membrane, cholesterol is converted to pregnenolone by the P450 side chain cleavage enzyme (P450scc). This is again a rate-limiting and hormonally regulated step (Miller, 1988). Similar to StAR, GtHs upregulate the gene expression of P450scc (Senthilkumaran et al., 2004), and exposure to EE_2 leads to a significant decrease in P450scc gene expression in male FHM testes (Garcia-Reyero et al., 2009).

In the following steroidogenesis steps, 3β-hydroxysteroid dehydrogenase (3β-HSD) catalyzes the conversion of pregnenolone to progesterone, which is a precursor for 17α-hydroxy-progesterone (17α-HDP). 17α-HDP is produced by $P450_{17\alpha}$ through hydroxylating progesterone, and is converted to androstenedione (a precursor of T) by enzyme $P450_{17,20}$ lyase. 17α-HDP is also a precursor of 17α, 20β-dihydroxy-4-pregnen-3-one (17α, 20β-DP), a maturation-inducing hormone (MIH) in most teleost fish (Nagahama, 1997). The conversion from 17α-HDP to 17α, 20β-DP is catalyzed by 20β-hydroxysteroid dehydrogenase (20β-HSD), a key enzyme to initiate maturational events. Androstenedione is converted to T by 17β-hydroxysteroid dehydrogenase (17β-HSD). T is then catalyzed by aromatase to E_2, or by 11β-hydroxysteroid dehydrogenase (11β-HSD) to KT (Miller, 1988). The conversion of T to E_2 occurs in male and female FHMs, while the production of KT usually only occurs in male FHMs (Jensen et al., 2001).

1.2.2.4 Steroid hormone metabolism

After being synthesized, steroid hormones are released into the bloodstream and circulate to other tissues (e.g., liver), where they may undergo metabolism. To better understand how steroid hormones or their mimics are metabolized in fish, I did an extensive literature search and summarized the information for the metabolism pathways of several steroid hormones (e.g., E_1 E_2, and T) and EE_2 in Figure 1.4.

A direct metabolite analysis shows that, similar to mammals, the liver is the major organ with the capability of metabolizing steroid hormones in fish (Butala et al., 2004; Snowberger and Stegeman, 1987). Distribution of E_2 among different tissues is observed by labeling E_2 with tritium (Myers and Avila, 1980). The results show that most tritiated E_2 is concentrated in the liver three hours post-exposure. Liver metabolism of steroid hormones is generally thought to occur in the microsomes (i.e., a granule in the cell cytoplasm). The metabolism pathway is associated with the P450 enzyme system (Hansson and Rafter, 1983). The P450 enzyme system is capable of hydroxylating E_2, T, and EE_2 at various positions on the steroid skeleton (e.g., 2^{nd}, 4^{th}, 6^{th}, 7^{th} and 16^{th} positions) and generates various hydroxylated steroid hormones (Li et al., 1999; Parks and LeBlanc, 1998a). In addition, 17β HSD converts E_1 to E_2 and T to androstenedione

reversibly; and aromatase converts E_2 to T and E_1 to androstenedione reversibly (Butala et al., 2004; Khan et al., 1997; Petkam et al., 2002).

Subsequently, the compounds and their hydroxylated metabolites can be conjugated and excreted into the environment. Glucuronosyltransferases (GTs) and sulfotransferases (STs) are two important enzymes responsible for steroid hormone conjugation (Li et al., 1999). They can move sulfate or glucuronide esters to the hydroxyl groups in the 3rd and 17th position of the steroid skeleton. Conjugation increases water solubility of steroid hormones, which eases excretion. Conjugated steroids and their mimics are mainly excreted through urine, and only a very small amount is excreted through feces in an unconjugated form.

The qualitative information above summarizes how steroid hormones and their mimics are metabolized and excreted in fish. However, kinetic data are unavailable to simulate these processes.

1.2.2.5 Estrogen-regulated Vitellogenesis

Steroid hormones are essential in a wide range of physiological and reproductive processes. For example, estrogens circulate to the liver where they bind to ERs and upregulate vitellogenesis. Vitellogenesis is a process of egg yolk formation, during which VTG is synthesized, secreted into blood, and taken up by growing oocytes where it serves as an egg yolk precursor and is processed to become egg yolk proteins (Sumpter and Jobling, 1995). VTG is synthesized in response to circulating estrogens (Hemmer et al., 2002; Stifani et al., 1990), and thus is dependent upon steroid hormone production and is a subsystem regulated by the HPG axis.

Under normal conditions, a large amount of VTG production occurs in the liver of females, but not males. Males also possess VTG genes, but their plasma VTG concentration typically remains very low, presumably due to low levels of circulating endogenous estrogens (Jensen et al., 2001). Exposure to estrogenic EDCs results in elevated plasma VTG concentration in males, which remains elevated for a long period

because there is no efficient elimination pathway (Kidd et al., 2007; Korte et al., 2000; Parrott and Blunt, 2005). The elevated plasma VTG concentration is due to VTG production in liver cells. VTG genes are transcribed in the gills of adult male FHMs exposed to EE_2, but the transcription level is relatively low compared to that in liver (Lattier et al., 2002). The physiological significance of VTG gene expression in FHM gills is open to future research. Because of a sensitive response to exogenous estrogens, VTG has been used as a biomarker for exposure to estrogenic EDCs in fish (Sumpter and Jobling, 1995). In addition, exposure to androgenic EDCs can result in decreased plasma VTG concentration in female FHMs (Ankley et al., 2003), which may be caused by decreased plasma estrogen concentrations.

Estrogenic compounds stimulate VTG gene expression through a ligand-receptor regulatory system. Estrogens such as E_2 bind to ERs to form estrogen-ER complexes. The complexes dimerize and stimulate the expression of *vtg* genes. ER belongs to a steroid receptor family whose members bind to their ligands, and the ligand-receptor complexes act as activators or inhibitors of target genes (Flouriot et al., 1997). Research on gene regulation by bound ER has shown that not only VTG but also ER gene expression can be upregulated by the estrogen-ER complex (Flouriot et al., 1997; Flouriot et al., 1996; Korte et al., 2000; Miracle et al., 2006). The upregulation of ER production in response to circulating estrogens accelerates VTG synthesis, and makes VTG production sensitive to estrogenic compound exposure.

1.2.2.6 Steroid feedback on the HPG axis

The steroid hormones also have feedback effects on the HPG axis. For example, as described above, T has a feedback on GnRH production, and E_2 has a feedback on LH production. Feedback regulation is an important part of the HPG axis signaling.

1.2.2.7 Oogenesis

The hormonal signaling of the HPG axis controls oogenesis in fish. However, very little information is available on FHMs. Therefore, this section focuses on the general processes of fish egg development.

Fish eggs develop from oocytes which develop from oogonia, the primitive egg cells that persist in ovaries. Fish ovaries consist of oogonia, oocytes and their surrounding tissues. Oogonia may produce clutches of new oogonia by mitotic divisions (oogonial proliferation), or they may undergo meiotic divisions to form oocytes throughout the fish's life (McMillan, 2007). As a result, it seems that there is no limit to the number of eggs a fish can spawn during its life (Tyler and Sumpter, 1996). However, although there is a variation caused by age, nutrition, health, and environmental conditions, the number of eggs spawned per fish is usually within a typical range for a fish species. This makes it particularly interesting to study the mechanisms controlling the onset of oocyte recruitment from oogonia. However, the mechanisms are not understood completely in any fish species studied so far.

After undergoing meiotic division, oogonia become oocytes and are recruited into a growth stage, during which all oocytes follow a similar basic pattern of growth for all teleosts studied to date (Tyler and Sumpter, 1996). At the beginning of the growth stage, each oocyte is surrounded by a follicle cell layer. With the oocyte growth, the follicle cells can proliferate and form a granulosa cell layer. The supporting tissue surrounding the follicle cell layer can form the outer thecal cell layer. The two cell layers are important in the production of estrogens, and thus the regulation of oocyte growth. During the oocyte growth period, there is considerable oocyte enlargement, which is mainly due to the absorption of VTG. For example, in FHMs the diameter of an oocyte before the vitellogenic stage is typically approximately 400 µm, and is roughly 1000 µm prior to spawning (Leino et al., 2005). Therefore, the absorption of VTG can result in a 10-fold increase in oocyte volume, which is more than 90% of the final oocyte content in FHMs.

When the vitellogenic stage comes to an end, fish oocytes enter a maturation stage. Post-vitellogenic oocytes resume meiosis under the regulation of a variety of hormones (e.g., LH and MIH), and then become fertilizable (Nagahama, 1994). In most teleosts, oocyte maturation is accomplished within 24 hours (Nagahama et al., 1994). For example, in FHMs the post-vitellogenic oocytes are only several hours away from

ovulation (Leino et al., 2005). As a result, usually no mature oocytes can be observed in a histological study using FHMs. During the oocyte maturation stage, hydration may contribute significantly to the final egg size. The proportion of the final egg size due to hydration varies from negligible to 88%, depending on the fish species (Tyler and Sumpter, 1996).

It is believed that the HPG axis regulates oogenesis in fish through a variety of hormones (e.g., FSH, LH, E_2, and MIH) (Nagahama, 1994; Patino et al., 2001; Schulz et al., 2001). FSH and LH have similar potencies in stimulating E_2 production in goldfish, tuna, and salmon; while the potency of LH in stimulating MIH production greatly exceeds that of FSH (Swanson et al., 2003). Generally speaking, FSH appears to regulate oocyte growth by stimulating the production of E_2. In contrast, LH appears to regulate oocyte maturation by stimulating the production of MIH (Nagahama and Yamashita, 2008).

1.3 Markov chain Monte Carlo Simulation

Following the biological fundamentals described in Section 1.2, I developed three physiologically based computational models. Two models simulate the HPG axis in male and female FHMs respectively, and the third model simulates oocyte growth dynamics in adult female FHMs. The conceptual models and mathematical formulations of each model are described in Chapters 2, 3, and 4, respectively. In the following section, I mainly focus on the Markov chain Monte Carlo method which was used to estimate parameter values of the two HPG axis models.

The computational models require input of a variety of model parameters such as FHM body weight, tissue compartment volumes, blood flow rates, equilibrium partition coefficients of chemicals of interest, kinetic rate constants for chemical reactions, volume of oogonia, and volume of mature oocytes. For the oocyte growth dynamics model, all parameters were fixed with values derived from experimental data or literature. For the HPG axis models, parameters were either fixed with certain values, or calibrated using

MCMC simulation following the method described in previous studies (Bois et al., 1996b; Gelman et al., 1995; Lin et al., 2004; Watanabe et al., 2005).

The MCMC simulations were performed with MCSim (Bois and Maszle, 1997), a software package freely available online (http://directory.fsf.org/math/mcsim.html), using the Metropolis-Hastings (MH) algorithm. Based upon Bayes' rule, MCMC simulation provides a joint posterior distribution of model parameters that is proportional to the product of the parameter prior distributions and the data likelihood. Figure 1.5 illustrates the principles of MCMC simulation. Generally, before performing MCMC simulation, one needs prior knowledge of the calibrated model parameters. In this dissertation, the knowledge is mainly from literature for mammals or other fish species. For each calibrated model parameter, the prior knowledge is used to specify a prior distribution which gives an approximate range of the parameter values. At the initial step of MCMC simulation, a value (θ_0) of each parameter is randomly sampled from its prior distribution. Then based upon the distribution, the prior probability of the parameter value ($P(\theta_0)$) is calculated. Subsequently, the parameter value is input into the model to calculate predictions that are compared to experimental data. Based upon the distributions of experimental data, data likelihood ($P(D/\theta_0)$) is calculated. According to Baye's rule, the posterior probability of the sampled model parameter ($P(\theta_0/D)$ is calculated as a product of the prior probability and data likelihood ($P(\theta_0/D) \propto P(D/\theta_0) \times P(\theta_0)$).

For the next step, a new parameter value (θ_c) is randomly sampled from its prior distribution as a candidate, and the MH algorithm is used to determine whether the candidate is accepted (Figure 1.5B). To be brief, the posterior probability of the candidate parameter value ($P(\theta_c/D)$) is calculated following the procedure described above. Then a ratio between the two posterior probabilities ($P(\theta_c/D)/ P(\theta_0/D)$) is calculated. According to the MH algorithm, if the ratio is greater than or equal to 1, θ_c is accepted as θ_1. Otherwise, the ratio is compared with U, a sample randomly generated from a uniform distribution ranging from 0 to 1. If the ratio is greater than or equal to U, θ_c is accepted as θ_1; otherwise, θ_c is rejected and another candidate parameter value is

randomly sampled from the prior distribution. The procedure is repeated until one candidate parameter value is accepted. Then the accepted parameter value is recorded, and the program moves to randomly sample another parameter value. The procedure is repeated until the MCMC simulation is stopped. The accepted parameter values constitute a chain with the step (i.e., iteration) number as 'x' and the parameter value as the 'y' (Figure 1.5C). Because the parameter values at the present state (step *n*) depend upon their values at the previous state (step *n*-1), this process is a Markov process and the chains constructed are Markov chains.

The MCMC simulations are stopped when stationary distributions (stable posterior distributions) are reached. During my dissertation research, I used a potential scale reduction method (Gelman et al., 1995) to assess if the stationary distributions were reached. Following the method, four Markov chains were run for the HPG axis models in male and female FHMs, respectively. For each parameter of each model, I compared the variance between and within the four Markov chains for the last *n* values from each chain (*n* is defined for each HPG axis model in Chapter 2 and 3, respectively). As recommended by Gelman et al. (1995), potential scale reduction values between 1.0 and 1.2 were used as the criteria for a convergence of the four Markov chains. Convergence indicates that all four Markov chains are stable, and the stationary distributions are reached.

The MCMC method has advantages over other parameter optimization methods. Through defining prior distributions, it combines existing knowledge about a range of possible parameter values with the experimental data. It allows determining confidence intervals (CIs) of model predictions. In addition, once new experimental data are available, the present posterior distributions can be used as the priors to estimate new posterior parameter distributions. As a result, it is relatively easy to update the information.

1.4 Dissertation organization

Three physiologically based computational models for the FHM constitute this dissertation. In Chapter two, I describe a model of the HPG axis in male FHMs exposed to E_2 and EE_2. This chapter contains a reproduction of a manuscript (permission to reproduce the manuscript granted by Oxford University Press) that has been published in Toxicological Sciences (Watanabe et al., 2009). The introduction section was modified to achieve smooth flow of writing. In addition, I added one more model evaluation study that was not published in the paper. Chapter three describes a computational model of the HPG axis in female FHMs exposed to EE_2 and TB. This chapter will be submitted for journal publication. In Chapter four, I describe a computational model for oocyte growth dynamics in FHMs, a manuscript that has been submitted and is under review (Canadian Journal of Fisheries and Aquatic Sciences).

CHAPTER 2

A Computational Model of the Hypothalamic-Pituitary-Gonadal Axis in Male FHMs Exposed to EE_2 and E_2

This chapter contains a reproduction of a manuscript (permission to reproduce the manuscript granted by Oxford University Press) that has been published in Toxicological Sciences (Watanabe et al., 2009). The introduction section was modified to achieve smooth flow of writing. In addition, one new model evaluation study (Brian et al., 2005) that was not published in the paper is added. The method, result, and discussion of the new study are incorporated into the method, result, and discussion sections of this chapter respectively.

2.1 Introduction

EE_2 and E_2, two estrogenic EDCs, have been found in the aquatic environment and are known to affect fish reproduction. The environment concentrations range from 0.5 to 15 ng EE_2/L (Desbrow et al., 1998; Ericson et al., 2002a; Ribeiro et al., 2008; Ying et al., 2008), and < 1 to 48 ng E_2/L (Desbrow et al., 1998; Labadie and Budzinski, 2005; Ribeiro et al., 2008; Ying et al., 2008). In a recent study, Kidd et al. (2007) found that additions of EE_2 to an experimental lake yielding water concentrations of approximately 5 ng EE_2/L resulted in a collapse of the native FHM population about 1.5 yrs (in Fall 2002) after the start of EE_2 additions to the lake. Moreover, in laboratory studies, environmentally relevant concentrations of either EE_2 or E_2 have been shown to affect function of the HPG axis in fish (Brion et al., 2004; Halm et al., 2002; Lange et al., 2001; Panter et al., 2000; Parrott and Blunt, 2005; Pawlowski et al., 2004). Most laboratory

studies focus on exposure to individual estrogens, whereas in the aquatic environment mixtures prevail. Some studies with FHMs have shown that mixtures of estrogens, including E_2 and EE_2, can produce additive effects within the HPG axis (Brian et al., 2005; Brian et al., 2007). Hence, it is clear that a mechanistic understanding is needed as to how estrogens, either singly or in mixtures, could affect key HPG-mediated processes in fish, including reproduction. This understanding would be greatly facilitated by a computational model describing the interaction of estrogens with the fish HPG axis.

To improve our understanding of how estrogenic EDCs affect reproductive endpoints, we developed a physiologically based computational model of the HPG axis for male FHMs exposed to EE_2 and E_2. This model captures the salient features of an HPG axis graphical systems model described by Villeneuve et al. (2007a), and simulates key reproductive endpoints such as plasma concentrations of T, KT, E_2, and VTG. Our physiologically based model is an advancement over prior non-physiologically based models of the HPG axis in fish (Kim et al., 2006; Murphy et al., 2005; Schultz et al., 2001), rats (Barton and Andersen, 1998; Inoue et al., 1970; Schlosser et al., 2006; Teeguarden and Barton, 2004), and humans (Enciso and Sontag, 2004; Plouffe and Luxenberg, 1992) because it is able to simulate responses for both EE_2 and E_2 exposure, and utilizes a probabilistic, Markov chain Monte Carlo method of model calibration that accounts for natural biological variability and provides model predictions with CIs.

2.2 Materials and methods

2.2.1 Experimental data

Reproductive endpoint data in unexposed FHMs were obtained from over 10 experiments conducted at the USEPA Duluth laboratory from 1999 to 2006, which were summarized in Watanabe et al. (2007). In total, there were 143 unexposed (control) male FHMs associated with these experiments. The data for 70 unexposed fish were used to calibrate the model and the remainder was used to evaluate the model. For each individual fish, measured model input parameters included body weight (BW), gonad weight (GW), and liver weight (LW). Model predictions of plasma T, KT, E_2 and VTG concentrations were compared to measurements of T, KT, E_2 and VTG through a

likelihood function (Gelman et al., 1995). Summary statistics of the unexposed FHM data used to calibrate the model are reported in Table 2.1.

Data for EE_2-exposed male FHMs were obtained from three studies: (i) a 48-hour static exposure to concentrations of 10 and 50 ng EE2/L (Garcia-Reyero et al., 2009); (ii) a continuous, flow-through exposure to concentrations of 10 and 100 ng EE_2/L (Ekman et al., 2008); (iii) two continuous, flow-through EE_2 exposures (exposure I: 0, 0.1, 0.5, 1, 2, 4, 10, and 50 EE_2/L; exposure II: 0, 0.05, 0.1, 0.2, 0.5, 2, 5, 10 EE_2/L) (Brian et al., 2005). Actual measured EE_2 water concentrations from the four studies were used as input into the model. In Garcia-Reyero et al.(2009), male FHMs were exposed to 10 and 50 ng EE_2/L for 48 hours, and plasma T and VTG concentrations were measured in four fish per exposure concentration (Table 2.2). As part of the study by Garcia-Reyero et al., EE_2 concentrations in carcass and liver also were measured in pooled tissues from 30 male FHMs exposed to 50 ng EE_2/L for 48 hours (unpublished data). After exposure, the average EE_2 concentration accumulated in liver was 57.8 ± 29.5 ng per g dry tissue, and the average EE_2 concentration accumulated in carcass was 13.9 ± 3.7 ng per g dry tissue. In Ekman et al. (2008), plasma VTG concentrations in male FHMs were measured in eight males per sampling period after days one, four and eight of exposure to EE_2, and eight days after EE_2 exposure (test day 16). In Brian et al. (2005), two separate experiments were performed in male FHMs exposed to EE_2 for 14 days. For each experiment, plasma VTG concentrations were measured in four fish per EE_2 concentration after exposure. Data from Garcia-Reyero et al. (2009) were used for model calibration, and data from Ekman et al. (2008) and Brian et al. (2005) were used for model evaluation.

Data from E_2 exposed male FHMs were obtained from two studies: (i) Korte et al. (2000); and (ii) Parks et al. (1999). Korte et al. (2000) injected 97 male FHMs with 0.5 or 5 mg E_2/kg, and measured plasma E_2 and VTG concentrations at 10 different times over 18 days (n = 5 fish/sample). Parks et al. (1999) injected three male FHMs with 25 mg E_2/kg on days zero, two and four, and measured plasma VTG concentrations on day

seven. The Korte et al. (2000) data were used to calibrate the model and Parks et al. (1999) data were used to evaluate our model predictions.

2.2.2 Computational model formulation

Our physiologically based model simulates the absorption, distribution, metabolism, and elimination of EE_2 and endogenous hormones of the HPG axis in male FHMs. Though a more detailed conceptual model has been described by Villeneuve et al. (2007a), the data needed to parameterize a corresponding computational model are currently unavailable. We simplified many of the biochemical processes reported in Villeneuve et al., and incorporated these processes into a model that contains six compartments (i.e., gill, brain, gonad, liver, venous blood, and ‘‘other’’) involved in HPG axis signaling and EE_2 disposition (Figure 2.1). Following principles of pharmacokinetic modeling, for each compartment and chemical of interest, a mass balance was formulated for the free (or unbound) chemicals of interest (Section 2.5 Eq. 1) to create a set of coupled ordinary differential equations that comprise the computational model. Total chemical concentrations were computed as the sum of free and specifically bound chemical concentrations (Section 2.5 Eq. 3). A comprehensive description of the model formulation with equations can be found in Section 2.5 Supplementary Information.

Gill. The gill compartment is where exogenous EE_2 uptake occurs from the aquatic environment. As water containing EE_2 flows across the gills, EE_2 is taken up into arterial blood that distributes throughout the body. In zebrafish, steroid binding proteins (SBPs) in gill have been found to facilitate EE_2 uptake from water (Miguel-Queralt and Hammond, 2008). In our model, EE_2 uptake is formulated using an equilibrium partition coefficient between blood and water, which simplifies the EE_2 uptake process and enables the entrance of EE_2 into the bloodstream. Similarly, we use partition coefficients to represent the fraction of EE_2 that leaves the blood to enter different tissues and organs. (Section 2.5 Eq. 5).

Brain. The brain regulates the HPG axis by producing hormones that circulate to target tissues (e.g., gonad). In the brain compartment, GnRH regulates the release of LH

(Yaron et al., 2003), but the dynamics of GnRH were not included in this model because GnRH data were unavailable. Instead, we represented the periodic nature of GnRH dynamics and its effect on LH by producing LH in brain according to a periodic function, which is similar to assumptions made by Murphy et al. (2005). Basal LH production is formulated as a periodic step function of 12 hrs on and 12 hrs off (Section 2.5 Figure 2.8). In addition, LH production can be stimulated by E_2 (Yaron et al., 2003), which is formulated as a positive feedback in our model, although Murphy et al. (2005) formulated the effect of E_2 on LH production as a negative feedback for Atlantic croaker. Our model simulates the production of E_2 from T that circulates to the brain in blood. Also, the model is formulated such that E_2 in the brain is able to bind to ERs, which serves as a "sink" in the brain's E_2 mass balance. Hormones produced in the brain are secreted into the blood and circulate throughout the body.

Gonad. A target tissue of LH is the gonad where LH binds to LH receptors to regulate steroidogenesis (Senthilkumaran et al., 2004). In our model, LH bound to LH receptors stimulates the production of StAR. The quantity of cholesterol available for steroidogenesis is formulated to be proportional to the quantity of StAR produced (Nunez and Evans, 2007). Cholesterol is the initial substrate in a cascade of reactions that produce T (Halm et al., 2002; Nagahama et al., 1994; Nagahama et al., 1995; Senthilkumaran et al., 2004). A more detailed computational model of steroidogenesis exists for FHM (Breen et al., 2007), however, we could not implement it here because concentrations of intermediate steroid hormones are unavailable. Thus, we simplified the complex process of T production from cholesterol by lumping the multiple reactions into one "effective" reaction (Murphy et al., 2005). This "effective" reaction was formulated as a Hill equation (Section 2.5 Eq. 12). Production of E_2 (and KT) from T is formulated as a Michaelis-Menten equation (Section 2.5 Eqs. 14 & 15). Because decreases in plasma T concentration, StAR gene expression, and P450scc gene expression were observed after EE_2 exposure (Garcia-Reyero et al., 2009), we assumed an autocrine/paracrine negative feedback process in the gonad (Callard, 1992) where E_2 or EE_2 binds to ER, and the E_2–ER or EE_2–ER complex inhibits T production (Section 2.5

Eq. 13). Hormones produced in the gonad are secreted into blood and circulate throughout the body.

Liver. When estrogens such as E_2 and EE_2 enter the liver, they bind to ERs forming E_2–ER and EE_2–ER complexes. These complexes then bind to EREs of target genes (e.g., ER and VTG) to regulate gene expression. The dominant ER subtype in FHM liver is ERα, which is the only ER subtype known to be induced by E_2 or EE_2 (Filby et al., 2007b; Filby and Tyler, 2005). In rainbow trout hepatocyte cultures, Flouriot et al. (1997; 1996) found that when exogenous E_2 concentration was zero, ER mRNA was expressed at low levels while VTG mRNA was not expressed. As a function of increasing exogenous E_2 concentration, both ER and VTG gene expression increased in a dose-dependent manner (Flouriot et al., 1996). Assuming that ER protein correlates with ER gene expression, in our model bound ER is formulated to increase the production of both ER itself and VTG. For example, we used measured changes in ER gene expression to provide limits to changes in ER protein induction. Moreover, we are modeling all ERs based on data from ERα. The ER kinetics in liver include background production, induction by bound ER, association and dissociation with E_2 and EE_2, and elimination (Section 2.5 Eq. 16).

In male FHMs, plasma VTG concentrations are normally very low, and are usually undetectable at the μg/ml level. Exposure to estrogens such as EE_2 has been shown to cause abnormal hepatic production of VTG, and raise plasma VTG concentrations to unusually high levels (Filby and Tyler, 2005; Lattier et al., 2002; Schmid et al., 2002). In our model, we associated the production rate of VTG protein in liver with the concentration of E_2-ER and EE_2-ER complexes (Section 2.5 Eq. 16). VTG produced in liver is secreted into blood and circulates throughout body.

We did not include steroid hormone or EE_2 metabolism reactions in liver, although they are known to exist (Ohkimoto et al., 2003; Snowberger and Stegeman, 1987). Liver metabolism serves to eliminate a parent compound from the body, and multiple reactions would need to be added to the model without sufficient data to provide parameter values. Adding these reactions would only increase the uncertainty and

complexity of our model without a significant improvement in model predictions. Thus, we formulated steroid hormone and EE_2 elimination as first order processes in the "other" compartment.

Venous blood. In the blood of most vertebrates E_2 and T are predominantly bound to SBPs, which modulate steroid hormone bioavailability and distribution to target tissues (Teeguarden and Barton, 2004; Tollefsen et al., 2004). In our model, free and SBP-bound T and E_2 concentrations are simulated in venous and arterial blood compartments (Section 2.5 equations for Venous Blood). KT also binds to SBPs, but with a much lower binding affinity than E_2 and T based on studies in other fish species (Laidley and Thomas, 1994; Miguel-Queralt and Hammond, 2008; Pasmanik and Callard, 1986). For EE_2, Tollefsen et al. (2004) reported that EE_2 binding to Arctic charr (*Salvelinus alpinus*) SBP was approximately 400-fold less than that of E_2. However, Gale et al. (2004) reported that the binding affinity of EE_2 for channel catfish (Ictalurus punctatus) SBP was threefold higher than that of E_2. More recently, Miguel-Queralt and Hammond (2008) reported that the binding affinity of EE_2 to recombinant SBPs from zebrafish was fivefold higher than that of E_2. These studies (Gale et al., 2004; Miguel-Queralt and Hammond, 2008; Tollefsen et al., 2004) suggest large interspecies variability in the binding affinity of EE_2 to SBPs, which may be a result of different fish species or different test methods. Inclusion of EE_2 binding to SBPs in our model would allow EE_2 to compete and displace E_2 and T from SBPs in blood, and as a result free E_2 and free T concentrations in blood would increase. However, the increase in free E_2 and T would not be significant because the total SBP concentration was defined as 20 nM, a relatively low value. Thus, KT and EE_2 binding to SBPs was not included in our model.

Other. In our model all tissues except for gill, brain, gonad and liver were grouped into a compartment called ‘‘other.’’ A unique function of the ‘‘other’’ compartment is the elimination of T, KT, E_2, and VTG according to first-order kinetics (S Section 2.5 Eq. 19). This is a simplifying assumption since Vermeirssen and Scott (1996) showed that rainbow trout steroid hormones, mainly in conjugated form, are excreted in urine and bile. However, without data to parameterize and calibrate kinetic equations of

steroid hormone biotransformation and conjugation in liver and subsequent elimination by the kidney, representing these complex reactions would introduce more uncertainty into the model. That is, the kinetic rate constants for these reactions could take on any value as long as the steroid hormone production parameters compensated for the increase or decrease in elimination. Thus, we chose to represent the elimination of steroid hormones, EE_2, and VTG with first-order kinetic processes in the ‘‘other’’ compartment where the kidney resides.

2.2.3 Model calibration

The model requires information about experimental conditions and 82 model parameters such as tissue compartment volumes, blood flow rates, equilibrium partition coefficients, and rate constants for chemical reactions. Sixty-two model parameters were fixed at values listed in Table 2.5 because they were either (1) measured directly in FHMs; (2) scaled allometrically to FHM from data in other species; (3) insensitive parameters with respect to the available measured data; or (4) they could not be uniquely identified given the other model parameters being calibrated and the available data. The remaining 20 model parameters (Table 2.3) were calibrated with data collected in FHMs. To account for biological uncertainty and variability, we used a probabilistic, Bayesian approach called MCMC simulation to calibrate 20 model parameters (see Table 2.3) following methods described in previous studies (Bois et al., 1996b; Gelman et al., 1995; Lin et al., 2004; Watanabe et al., 2005). MCMC simulation is a computational method based on Bayes’ rule that provides a joint posterior distribution of model parameters that is proportional to the product of the parameter prior distributions and the data likelihood. This method has advantages over other parameter optimization methods in that it: (1) provides a method of incorporating existing knowledge about a range of possible parameter values through specification of a prior distribution; (2) accounts for covariance between the 20 calibrated model parameters; and (3) allows for determination of model prediction CIs (e.g., Table 2.4). To perform MCMC simulation, one must specify prior parameter distributions, and experimental conditions and data for computing the likelihood function as described below.

We specified model parameter prior distributions based on data available in the literature. When little or no data were available, we assigned a vague prior distribution such as a uniform or log-uniform distribution with a large range to allow the experimental data to refine the posterior parameter distribution. For example, we could not find a published value for the Hill coefficient for VTG production in liver, but we assumed that it would be approximately two based on the dimerization of ER complexes needed to stimulate gene expression. Thus, we assigned a log-uniform distribution with a lower bound of two and an upper bound of 10 (Table 2.3). Similarly, an EE_2 partition coefficient for blood to water was reported for rainbow trout (Kim, 2004), but not FHM, so we assigned a lognormal distribution with a geometric mean of 600 and a geometric standard deviation of three, which corresponds to a coefficient of variation equal to 1.5.

Two of the 20 calibrated parameters were the variances of measured plasma T and E_2 concentrations. Measurements were made for these two endpoints in unexposed and E_2- or EE_2-exposed FHMs, but relatively few measurements were made in the exposed FHMs. Thus, the plasma T and E_2 concentration variances were treated as unknowns and calibrated with MCMC simulations. Following methods used previously (Bois et al., 1996b; Lin et al., 2004), inverse gamma prior distributions were assigned to the variances based upon a natural logarithm transformation of the measured plasma E_2 and T concentrations.

Simulation of EE_2 or E_2 exposure experiments with our model began at model simulation time equal to 3600 h in order to allow the model to reach homeostasis/steady-state before starting the exposure. Starting an experimental exposure at 3600 h was necessary because at the start of a simulation (i.e., 0 h), most model output variables (e.g., plasma T, KT, and E_2 concentrations) were set to equal zero because they have not been measured at birth. For each simulated experiment, the exposure duration was defined by the experimental conditions, and model predictions were made at times corresponding to each measurement. Thus, a 48-h exposure to EE_2 was started at 3600 h and ended at 3648 h; plasma VTG predictions were output at 3648 h to correspond to measured plasma VTG concentrations at the end of the 48-h exposure period.

MCMC simulations were performed with MCSim (Bois and Maszle, 1997), a software package freely available online (http://directory.fsf.org/math/mcsim.html), using the MH algorithm. Four independent Markov chains were run that started with parameter values randomly selected from their assigned prior distributions. Simulations were performed until the four chains converged for all 20 parameters. Convergence was assessed by the potential scale reduction method (Gelman et al., 1995) that compares the variance between and within Markov chains for the last *n* values from each chain (*n* = 1000 in this study). As recommended by Gelman et al. (1995), we used potential scale reduction values between 1.0 and 1.2 as our criteria for convergence.

2.2.4 Model evaluation

We evaluated the predictive ability of our model by simulating plasma VTG concentrations from four studies that used different experimental (including exposure) conditions compared to the studies used to calibrate the model. Four thousand sets of 20 calibrated model parameters were used to simulate two different experiments from Ekman et al. (2008) (see Section 2.2.1 Experimental Data). Exposure to EE_2 was started at simulation time equal to 3600 hrs for reasons described in the Section 2.2.3 Model Calibration. Simulated exposures to 10 and 100 ng EE_2/L lasted for 8 days, and plasma VTG concentrations were output at days 1, 4, 8 and 16 (i.e., 8 days post-exposure). Similarly, we simulated the two separate experiments from Brian et al. (2005) (see Experimental data section). Plasma VTG concentrations were output at the 14^{th} day of EE_2 exposure. We also simulated the plasma concentrations of VTG in male FHMs 7 days after three doses of E_2 injection, and compared the predictions to measurements from an independent study by Parks et al. (1999). Parks et al. reported that the plasma concentration of VTG on the seventh day after three injections of E_2 on days 0, 2, and 4 was 21.3 ± 1.3 mg/ml. The model predictions were compared with the measured data visually.

2.3 Results

2.3.1 Model Calibration

Four separate Markov chains of 6500 iterations were run in order to reach convergence for all 20 parameters treated as unknown random variables. The speed of each chain was approximately 90 h per 1000 iterations on a 2.8-GHz Linux workstation. Figure 2.2 plots the progression of parameter values for two of the 20 calibrated parameters: (a) blood to water partition coefficient for EE_2 uptake; and (b) Hill coefficient for VTG production in liver. For these two parameters, convergence or mixing of the four Markov chains is achieved much earlier than the 6,500 iterations needed for all 20 parameters to converge. Summary statistics for posterior parameter values (the last 1000 parameter sets from each Markov chain for a total of 4000) are reported in Table 2.3. Two calibrated model parameters Kd_E2ER,brn, qChol,gon) had posterior 95% CIs slightly larger than their prior distribution 95% CIs; three calibrated parameters (k1_E2ER,brn, qLH,brn, qSTAR,gon) had similar prior and posterior 95% CIs; and 14 calibrated model parameters had posterior 95% CIs smaller than their prior distribution 95% CIs. One calibrated parameter, the variance of the natural logarithm of plasma E_2 concentration (Var_ Ln_CE2tot_pla_ngml), had a posterior 95% CI that did not overlap with the 95% CI of its prior distribution because its assigned prior distribution was based on plasma E_2 concentrations from unexposed control fish only. Values of the posterior distribution of Var_Ln_CE2tot_pla_ngml are consistent with the variance in the data used to calibrate with model, which include both unexposed control FHM and FHM injected with E_2 in Korte et al. (2000). That is, the variance of the natural logarithms of plasma E_2 concentrations used to calibrate the model is 15, and the posterior 95% CI is 7.3–12. In summary, model calibration with FHM data improved estimates of the majority of model parameters.

2.3.2 Model Evaluation

With the 4000 calibrated parameter sets, we simulated plasma concentrations of T, KT, E_2, and VTG in unexposed male FHMs. Table 2.4 compares model predictions with plasma concentrations of T, KT, E_2, and VTG measured in 73 unexposed (control) male

FHMs; data that were not used to calibrate the model. Model-predicted 95% CIs for T, KT, and E_2 fall within the measured 95% CI for each endpoint. The model-predicted 95% CI for VTG overlaps the measured 95% CI, but its lower bound is 80% that of the lower bound for the measured data. In unexposed FHMs, our model under-predicts the variance in the measured data.

We simulated plasma VTG concentrations of male FHMs exposed to 10 and 100 ng EE_2/L reported in Ekman et al. (2008) (Figure 2.3). Predicted plasma VTG concentrations followed the same general trend as the measured concentrations. However, although the model predictions appear to be leveling-off by day 16, they do not start to decrease on day 16 like the measured concentrations. For the 10 ng EE_2/L exposure, the 95% CI of predicted VTG concentrations encompassed the median concentration measured on all days. For the 100 ng EE_2/L exposure, the 95% upper confidence limit (or 97.5 percentile) of the simulated VTG concentrations was 1.4–2 times lower than the median measured plasma VTG concentration, except on day 16 where the median measured VTG concentration fell within the 95% CI. These results suggest that the model is useful for predicting plasma VTG responses for exposures up to 8 days, and up to 8 days post-exposure.

Figure 2.4 compares model predictions with experimental data for plasma VTG concentrations in male FHMs exposed to EE_2 for 14 days (Brian et al., 2005). Figure 2.4A compares the absolute values of plasma VTG concentration. It is obvious that model predictions captured the general trend of experimental data, although model-predicted plasma VTG concentration were constantly higher (1 to 5 orders of magnitude) than the measured data, presumably due to different methods used in VTG measurements (Korte et al., 2004). Figure 2.4B compared the percentages of VTG induction. Model-predicted dose-response curve was comparable to that generated from measured data, but slightly shifted to the left. For model predictions, EC50 was around 0.1 ng EE_2/L; while for the measured data, EC50 was around 0.6 ng EE_2/L.

Parks et al. (1999) reported that the plasma VTG concentration on the seventh day after three injections of E_2 over a period of 4 days was 21.3 ± 1.3 mg/ml. We used our

model and the 4000 calibrated parameter sets to simulate plasma VTG concentrations (mg VTG/ml) from Parks et al. (1999). Our simulations resulted in a mean = 29, standard deviation = 10 mg VTG/ml, median = 27.5 mg VTG/ml, and 95% CI = (14, 54). The predicted standard deviation in plasma VTG concentration was larger than the measured data, and all of the measured data were within the 95% CI of the model predictions. In this case, our model predicts the mean measured plasma VTG concentration well, but overpredicts the variance.

2.3.3 Model Predictions of Unmeasured Endpoints in Male FHMs Exposed to EE_2

As a demonstration of our model's hypothesis generating capability, we used it to simulate 48-h exposures to four EE_2 exposure concentrations: 5, 10, 50, and 100 ng EE_2/L. The predictions shown in Figure 2.5 are a result of our model formulation and calibration, and experimental data to evaluate these predictions are needed. For the four different exposure concentrations, plasma concentrations of E_2, T, KT, and VTG as a function of time were predicted (Figures 2.5A–D, respectively). Plasma concentrations of all three steroids are predicted to decrease as plasma EE_2 concentration (Figure 2.5E) increases. In contrast, plasma VTG concentrations are predicted to increase as plasma EE_2 concentration increases, and plasma VTG concentrations remain elevated compared with unexposed FHM levels for at least 2400 h (100 days).

In addition to the measured reproductive endpoints, our model can also predict a number of model endpoints that, to date, have not been measured in FHMs such as plasma LH concentration (Figure 2.5F), StAR protein concentration in gonads (Figure 2.5G), and liver ER concentration (Figure 2.5H). After exposure to EE_2, the plasma concentration of LH and the concentration of StAR in the gonads are predicted to decrease in a dose-dependent manner, whereas the concentration of ER in the liver increases in a dose-dependent manner. These predictions provide hypotheses that can be tested experimentally illustrating the value of this model in providing a better understanding of the HPG axis in male FHMs.

2.4 Discussion

2.4.1 Experimental Data

At first glance, experimental data from different studies suggest a large amount of variability, possibly due to different laboratory conditions, exposure designs, chemical analysis methods, or FHM cultures. Although the data from different studies may appear variable, after experimental differences such as exposure design have been accounted for, the data become much more consistent. A reliable computational model can be used to evaluate whether data from different studies are in fact consistent. For example, Garcia-Reyero et al. (2009) exposed adult male FHMs to nominal concentrations of 10 and 50 ng EE_2/L for 48 h, and measured plasma VTG concentrations using a monoclonal carp-based enzyme-linked immunosorbent assay (ELISA) (Hemming *et al.*, 2001). Garcia-Reyero et al. (2009) reported plasma concentrations of 13 and 29 mg VTG/ml, 48 h after the 10 and 50 ng EE_2/L exposures, respectively. Ekman et al. (2008) exposed FHMs to nominal concentrations of 10 and 100 ng EE_2/L for 8 days, and measured plasma VTG using a polyclonal FHM-based ELISA (Parks *et al.*, 1999). For the 10 and 100 ng EE_2/L exposures, Ekman et al. (2008) reported the following plasma VTG concentrations: on day 1, 1.2 and 8.7 mg VTG/ml, respectively; on day 4, 28 and 62 mg VTG/ml, respectively; and on day 8, 52 and 97 mg VTG/ml, respectively. For the 10 ng EE_2/L exposures from Garcia-Reyero et al. (2009) and Ekman et al. (2008) we found that our computational model fits both data sets well, and concluded that these results are consistent despite differences in measured water EE_2 test concentrations, exposure duration, and VTG analytical methods used in the two laboratories.

Another independent study by Brian et al. (2005) exposed male adult FHMs to several concentrations of EE_2 for 14 days, and measured the plasma VTG concentrations using a polyclonal carp-based ELISA. Generally, the plasma VTG concentrations are several orders of magnitude lower than those reported by Garcia-Reyero et al. (2009) and Ekman et al. (2008). For example, Brian et al. reported an average plasma concentration of 0.7 mg VTG/ml in FHMs exposed to 50 ng EE_2/L for 14 days, which is 40 fold lower than that in FHMs exposed to 50 ng EE_2/L for 48 hrs (Garcia-Reyero et al., 2009), and 74

fold lower than that in FHMs exposed to 10 ng EE_2/L for 8 days (Ekman et al., 2008). The significant difference may be caused by the polyclonal carp-based ELISA method used by Brian et al. (2005). A comparison between the ELISA methods using polyclonal carp and FHM antibodies was performed by Mylchreest et al (2003), and deep discussions were made between scientific groups using the two ELISA methods (Korte et al., 2004; Mylchreest et al., 2003; Tyler et al., 2004). These studies concluded that, in FHMs, the polyclonal FHM-based ELISA produced more accurate and reproducible measurements. Our model was calibrated using experimental data from Garcia-Reyero et al (2009), which agree with data measured using a polyclonal FHM ELISA by Ekman et al. (2008). As a result, it is not surprising that our model failed to predict the plasma VTG concentrations from Brian et al. (2005b) (Figure 2.4A).

The polyclonal carp-based ELISA has already been widely used and is still widely used to measure the plasma VTG concentrations in FHMs. Therefore, it is meaningful to find a way to compare the VTG concentrations measured by the two ELISA methods. In order to do this comparison, we calculated and compared the percentages of VTG induction for model predictions and experimental data (Figure 2.4B). Model-predicted EC50 was one sixth of the measured one (0.1 versus 0.6 ng EE_2/L). The difference may be caused by experimental conditions. For example, Brian et al. (2005b) used N,N-dimethylformamide as a carrier solvent, while Garcia-Reyero et al. (2009) and Ekman et al. (2008) did not use any chemical carrier. In addition, this might also be caused by the inaccurate EE_2 concentration in exposure water. As pointed out by Brian et al., they encountered some analytical problems, and did not obtain full sets of reliable data for EE_2 concentrations (2005b). As a result, we cannot conclude if the VTG induction effect reported by Brian et al is consistent with those reported by Garcia-Reyero et al. (2009) and Ekman et al. (2008). However, our attempt to compare the two data sets using percentage VTG induction is plausible, which suggests that the percentages of VTG induction should be useful in comparing the VTG induction effects measured using different ELISA methods.

2.4.2 Model Structure and Formulation

Many simplifying assumptions were made in formulating this computational model because many processes and parameter values are unknown for FHMs. There are too many to discuss them all in great detail, but in the following we discuss some of our assumptions that have alternative formulations.

In the brain, LH production is affected by E_2, which is formulated in our model as a positive feedback based on studies in other fishes where T and E_2 increased mRNA levels of LHβ subunit (Yaron *et al.*, 2003). In addition, Yaron et al. (2003) describe an ERE in the promoter region of the Chinook salmon LHβ gene which suggests that bound ER (E2-ER or EE2-ER) would be a more realistic quantity than free E_2 for positive feedback regulation of LH production. Such a modification to the model would allow all estrogenic chemicals (e.g., EE_2) to stimulate LH production in brain.

In vertebrates, E_2 production from T occurs in the brain and gonads catalyzed by the aromatase enzyme. Moreover, in teleost fishes, aromatase activity is relatively high in brain compared to gonads, and compared to brain aromatase in other vertebrate species (Callard *et al.*, 2001; Sawyer *et al.*, 2006), though E_2 production rates depend on the number of cells in the respective tissues. Our model resulted in E_2 production in brain at higher rates than in the testis. Calculations using fixed parameter values for BW (= 0.0041 kg), BW (= 3.8×10^{-5} kg), GW (= 5.5×10^{-5} kg), scaling coefficients of aromatase Vmax in brain and gonad ($sc\_Vmax_{aro,brn}$ = 1.05×10^{-2} nmol/h/mg protein and $sc\_Vmax_{aro,gon}$ = 2.3×10^{-3} nmol/h/mg protein, respectively), and the median calibrated concentrations of microsomal protein in brain (D_m_mp_brn = 500 mg protein/l) and gonad (D_m_mp_gon = 800 mg protein/l), we found E_2 production in brain to be twice as high as E_2 production in testis, 2.0×10^{-4} nmol/h and 1.0×10^{-4} nmol/h, respectively. This is consistent with studies in teleost fish that describe higher aromatase activity in brain compared to gonads (Callard *et al.*, 2001; Halm *et al.*, 2001; Sawyer *et al.*, 2006).

2.4.3 Model Calibration

The posterior parameter distributions obtained through model calibration depend upon values of the fixed parameters (Table 2.5), the prior parameter distributions (Table 2.3), and the measured reproductive endpoints (Table 2.1). In developing our model, we relied upon values based on data from other species (e.g., zebrafish, or Japanese medaka) and some in vitro studies because of the lack of FHM-specific data. It is important to note that the FHM is a small aquarium sized fish and an asynchronous spawner (i.e., multiple spawns in a season with oocytes present in all stages of maturation simultaneously in the gonads) as opposed to synchronous spawners (e.g., salmon, rainbow trout, or channel catfish) in which the oocytes more or less mature synchronously during a spawning season. Conditional upon the fixed model parameter values, we believe that our model and the calibrated model parameters provide a good representation of the HPG axis in FHMs. If FHM-specific values of our fixed model parameters were appreciably different from what we used in this modeling study, then the calibrated model parameters would probably have different values, but the physiologically based model as formulated could perform as well as shown here or better.

2.4.4 Model Evaluation

We evaluated our model's predictive ability by simulating EE_2 and E_2 laboratory experiments in FHMs from two studies (Ekman et al., 2008; Parks et al., 1999). In each of these studies, the exposure pattern of EE_2 or E_2 differed from the exposure patterns used to obtain the model calibration data. It is noteworthy that the model was able to accurately predict plasma VTG concentrations after an 8-day continuous exposure to a nominal concentration of 10 ng EE_2/L from Ekman et al. (2008) (Figure 2.3A). The model under-predicted all plasma VTG concentrations in FHM exposed to a nominal water concentration of 100 ng EE_2/L, but this exposure concentration is higher than either of the 48-hr exposure concentrations used to calibrate the model, and is therefore an extrapolation of the model's capability. For the Parks et al. (1999) study, three injections of E_2 were given at a higher dose than either of those used to calibrate the model. Thus, it is remarkable that the model-predicted plasma VTG concentrations encompass the

measured data. These results suggest that our model has captured the processes important for steroid hormone and VTG production in male FHMs.

A limitation of our model is that it significantly under-predicts variance in measured plasma steroid hormone and VTG concentrations for unexposed fish (Table 2.4), though it predicts median concentrations well. Interestingly, this is not the case for exposed fish. Indeed, the model tends to slightly over-predict variance in measured plasma VTG concentrations for fish exposed to EE_2 from Ekman et al. (2008) (Figure 2.3). Furthermore, the model significantly over-predicts variance in measured plasma VTG for fish exposed to E_2 from the Parks et al. (1999) study.

Perhaps this tendency of the model to under-predict variance in unexposed fish, and to over-predict variance in exposed fish is not surprising, given the nature of inter-individual variation that is often observed in molecular profiling studies for chemical exposures. Namely, researchers often find that inter-individual variation in measured values for controls is larger than that for exposed animals (Parsons *et al.*, 2008). For example, using ^1H nuclear magnetic resonance (NMR) spectroscopy for hepatic metabolite profiling, unexposed female fathead minnows were found to exhibit considerably more variation than females that were exposed to estrogenic compounds (Ekman *et al.*, 2006). This was attributed to unexposed fish being in different stages of the reproductive cycle. However, upon exposure, the reproductive status of the female fish was more homogenous, resulting in a more ‘‘focused’’ metabolic response. Beyond this specific example using female fish, this effect of focusing upon exposure appears to be quite common regardless of animal, gender or tissue/fluid type (Parsons *et al.*, 2008).

Indeed, we see a striking example of this focusing effect when examining lipid metabolite profiles of plasma samples from the same male FHMs used to evaluate this model (i.e., fish from Ekman et al, 2008). Figure 2.6 is a principle components analysis scores plot built from NMR spectra of the pool of plasma lipid metabolites from male FHMs sampled on day 4 of the exposure. Results are shown for unexposed controls and fish exposed to 100 ng EE_2/L. Although the metabolites measured here by NMR are not the same as those used in the model, it is clear that variability in metabolic status is much

greater in controls. Therefore, it is not unreasonable that the model (which does not account for this ill-defined change in variation) under-predicts variance in measurements from unexposed fish while over-predicting that for exposed fish.

The model described here utilizes data collected in a wide variety of species and postulates mathematical formulations for biological processes in the HPG axis of male FHMs. This study has shown that the model can predict plasma steroid hormone and VTG concentrations after exposures to E_2 or EE_2 through different routes (i.e., water or injection) and for different patterns of exposure. More experimental data are needed to evaluate model predictions of reproductive endpoints and other endpoints such as plasma LH concentration, StAR concentration in gonads, and ERα concentration in liver. Furthermore, measurements of other signaling molecules in the HPG axis (e.g., concentrations of follicle stimulation hormone, maturation inducing hormone, and receptors) would enable the extension of this model and allow it to better represent the HPG axis, and its regulation of reproduction.

The unique features of this model over previously developed models are (1) its ability to generate hypotheses about biological endpoints that may not have been measured, (2) the ability to simulate exposures to mixtures of EE_2 and E_2, and the capability to extend the model to simulate other estrogen exposures, and (3) most importantly, the ability to estimate CIs for all model predictions. In the context of toxicology and risk assessment, this model provides a framework for interpreting available FHM reproductive endpoint data and postulating a population of FHMs (i.e., this study provides a ‘‘population’’ of 4000 FHMs characterized by each set of 20 calibrated model parameters) that are represented by the measured data. Changes in reproductive endpoints as they relate to the ‘‘population’’ can then be assessed for new exposure conditions. Furthermore, with the appropriate modifications and initial conditions (e.g., plasma T, KT, and E_2 concentrations at birth), our model could be extended to simulate FHM early life stages.

2.5 Supplementary Information

2.5.1 General equations

In the physiologically based model, compartments were chosen to represent tissues that have an effect on the absorption, distribution, metabolism, and elimination of a compound or hormone of interest. Equations were formulated based upon a mass balance within each compartment (Figure 2.1). Equation 1 is a general form of a mass balance. The left side represents the rate of change of a chemical quantity in a compartment that is equal to the quantity of chemical that flows into the compartment minus the quantity of chemical removed from the compartment.

$$\frac{d(C_{i,j}V_j)}{dt} = F_j \mathrm{CArt}_i - F_j \frac{C_{i,j}}{\lambda_{i,j}} + \sum_i P_{i,j} - \sum_i R_{i,j} \quad (1)$$

where, $C_{i,j}$ (nmol/L) is the concentration of free compound i in compartment j (e.g., gill, brain, liver, gonad, venous blood, other); CArt_i (nmol/L) is the arterial blood concentration of free compound i; the concentration of free compound i in venous blood leaving compartment j is equal to $C_{i,j}/\lambda_{i,j}$, where $\lambda_{i,j}$ is the tissue to blood partition coefficient for free compound i in compartment j; V_j (L) is volume of compartment j; t (hr) is time; F_j (L/hr) is volumetric blood flow rate entering and leaving compartment j; $P_{i,j}$ (nmol/hr) is the rate of a reaction that produces free compound i in compartment j; $R_{i,j}$ (nmol/hr) is the rate of a reaction that consumes free compound i or an elimination process (e.g., hormone conjugation and excretion) of free compound i in compartment j.

Ligand-receptor binding is an important process in endocrine signaling, and in our model the process is simulated in compartments such as brain, liver, gonad, and venous blood. In brain, liver, and gonads, hormones (e.g., E_2, EE_2, T, and LH) assert their roles in HPG axis regulation by binding to their receptors. In blood, SBPs can associate and dissociate with steroid hormones, thus regulating their bioavailability and distribution among different tissues. Equation 2 is a general dynamic formulation of a ligand-receptor binding process.

$$\frac{d(C_{iR,j}V_j)}{dt} = k_{1\_iR,j}C_{i,j}C_{R,j}V_j - K_{d\_iR,j}k_{1\_iR,j}C_{iR,j}V_j \quad (2)$$

where $C_{iR,j}$ (nmol/L) is the concentration of the complex of compound *i* bound to its receptor *R* in compartment *j*; $k_{1\_iR,j}$ (1/nM/hr) is the association rate of compound *i* with its receptor in compartment *j*; $C_{R,j}$ (nmol/L) is the concentration of unbound receptor in compartment *j*; $K_{d\_iR,j}$ (nmol/L) is the equilibrium dissociation rate constant of compound *i* with its receptor in compartment *j*. The term $k_{1\_iR,j}C_{i,j}C_{R,j}V_j$ (nmol/hr) is the production rate of compound *i* bound to its receptor, which corresponds to $P_{i,j}$ in equation 1; the term $K_{d\_iR,j}k_{1\_iR,j}C_{iR,j}V_j$ (nmol/hr) is the dissociation rate of the ligand-receptor complex, which corresponds to $R_{i,j}$ in equation 1.

The total concentration of compound *i* in compartment *j* is calculated as a sum of the concentration of free compound *i* and compound *i* bound to its receptor in compartment *j*, as shown in equation 3; where the $C_{itot,j}$ represents the total concentration of compound *i* in compartment *j*.

$$C_{itot,j} = C_{i,j} + C_{iR,j} \quad (3)$$

2.5.2 Equations in the Gill compartment

In this study, male FHMs were exposed to EE_2 in aquarium water. To allow the model to reach a steady-state prior to a simulated EE_2 exposure, we simulated the EE_2 exposure starting from 3600 hrs using a PerDose function in MCSim software (equation 4). In equation 4, $C_{EE2,H20}$ (nmol/L) is the concentration of EE_2 in aquarium water as a function of time; 'Mag_{EE2}' (nmol/L) is the EE_2 concentration in aquarium water; 'Per_{EE2}' (hr) represents the period for a repeated dose. For a continuous exposure, Per_{EE2} is set to the total simulation time; '$IniT_{EE2}$' (hr) is the time when EE_2 exposure starts (e.g. 3600 hrs); and '$ExpT_{EE2}$' (hr) represents the exposure duration (Figure 2.7).

$$C_{EE2,H2O} = \text{PerDose}\ (Mag_{EE2}, Per_{EE2}, IniT_{EE2}, ExpT_{EE2}) \quad (4)$$

Equation 5 is the mass balance equation for the gill compartment, which involves flows of EE_2 into the compartment from the surrounding aquatic environment and from venous blood.

$$\frac{d(V_{gil}C_{EE2gil})}{dt} = FW_{gil}(C_{EE2H2O} - C_{EE2exp}) + F_{car}(C_{EE2ven} - CArt_{EE2}) \quad (5)$$

where, V_{gil} (L) is the volume of the gills; $C_{EE2,gil}$ (nmol/L) is the concentration of EE_2 in the gills; FW_{gil} (L/hr) is the volumetric flow rate of water through the gills; $C_{EE2,Exp}$ (nmol/L) is the concentration of EE_2 in the expired water, which is equal to $CArt_{EE2}$ divided by $\lambda_{EE2,bld,}$ the blood to water partition coefficient for free EE_2; F_{car} (L/hr) is cardiac output; $C_{EE2,ven}$ (nmol/L) is the concentration of EE_2 in the venous blood; and $CArt_{EE2}$ (nmol/L) is the concentration of EE_2 in the arterial blood, which is equal to . In our model, we assumed that the gills act only as permeable membranes and do not accumulate EE_2 (Nichols *et al.*, 1996). Therefore, the left side of equation 5 was set to zero (equation 6).

$$0 = FW_{gil}(C_{EE2,H2O} - C_{EE2,exp}) + F_{car}(C_{EE2,ven} - CArt_{EE2}) \quad (6)$$

2.5.3 Equations in the Brain compartment

Luteinizing hormone is produced in brain in response to GnRH. We did not have measurements of GnRH, and hence assumed a diurnal cycle of LH production based upon a similar assumption by Murphy *et al.* (2005). That is, the background production of LH in brain was simulated as a periodic cycle. The 'PerDose' function in MCSim was used as shown below:

$$P_{LH,brn} = \text{PerDose}\ (Mag_{LH}, Per_{LH}, IniT_{LH}, ExpT_{LH}) \quad (7)$$

where $P_{LH,brn}$ (nmol/hr) is the input rate of LH in compartment brain as a function of time; 'Mag_{LH}' (nmol/hr) is the input magnitude of LH; 'Per_{LH}' (hr) is the period of one cycle of LH production (set as 24 hrs); '$IniT_{LH}$' (hr) is the time when LH production starts in one cycle (set as 0 hr); and '$ExpT_{LH}$' (hr) is the duration of LH production in one cycle (set as 12 hrs). In our model, LH production began at time '$IniT_{LH}$' (set as 0 hr) in the period 'Per_{LH}' (set as 24 hrs) and lasts for '$ExpT_{LH}$' (set as 12 hrs) (Figure 2.8).

An increase in LH production based on the quantity of free E_2 in brain was formulated by making the LH production rate directly proportional to the quantity of free E_2 in brain as shown in equation 8. In the equation, $P'_{LH,brn}$ (nmol/hr) is the production

rate of LH caused by free E_2 in brain; $\rho_{LH,brn}$ (1/hr) is a first order rate constant for LH production induced by free E_2 in brain; $C_{E2,brn}$ (nmol/L) is the concentration of free E_2 in brain; V_{brn} (L) is the volume of brain.

$$P'_{LH,brn} = \rho_{LH,brn} \times C_{E2,brn} \times V_{brn} \tag{8}$$

The production of E_2 from T in brain is catalyzed by brain P450 aromatase enzyme (Zhao *et al.*, 2001). Studies in teleost fishes (Callard et al., 2001; Halm et al., 2001; Sawyer et al., 2006) have found higher levels of aromatase mRNA expression in brain than in ovaries or testes. Moreover, mRNA levels are a reliable predictor of functional protein (Sawyer *et al.*, 2006). In our model, E_2 production from T in brain was formulated using a Michaelis-Menten kinetic equation.

$$P_{E2,brn} = \frac{Vmax_{aro,brn} C_{T,brn}}{Km_{aro,brn} + C_{T,brn}} \tag{9}$$

where, $P_{E2,brn}$ (nmol/hr) is the production rate of E_2 in brain; $Vmax_{aro,brn}$ (nmol/hr) is the maximum production rate of E_2 by brain aromatase; $Km_{aro,brn}$ (nmol/L) is the Michaelis-Menten constant of brain aromatase for E_2 production; $C_{T,brn}$ (nmol/L) is the concentration of T in brain.

2.5.4 Equations in the Gonad compartment

The concentration of StAR in gonads was formulated as being directly proportional to the concentration of bound LH.

$$C_{StAR,gon} = \rho_{StAR,gon} \times C_{LHLR,gon} \tag{10}$$

where, $C_{StAR,gon}$ (nmol/L) is the concentration of StAR in gonads; $C_{LHLR,gon}$ (nmol/L) is the concentration of bound LH in gonads; $\rho_{StAR,gon}$ is the ratio of the concentration of StAR to the concentration of bound LH in gonads.

The concentration of cholesterol in gonads was formulated as being directly proportional to the concentration of StAR.

$$C_{\text{Chol,gon}} = \rho_{\text{Chol,gon}} \times C_{\text{StAR,gon}} \tag{11}$$

where, $C_{\text{Chol,gon}}$ (nmol/L) is the concentration of cholesterol in gonads; $\rho_{\text{Chol,gon}}$ is the ratio of the concentration of cholesterol to the concentration of StAR.

The production of T was formulated using a Hill equation. The substrate for T production is cholesterol, and the synthesis of T from cholesterol is a complicated process involving a cascade of multiple intermediate reactions (Halm et al., 2002; Nagahama et al., 1995; Senthilkumaran et al., 2004). In the model, we simplified the complex process of T production from cholesterol by lumping the multiple reactions into one "effective" reaction (Murphy *et al.*, 2005), which was formulated as a Hill equation.

$$P_{\text{T gon}} = \frac{\text{Vmax}_{\text{Scc,gon}} C_{\text{Cholgon}}^{n_T}}{K_{0.5\text{Sccgon}}^{n_T} + C_{\text{Cholgon}}^{n_T}} \tag{12}$$

where, $P_{\text{T,gon}}$ (nmol/hr) is the production rate of T in gonads; $\text{Vmax}_{\text{Scc,gon}}$ (nmol/hr) is the effective maximum production rate of T in gonads; $K_{0.5\text{Scc,gon}}$ (nmol/L) is the concentration of cholesterol which gives a production rate equal to half of the $\text{Vmax}_{\text{Scc,gon}}$; and n_T is a Hill coefficient for T production.

The inhibition of T production by bound estrogen receptor (ER) was formulated as a noncompetitive process (equation 13). In the equation, $P_{\text{T gon}}^{I}$ (nmol/hr) is the production rate of T after inhibition; $C_{\text{E2ER,gon}}$ (nmol/L) is the concentration of ER bound to E_2; $C_{\text{EE2ER,gon}}$ (nmol/L) is the concentration of ER bound to EE_2; and K_{T} (nmol/L) is the inhibition factor.

$$P_{\text{T,gon}}^{I} = \frac{P_{\text{T,gon}}}{1 + \dfrac{(C_{\text{E2ER,gon}} + C_{\text{EE2ER,gon}})}{K_{\text{T}}}} \tag{13}$$

The production of E_2 in gonads was formulated using a Michaelis-Menten kinetic equation (equation 14). The substrate for E_2 production is T, and the process is catalyzed by gonad aromatase.

$$P_{\mathrm{E2,gon}} = \frac{\mathrm{Vmax}_{\mathrm{aro,gon}} C_{\mathrm{T,gon}}}{\mathrm{Km}_{\mathrm{aro,gon}} + C_{\mathrm{T,gon}}} \tag{14}$$

In equation 14, $P_{\mathrm{E2,\ gon}}$ (nmol/hr) is the production rate of E_2 in gonad; $\mathrm{Vmax}_{\mathrm{aro,gon}}$ (nmol/hr) is the maximum production rate of E_2 by gonad aromatase; $\mathrm{Km}_{\mathrm{aro,gon}}$ (nmol/L) is the Michaelis-Menten constant of gonad aromatase for E_2 production; $C_{\mathrm{T,gon}}$ (nmol/L) is the concentration of T in gonads.

The production of KT in gonads was formulated using a Michaelis-Menten kinetic equation (equation 15). The substrate for KT production is T, and the process is catalyzed by 11β-HSD (Ge *et al.*, 1997).

$$P_{\mathrm{KT,gon}} = \frac{\mathrm{Vmax}_{\mathrm{11bHSD,gon}} C_{\mathrm{T,gon}}}{\mathrm{Km}_{\mathrm{11bHSD,gon}} + C_{\mathrm{T,gon}}} \tag{15}$$

In equation 15, $P_{\mathrm{KT,gon}}$ (nmol/hr) is the production rate of KT in gonads; $\mathrm{Vmax}_{\mathrm{11bHSD,gon}}$ (nmol/hr) is the maximum production rate of KT by 11β-HSD; $\mathrm{Km}_{\mathrm{11bHSD,gon}}$ (nmol/L) is the Michaelis-Menten constant of 11β-HSD for KT production.

2.5.5 Equations in the Liver compartment

In liver, an ER self-regulation process was simulated. When E_2-ER or EE_2-ER combine to form a dimer, the dimer binds to EREs on the regulation sequence of the ER gene, and stimulates ER protein synthesis. We assumed a background production rate of ER based on published experiments in rainbow trout hepatocytes (Flouriot et al., 1997; Flouriot et al., 1996) which showed that when E_2 concentration was 0, ER mRNA was present at a low level. When ERs are produced, some ERs will again bind to E_2 or EE_2, while some ERs will be subject to degradation. The mass balance for the whole process is listed in equation 16.

$$\begin{aligned} \frac{d(C_{\mathrm{ER,liv}} V_{\mathrm{liv}})}{dt} = {} & \mathrm{Pbg}_{\mathrm{ER,liv}} V_{\mathrm{liv}} + k_{\mathrm{ER,liv}} (C_{\mathrm{E2ER\_liv}} + C_{\mathrm{EE2ER\_liv}}) V_{\mathrm{liv}} \\ & - (k_{\mathrm{1\_EE2ER,liv}} C_{\mathrm{EE2,liv}} C_{\mathrm{ER,liv}} - K_{\mathrm{d\_EE2ER,liv}} k_{\mathrm{1\_EE2ER,liv}} C_{\mathrm{EE2ER,liv}}) V_{\mathrm{liv}} \\ & - (k_{\mathrm{1\_E2ER,liv}} C_{\mathrm{E2,liv}} C_{\mathrm{ER,liv}} - K_{\mathrm{d\_E2ER,liv}} k_{\mathrm{1\_E2ER,liv}} C_{\mathrm{E2ER,liv}}) V_{\mathrm{liv}} \\ & - \mathrm{kelim}_{\mathrm{ER,liv}} C_{\mathrm{ER,liv}} V_{\mathrm{liv}} \end{aligned} \tag{16}$$

where, $C_{ER,liv}$ (nmol/L) is the free ER concentration in liver; $Pbg_{ER,liv}$ (nmol//L/hr) is the background production rate of ER in liver; V_{liv} (L) is the volume of liver; $k_{ER,liv}$ (1/hr) is the induction rate constant for ER production by E_2-ER or EE_2-ER complexes; C_{E2ER_liv} (nmol/L) is the concentration of E_2-ER complex in liver; C_{EE2ER_liv} (nmol/L) is the concentration of EE_2-ER complex in liver; $kelim_{ER,liv}$ (1/hr) is the elimination rate constant for free ER; the term $(k_{1\_EE2ER,liv}C_{EE2,liv}C_{ER,liv} - K_{d\_EE2ER,liv}k_{1\_EE2ER,liv}C_{EE2ER,liv})V_{liv}$ represents the rate of ER binding to EE_2; $(k_{1\_E2ER,liv}C_{E2,liv}C_{ER,liv} - K_{d\_E2ER,liv}k_{1\_E2ER,liv}C_{E2ER,liv})V_{liv}$ represents the rate of ER binding to E_2; $kelim_{ER,liv}C_{ER,liv}V_{liv}$ is the rate of free ER elimination in liver.

In our model, another process regulated by E_2-ER and EE_2-ER is VTG production in liver. When E_2-ER or EE_2-ER combine to form a dimer, the dimer binds to EREs on the regulation sequence of VTG gene, and stimulates the synthesis of VTG protein. In our model, we assumed that the VTG production process could be simulated using a Hill equation dependent upon the concentration of bound ER (E_2–ER or EE_2–ER complexes).

$$P_{Vtg,liv} = \frac{Vmax_{Vtg,liv}(C_{E2ER,liv} + C_{EE2ER,liv})^{n_{vtg}}}{K_{0.5Vtg,liv}^{n_{Vtg}} + (C_{E2ER,liv} + C_{EE2ER,liv})^{n_{Vtg}}} \quad (17)$$

where $P_{Vtg,liv}$ (nmol/hr) is the production rate of VTG in liver; $Vmax_{Vtg,liv}$ (nmol/hr) is the maximum production rate of VTG in liver; $K_{0.5Vtg,liv}$ (nmol/L) is the concentration of bound ER which gives a production rate equal to half of the $Vmax_{Vtg,liv}$; and n_{Vtg} is Hill coefficient for VTG production.

To compare our model predicted total liver concentration of EE_2 to measured experimental data, we calculated the total concentration of EE_2 in dry liver tissue as shown in equation 18:

$$C_{EE2tot,liv\_dry\_ngg} = (C_{EE2,liv} + C_{EE2ER,liv}) \times Conv_{EE2,nmol/L\_ngg} \div 0.3 \quad (18)$$

where, $C_{EE2tot,liv\_dry\_ng/g}$ is the total EE_2 concentration in dry liver tissue (ng EE_2 /g dry liver tissue); $C_{EE2,liv}$ is the concentration of free EE_2 in wet liver tissue (nmol EE_2 / L wet

liver tissue); $C_{EE2ER,liv}$ is the concentration of EE_2 bound to estrogen receptor in wet liver tissue (nmol EE_2ER complex /L wet liver tissue), and $Conv_{EE2,nmol/L\_ng/g}$ (= 0.296) is a constant to convert EE_2 from nmol/L to ng/g. To convert wet liver tissue EE_2 concentration to dry liver tissue EE_2 concentration, a conversion factor (= 0.3) is used since approximately 70% of liver tissue is water, and after being dried only 30% of the original tissue mass remains.

2.5.6 Equations in the Other compartment

The elimination of EE_2, E_2, T, KT, VTG, and LH from the "other" tissue compartment was assumed to follow first order reaction kinetics (equation 19).

$$R_{i,\text{oth}} = k_{i,\text{oth}} C_{i,\text{oth}} V_{\text{oth}} \tag{19}$$

where $R_{i,\text{oth}}$ (nmol/hr) is the elimination rate of free compound *i* (e.g., EE_2, E_2, T, KT, VTG, LH) in the "other" compartment; $k_{i,\text{oth}}$ (1/hr) is the elimination rate constant for free compound *i* in the "other" compartment; $C_{i,\text{oth}}$ (nmol/L) is the concentration of the free compound *i* in the "other" compartment; and V_{oth} (1/L) is the volume of the "other" compartment;.

The E_2 injection experiments in the "other" compartment were simulated using a PerDose function (equation 20); where $P_{E2,\text{oth}}$ (nmol/hr) is the injection rate of E_2 in the "other' compartment as a function of time; 'Mag_{E2}'(nmol/hr) is the injection magnitude of E_2; 'Per_{E2}' (hr) is the whole period of one E_2 injection experiment; '$IniT_{E2}$' (hr) is the time when E_2 injection starts in one experiment; and '$ExpT_{E2}$' (hr) is the E_2 injection time in one experiment (set as 2 seconds). The equation 20 describes that E_2 injection begins at time '$IniT_{E2}$' in the period 'Per_{E2}' and lasts for '$ExpT_{E2}$' (2 seconds) time units (Figure 2.9).

$$P_{E2,\text{oth}} = \text{PerDose}\ (Mag_{E2},\ Per_{E2},\ IniT_{E2},\ ExpT_{E2}) \tag{20}$$

To compare our model predicted total concentration of EE_2 in carcass to measured experimental data, we calculated the total concentration of EE_2 in dry carcass as shown in equation 21:

$$C_{EE2tot,car\_dry\_ng/g} = C_{EE2,oth} \times Conv_{EE2,nmol/L\_ng/g} \div 0.3 \quad (21)$$

where, $C_{EE2tot,car\_dry\_ng/g}$ is the total EE_2 concentration in dry carcass (ng EE_2 /g dry carcass); $C_{EE2,oth}$ is the concentration of free EE_2 in wet carcass (nmol EE_2 /L wet carcass) (We did not include any estrogen receptor in the 'other' tissue in our model, and all EE_2 in the 'other' tissue are free EE_2); and $Conv_{EE2,nmol/L\_ng/g}$ (=0.296) is a constant to convert EE_2 from nmol/L to ng/g. To convert wet carcass EE_2 concentration to dry carcass EE_2 concentration, a conversion factor (= 0.3) is used since approximately 70% of carcass tissue is water, and after being dried only 30% of the original tissue mass remains.

2.5.7 Equations in the Venous Blood compartment

In the compartment of venous blood, we simulated the association and dissociation processes of E_2 and T to SBPs. SBPs in the blood can bind to steroid hormones, serving as a reservoir and regulating the bioavailability and distribution of steroid hormones to other tissues. The general formulation of the processes was described in equation 2.

The total concentration of E_2 in venous blood was calculated as free E_2 concentration plus the SBP-bound E_2 concentration, as shown in equation 3. In a same way, we calculated the total T concentration in venous blood.

The total concentrations of E_2 and T in plasma were calculated using equation 22.

$$C_{itot,plasma\_ng/ml} = (C_{i,ven} + C_{iSBP,ven}) \div frc_{plasma\_venous} \times Conv_{i,nmol/L\_ng/ml} \quad (22)$$

where, $C_{itot,plasma\_ng/ml}$ is the total concentration of chemical *i* in plasma (ng chemical *i* /ml plasma, and *i* can be E_2 or T); $C_{i,ven}$ is the concentration of free chemical *i* in venous blood (nmol chemical *i* /L venous blood); C_{iSBP_ven} is the concentration of chemical *i* bound to SBP in venous blood (nmol chemical *i*-SBP complex /L venous blood); frc_{plasma_venous} is the fraction of plasma to blood by volume; $Conv_{i,nmol/L\_ng/ml}$ is a conversion constant for chemical *i* (for E_2, its value is 0.272; for T, its value is 0.288) to convert from nmol/L to ng/mL.

2.5.8 Assumptions for Arterial blood

In arterial blood, we set the concentrations of both free and bound compound *i* equal to those in venous blood compartment, unless there is a water exposure of compound *i*. When a water exposure of compound *i* presents, we use equation 6 to calculate the concentration of free compound *i* in arterial blood.

2.5.9 Differential equation list

Brain

$$\frac{d(C_{\mathrm{EE2ER,brn}})}{dt} = k_{1\_\mathrm{EE2ER,brn}} C_{\mathrm{EE2,brn}} C_{\mathrm{ER,brn}} - K_{\mathrm{d\_EE2ER,brn}} k_{1\_\mathrm{EE2ER,brn}} C_{\mathrm{EE2ER,brn}}$$

$$\frac{d(C_{\mathrm{E2ER,brn}})}{dt} = k_{1\_\mathrm{E2ER,brn}} C_{\mathrm{E2,brn}} C_{\mathrm{ER,brn}} - K_{\mathrm{d\_E2ER,brn}} k_{1\_\mathrm{E2ER,brn}} C_{\mathrm{E2ER,brn}}$$

$$\frac{d(C_{\mathrm{LH,brn}} V_{\mathrm{brn}})}{dt} = F_{\mathrm{brn}}(\mathrm{CArt}_{\mathrm{LH}} - C_{\mathrm{LH,brn}}) + \rho_{\mathrm{LH,brn}} C_{\mathrm{E2,brn}} V_{\mathrm{brn}} + \mathrm{PerDose}(\mathrm{Mag}_{\mathrm{LH}}, \mathrm{Per}_{\mathrm{LH}}, \mathrm{IniT}_{\mathrm{LH}}, \mathrm{ExpT}_{\mathrm{LH}})$$

$$\frac{d(C_{\mathrm{T,brn}} V_{\mathrm{brn}})}{dt} = F_{\mathrm{brn}}(\mathrm{CArt}_{\mathrm{T}} - \frac{C_{\mathrm{T,brn}}}{\lambda_{\mathrm{T,brn}}}) - \frac{\mathrm{Vmax}_{\mathrm{aro,brn}} C_{\mathrm{T,brn}}}{\mathrm{Km}_{\mathrm{aro,brn}} + C_{\mathrm{T,brn}}}$$

$$\frac{d(C_{\mathrm{KT,brn}} V_{\mathrm{brn}})}{dt} = F_{\mathrm{brn}}(\mathrm{CArt}_{\mathrm{KT}} - \frac{C_{\mathrm{KT,brn}}}{\lambda_{\mathrm{KT,brn}}})$$

$$\frac{d(C_{\mathrm{E2,brn}} V_{\mathrm{brn}})}{dt} = F_{\mathrm{brn}}(\mathrm{CArt}_{\mathrm{E2}} - \frac{C_{\mathrm{E2,brn}}}{\lambda_{\mathrm{E2,brn}}}) + \frac{\mathrm{Vmax}_{\mathrm{aro,brn}} C_{\mathrm{T,brn}}}{\mathrm{Km}_{\mathrm{aro,brn}} + C_{\mathrm{T,brn}}} - V_{\mathrm{brn}}(k_{1\_\mathrm{E2ER,brn}} C_{\mathrm{E2,brn}} C_{\mathrm{ER,brn}} - K_{\mathrm{d\_E2ER,brn}} k_{1\_\mathrm{E2ER,brn}} C_{\mathrm{E2ER,brn}})$$

$$\frac{d(C_{\mathrm{Vtg,brn}} V_{\mathrm{brn}})}{dt} = F_{\mathrm{brn}}(\mathrm{CArt}_{\mathrm{Vtg}} - C_{\mathrm{Vtg,brn}})$$

$$\frac{d(C_{\mathrm{EE2,brn}} V_{\mathrm{brn}})}{dt} = F_{\mathrm{brn}}(\mathrm{CArt}_{\mathrm{EE2}} - \frac{C_{\mathrm{EE2,brn}}}{\lambda_{\mathrm{EE2,brn}}}) - V_{\mathrm{brn}}(k_{1\_\mathrm{EE2ER,brn}} C_{\mathrm{EE2,brn}} C_{\mathrm{ER,brn}} - K_{\mathrm{d\_EE2ER,brn}} k_{1\_\mathrm{EE2ER,brn}} C_{\mathrm{EE2ER,brn}})$$

Gonad

$$\frac{d(C_{\mathrm{LHLR,gon}})}{dt} = k_{1\_\mathrm{LHLR,gon}} C_{\mathrm{LH,gon}} C_{\mathrm{LR,gon}} - K_{\mathrm{d\_LHLR,gon}} k_{1\_\mathrm{LHLR,gon}} C_{\mathrm{LHLR,go}}$$

$$\frac{d(C_{\mathrm{EE2ER,gon}})}{dt} = k_{1\_\mathrm{EE2ER,go}} C_{\mathrm{EE2,gon}} C_{\mathrm{ER,gon}} - K_{\mathrm{d\_EE2ER,go}} k_{1\_\mathrm{EE2ER,go}} C_{\mathrm{EE2ER,go}}$$

$$\frac{d(C_{\mathrm{E2ER,gon}})}{dt} = k_{1\_\mathrm{E2ER,gon}} C_{\mathrm{E2,gon}} C_{\mathrm{ER,gon}} - K_{\mathrm{d\_E2ER,gon}} k_{1\_\mathrm{E2ER,gon}} C_{\mathrm{E2ER,go}}$$

$$\frac{d(C_{\mathrm{LH,gon}} V_{\mathrm{gon}})}{dt} = F_{\mathrm{gon}}(\mathrm{CArt}_{\mathrm{LH}} - C_{\mathrm{LH,gon}}) - V_{\mathrm{gon}}(k_{1\_\mathrm{LHLR,gon}} C_{\mathrm{LH,gon}} C_{\mathrm{LR,gon}} - K_{\mathrm{d\_LHLR,gon}} k_{1\_\mathrm{LHLR,gon}} C_{\mathrm{LHLR,gon}})$$

$$\frac{d(C_{\mathrm{T,gon}} V_{\mathrm{gon}})}{dt} = F_{\mathrm{gon}}(\mathrm{CArt}_{\mathrm{T}} - \frac{C_{\mathrm{T,gon}}}{\lambda_{\mathrm{T,gon}}}) - \frac{\mathrm{Vmax}_{\mathrm{11bHSD,gon}} C_{\mathrm{T,gon}}}{\mathrm{Km}_{\mathrm{11bHSD,gon}} + C_{\mathrm{T,gon}}} - \frac{\mathrm{Vmax}_{\mathrm{aro,gon}} C_{\mathrm{T,gon}}}{\mathrm{Km}_{\mathrm{aro,gon}} + C_{\mathrm{T,gon}}}$$

$$+ \frac{\mathrm{Vmax}_{\mathrm{Scc,gon}} C_{\mathrm{Chol,gon}}^{n_{\mathrm{T}}}}{\mathrm{K}_{0.5\mathrm{Scc,gon}}^{n_{\mathrm{T}}} + C_{\mathrm{Chol,gon}}^{n_{\mathrm{T}}}} \div (1 + \frac{C_{\mathrm{E2ER,gon}} + C_{\mathrm{EE2ER,gon}}}{K_{\mathrm{T}}})$$

$$\frac{d(C_{\mathrm{KT,gon}} V_{\mathrm{gon}})}{dt} = F_{\mathrm{gon}}(\mathrm{CArt}_{\mathrm{KT}} - \frac{C_{\mathrm{KT,gon}}}{\lambda_{\mathrm{KT,gon}}}) + \frac{\mathrm{Vmax}_{\mathrm{11bHSD,gon}} C_{\mathrm{T,gon}}}{\mathrm{Km}_{\mathrm{11bHSD,gon}} + C_{\mathrm{T,gon}}}$$

$$\frac{d(C_{\mathrm{E2,gon}} V_{\mathrm{gon}})}{dt} = F_{\mathrm{gon}}(\mathrm{CArt}_{\mathrm{E2}} - \frac{C_{\mathrm{E2,gon}}}{\lambda_{\mathrm{E2,gon}}}) + \frac{\mathrm{Vmax}_{\mathrm{aro,gon}} C_{\mathrm{T,gon}}}{\mathrm{Km}_{\mathrm{aro,gon}} + C_{\mathrm{T,gon}}}$$

$$- V_{\mathrm{gon}}(k_{1\_\mathrm{E2ER,gon}} C_{\mathrm{E2,gon}} C_{\mathrm{ER,gon}} - K_{\mathrm{d\_E2ER,gon}} k_{1\_\mathrm{E2ER,gon}} C_{\mathrm{E2ER,gon}})$$

$$\frac{d(C_{\mathrm{Vtg,gon}} V_{\mathrm{gon}})}{dt} = F_{\mathrm{gon}}(\mathrm{CArt}_{\mathrm{Vtg}} - C_{\mathrm{Vtg,gon}})$$

$$\frac{d(C_{\mathrm{EE2,gon}} V_{\mathrm{gon}})}{dt} = F_{\mathrm{gon}}(\mathrm{CArt}_{\mathrm{EE2}} - \frac{C_{\mathrm{EE2,gon}}}{\lambda_{\mathrm{EE2,gon}}}) - V_{\mathrm{gon}}(k_{1\_\mathrm{EE2ER,gon}} C_{\mathrm{EE2,gon}} C_{\mathrm{ER,gon}} - K_{\mathrm{d\_EE2ER,gon}} k_{1\_\mathrm{EE2ER,gon}} C_{\mathrm{EE2ER,gon}})$$

Liver

$$\frac{d(C_{\mathrm{ER,liv}})}{dt} = \mathrm{Pbg}_{\mathrm{ER,liv}} + k_{\mathrm{ER,liv}}(C_{\mathrm{E2ER\_liv}} + C_{\mathrm{EE2ER\_liv}}) - (k_{1\_\mathrm{EE2ER,liv}} C_{\mathrm{EE2,liv}} C_{\mathrm{ER,liv}} - K_{\mathrm{d\_EE2ER,liv}} k_{1\_\mathrm{EE2ER,liv}} C_{\mathrm{EE2ER,liv}})$$

$$- (k_{1\_\mathrm{E2ER,liv}} C_{\mathrm{E2,liv}} C_{\mathrm{ER,liv}} - K_{\mathrm{d\_E2ER,liv}} k_{1\_\mathrm{E2ER,liv}} C_{\mathrm{E2ER,liv}}) - \mathrm{kelim}_{\mathrm{ER,liv}} C_{\mathrm{ER,liv}}$$

$$\frac{d(C_{\mathrm{EE2ER,liv}})}{dt} = k_{1\_\mathrm{EE2ER,liv}} C_{\mathrm{EE2,liv}} C_{\mathrm{ER,liv}} - K_{\mathrm{d\_EE2ER,liv}} k_{1\_\mathrm{EE2ER,liv}} C_{\mathrm{EE2ER,li}}$$

$$\frac{d(C_{\mathrm{E2ER,liv}})}{dt} = k_{1\_\mathrm{E2ER,liv}} C_{\mathrm{E2,liv}} C_{\mathrm{ER,liv}} - K_{\mathrm{d\_E2ER,liv}} k_{1\_\mathrm{E2ER,liv}} C_{\mathrm{E2ER,li}}$$

$$\frac{d(C_{\mathrm{LH,liv}} V_{\mathrm{liv}})}{dt} = F_{\mathrm{liv}}(\mathrm{CArt}_{\mathrm{LH}} - C_{LH,liv})$$

$$\frac{d(C_{\mathrm{T,liv}} V_{\mathrm{liv}})}{dt} = F_{\mathrm{liv}}(\mathrm{CArt}_{\mathrm{T}} - \frac{C_{\mathrm{T,liv}}}{\lambda_{\mathrm{T,liv}}})$$

$$\frac{d(C_{\mathrm{KT,liv}} V_{\mathrm{liv}})}{dt} = F_{\mathrm{liv}}(\mathrm{CArt}_{\mathrm{KT}} - \frac{C_{\mathrm{KT,liv}}}{\lambda_{\mathrm{KT,liv}}})$$

$$\frac{d(C_{\mathrm{E2,liv}} V_{\mathrm{liv}})}{dt} = F_{\mathrm{liv}}(\mathrm{CArt}_{\mathrm{E2}} - \frac{C_{\mathrm{E2,liv}}}{\lambda_{\mathrm{E2,liv}}}) - V_{\mathrm{liv}}(k_{1\_\mathrm{E2ER,liv}} C_{\mathrm{E2,liv}} C_{\mathrm{ER,liv}} - K_{\mathrm{d\_E2ER,liv}} k_{1\_\mathrm{E2ER,liv}} C_{\mathrm{E2ER,liv}})$$

$$\frac{d(C_{\mathrm{Vtg,liv}}V_{\mathrm{liv}})}{dt} = F_{\mathrm{liv}}(\mathrm{CArt}_{\mathrm{Vtg}} - C_{\mathrm{Vtg,liv}}) + \frac{\mathrm{Vmax}_{\mathrm{Vtg,liv}}(C_{\mathrm{E2ER,liv}} + C_{\mathrm{EE2ER,liv}})^{n_{\mathrm{Vtg}}}}{\mathrm{K}_{0.5\mathrm{Vtg,liv}}^{n_{\mathrm{Vtg}}} + (C_{\mathrm{E2ER,liv}} + C_{\mathrm{EE2ER,liv}})^{n_{\mathrm{Vtg}}}}$$

$$\frac{d(C_{\mathrm{EE2,liv}}V_{\mathrm{liv}})}{dt} = F_{\mathrm{liv}}(\mathrm{CArt}_{\mathrm{EE2}} - \frac{C_{\mathrm{EE2,liv}}}{\lambda_{\mathrm{EE2,liv}}}) - V_{\mathrm{liv}}\,(k_{1\_\mathrm{EE2ER,liv}}C_{\mathrm{EE2,liv}}C_{\mathrm{ER,liv}} - K_{\mathrm{d\_EE2ER,liv}}k_{1\_\mathrm{EE2ER,liv}}C_{\mathrm{EE2ER,liv}})$$

Other

$$\frac{d(C_{\mathrm{LH,oth}}V_{\mathrm{oth}})}{dt} = F_{\mathrm{oth}}(\mathrm{CArt}_{\mathrm{LH}} - C_{\mathrm{LH,oth}}) - \mathrm{kelim}_{\mathrm{LH,oth}}C_{\mathrm{LH,oth}}V_{\mathrm{oth}}$$

$$\frac{d(C_{\mathrm{T,oth}}V_{\mathrm{oth}})}{dt} = F_{\mathrm{oth}}(\mathrm{CArt}_{\mathrm{T}} - \frac{C_{\mathrm{T,oth}}}{\lambda_{\mathrm{T,oth}}}) - \mathrm{kelim}_{\mathrm{T,oth}}C_{\mathrm{T,oth}}V_{\mathrm{oth}}$$

$$\frac{d(C_{\mathrm{KT,oth}}V_{\mathrm{oth}})}{dt} = F_{\mathrm{oth}}(\mathrm{CArt}_{\mathrm{KT}} - \frac{C_{\mathrm{KT,oth}}}{\lambda_{\mathrm{KT,oth}}}) - \mathrm{kelim}_{\mathrm{KT,oth}}C_{\mathrm{KT,oth}}V_{\mathrm{oth}}$$

$$\frac{d(C_{\mathrm{E2,oth}}V_{\mathrm{oth}})}{dt} = F_{\mathrm{oth}}(\mathrm{CArt}_{\mathrm{E2}} - \frac{C_{\mathrm{E2,oth}}}{\lambda_{\mathrm{E2,oth}}}) - \mathrm{kelim}_{\mathrm{E2,oth}}C_{\mathrm{E2,oth}}V_{\mathrm{oth}} + \mathrm{PerDose}(\mathrm{Mag}_{\mathrm{E2}}, \mathrm{Per}_{\mathrm{E2}}, \mathrm{IniT}_{\mathrm{E2}}, \mathrm{ExpT}_{\mathrm{E2}})$$

$$\frac{d(C_{\mathrm{Vtg,oth}}V_{\mathrm{oth}})}{dt} = F_{\mathrm{oth}}(\mathrm{CArt}_{\mathrm{Vtg}} - C_{\mathrm{Vtg,oth}}) - \mathrm{kelim}_{\mathrm{Vtg,oth}}C_{\mathrm{Vtg,oth}}V_{\mathrm{oth}}$$

$$\frac{d(C_{\mathrm{EE2,oth}}V_{\mathrm{oth}})}{dt} = F_{\mathrm{oth}}(\mathrm{CArt}_{\mathrm{EE2}} - \frac{C_{\mathrm{EE2,oth}}}{\lambda_{\mathrm{EE2,oth}}}) - \mathrm{kelim}_{\mathrm{EE2,oth}}C_{\mathrm{EE2,oth}}V_{\mathrm{oth}}$$

Venous blood

$$\frac{d(C_{\mathrm{E2SBP,ven}})}{dt} = k_{1\_\mathrm{E2SBP,ven}}C_{\mathrm{E2,ven}}C_{\mathrm{SBP,ven}} - K_{\mathrm{d\_E2SBP,ven}}k_{1\_\mathrm{E2SBP,ven}}C_{\mathrm{E2SBP,ven}}$$

$$\frac{d(C_{\mathrm{TSBP,ven}})}{dt} = k_{1\_\mathrm{TSBP,ven}}C_{\mathrm{T,ven}}C_{\mathrm{SBP,ven}} - K_{\mathrm{d\_TSBP,ven}}k_{1\_\mathrm{TSBP,ven}}C_{\mathrm{TSBP,ven}}$$

$$\frac{d(C_{\mathrm{E2,ven}}V_{\mathrm{ven}})}{dt} = F_{\mathrm{oth}}\frac{C_{\mathrm{E2,oth}}}{\lambda_{\mathrm{E2,oth}}} + F_{\mathrm{liv}}\frac{C_{\mathrm{E2,liv}}}{\lambda_{\mathrm{E2,liv}}} + F_{\mathrm{brn}}\frac{C_{\mathrm{E2,brn}}}{\lambda_{\mathrm{E2,brn}}} + F_{\mathrm{gon}}\frac{C_{\mathrm{E2,gon}}}{\lambda_{\mathrm{E2,gon}}} - F_{\mathrm{car}}C_{\mathrm{E2,ven}}$$
$$- V_{\mathrm{ven}}(k_{1\_\mathrm{E2SBP,ven}}C_{\mathrm{E2,ven}}C_{\mathrm{SBP,ven}} - K_{\mathrm{d\_E2SBP,ven}}k_{1\_\mathrm{E2SBP,ven}}C_{\mathrm{E2SBP,ven}})$$

$$\frac{d(C_{\mathrm{T,ven}}V_{\mathrm{ven}})}{dt} = F_{\mathrm{oth}}\frac{C_{\mathrm{T,oth}}}{\lambda_{\mathrm{T,oth}}} + F_{\mathrm{liv}}\frac{C_{\mathrm{T,liv}}}{\lambda_{\mathrm{T,liv}}} + F_{\mathrm{brn}}\frac{C_{\mathrm{T,brn}}}{\lambda_{\mathrm{T,brn}}} + F_{\mathrm{gon}}\frac{C_{\mathrm{T,gon}}}{\lambda_{\mathrm{T,gon}}} - F_{\mathrm{car}}C_{\mathrm{T,ven}}$$
$$- V_{\mathrm{ven}}(k_{1\_\mathrm{TSBP,ven}}C_{\mathrm{T,ven}}C_{\mathrm{SBP,ven}} - K_{\mathrm{d\_TSBP,ven}}k_{1\_\mathrm{TSBP,ven}}C_{\mathrm{TSBP,ven}})$$

$$C_{\mathrm{LH,ven}}V_{\mathrm{ven}} = F_{\mathrm{oth}}C_{\mathrm{LH,oth}} + F_{\mathrm{liv}}C_{\mathrm{LH,liv}} + F_{\mathrm{brn}}C_{\mathrm{LH,brn}} + F_{\mathrm{gon}}C_{\mathrm{LH,gon}}$$

$$C_{\mathrm{VTG,ven}}V_{\mathrm{ven}} = F_{\mathrm{oth}}C_{\mathrm{VTG,oth}} + F_{\mathrm{liv}}C_{\mathrm{VTG,liv}} + F_{\mathrm{brn}}C_{\mathrm{VTG,brn}} + F_{\mathrm{gon}}C_{\mathrm{VTG,gon}}$$

$$C_{\mathrm{EE2,ven}}V_{\mathrm{ven}} = F_{\mathrm{oth}}\frac{C_{\mathrm{EE2,oth}}}{\lambda_{\mathrm{EE2,oth}}} + F_{\mathrm{liv}}\frac{C_{\mathrm{EE2,liv}}}{\lambda_{\mathrm{EE2,liv}}} + F_{\mathrm{brn}}\frac{C_{\mathrm{EE2,brn}}}{\lambda_{\mathrm{EE2,brn}}} + F_{\mathrm{gon}}\frac{C_{\mathrm{EE2,gon}}}{\lambda_{\mathrm{EE2,gon}}}$$

$$C_{\mathrm{KT,ven}}V_{\mathrm{ven}} = F_{\mathrm{oth}}\frac{C_{\mathrm{KT,oth}}}{\lambda_{\mathrm{KT,oth}}} + F_{\mathrm{liv}}\frac{C_{\mathrm{KT,liv}}}{\lambda_{\mathrm{KT,liv}}} + F_{\mathrm{brn}}\frac{C_{\mathrm{KT,brn}}}{\lambda_{\mathrm{KT,brn}}} + F_{\mathrm{gon}}\frac{C_{\mathrm{KT,gon}}}{\lambda_{\mathrm{KT,gon}}}$$

Arterial blood

$$\mathrm{CArt}_{\mathrm{E2}} = C_{\mathrm{E2,ven}}$$

$$\mathrm{CArt}_{\mathrm{E2SBP}} = C_{\mathrm{E2SBP,ven}}$$

$$\mathrm{CArt}_{\mathrm{T}} = C_{\mathrm{T,ven}}$$

$$\mathrm{CArt}_{\mathrm{TSBP}} = C_{\mathrm{TSBP,ven}}$$

$$\mathrm{CArt}_{\mathrm{LH}} = C_{\mathrm{LH,ven}}$$

$$\mathrm{CArt}_{\mathrm{VTG}} = C_{\mathrm{VTG,ven}}$$

$$\mathrm{CArt}_{\mathrm{KT}} = C_{\mathrm{KT,ven}}$$

$$\mathrm{CArt}_{\mathrm{EE2}} = \frac{\mathrm{FW}_{\mathrm{gil}} \times C_{\mathrm{EE2,H2O}} + F_{\mathrm{car}} \times C_{\mathrm{EE2,ven}}}{F_{\mathrm{car}} + \dfrac{\mathrm{FW}_{\mathrm{gil}}}{\lambda_{\mathrm{EE2,bld}}}}$$

CHAPTER 3

A Computational Model of the Hypothalamic – Pituitary – Gonadal Axis in Female FHMs Exposed to EE_2 and TB

Adapted from a manuscript in preparation: Li Z., Kroll K., Jensen K., Villeneuve D., Ankley G., Ekman D., Collette T., Brian J., Sepulveda M., Orlando E., Lazorchak J., Kostich M., Armstrong B., Denslow N., Watanabe K.

3.1 Introduction

Besides estrogenic EDCs (e.g., EE_2 and E_2), androgenic EDCs (e.g., TB) have also been found in the aquatic environment, and are known to affect fish reproduction. TB is a relatively stable metabolic product of trenbolone acetate, a synthetic androgen used as a growth promoter in livestock (e.g., cattle). TB enters the environment mainly as runoff from livestock feedlots. Schiffer et al. (2001) reported that the TB concentration in effluents of solid cattle dung was around 19 ng/L. Durhan et al. (2006) studied a cattle feedlot located in southwest central Ohio, and reported that the TB concentration in feedlot discharge was between 10 and 20 ng/L. TB has a high binding affinity for the AR. Exposure to TB at concentrations similar to those found in the environment decreases egg production in FHM in conjunction with changes in plasma concentrations of E_2, T, and VTG in females (Ankley et al., 2003). Interestingly, concentration-response relationships for the alterations in E_2, T and VTG were not monotonic, exhibiting a "U-shaped" nature (Ankley et al., 2003).

To better understand the dynamics of the HPG axis in female FHMs and to evaluate risks of both estrogenic and androgenic EDC exposure, we developed a

physiologically based computational model to simulate key reproductive endpoints, such as plasma concentrations of E_2, T, and VTG, in unexposed, TB-, or EE_2-exposed adult female FHMs. The model simulates absorption, distribution, and elimination of TB and EE_2, and converts their concentrations in exposure water to tissue concentrations. Through taking into account physiological characteristics of FHMs, the model predicts reproductive endpoints through modeling biochemical pathways and reactions. After being calibrated using MCMC simulations, the model predicted independent experimental data well. For more than 80% of the simulation results, the 95% CIs of model predictions encompassed the median of the experimental data. We concluded that the physiologically-based computational model represents the HPG axis in adult female FHM robustly. The model would be useful to estimate how estrogens (e.g., EE_2) or androgens (e.g., TB) affect plasma concentrations of E_2, T and VTG, which are important determinants of fecundity in fish.

3.2 Materials and methods

3.2.1 Experimental Data

To calibrate model parameters and to evaluate model predictions, we used data from unexposed, TB-exposed, and EE_2-exposed adult female FHMs from 18 different studies. For each fish, physiological parameters, including BW, gonadosomatic index (GSI), and hepatosomatic index (HSI), were input into the model. For all experimental data used in model calibration or validation, when any measurements of BW, GSI, or HSI were missing, we used the medians of measured BW, GSI, or HIS, respectively (Watanabe et al., 2007).

From Watanabe et al. (2007), we obtained reproductive endpoint data in unexposed (control) adult female FHMs. Watanabe et al. (2007) summarized the data in unexposed adult female FHMs from experiments conducted at the USEPA Duluth laboratory from 1999 to 2006. All (or a subset of) reproductive endpoints such as plasma E_2, T, and VTG concentrations were measured in a total of 170 unexposed adult female FHMs. We randomly split the data; the first 75 records were used to calibrate our model; the remaining 95 records were used in model validation.

Experimental data from TB exposed adult female FHMs were obtained from three studies: (i) a flow-through water exposure to nominal concentrations of 0.005, 0.05, 0.5, 5.0, and 50 µg TB/L for 21 days by Ankley et al. (2003); (ii) a static exposure to nominal concentrations of 0.05, 0.5, 5 µg TB/L for 48 hours by Garcia-Reyero et al. (2009); and (iii) a flow-through water exposure to nominal concentrations of 0.05 and 0.5 µg TB/L in adult female FHMs for eight days, followed by an eight-day depuration described by Ekman et al. (in review). In Ankley et al. (2003), 12 female FHMs were exposed in each treatment group. On the 21st day of exposure, all FHMs were sacrificed; plasma concentrations of E_2, T, and VTG were measured in each fish. In Garcia-Reyero et al. (2009) eight FHMs were exposed in each treatment group. After a 48-hour exposure, the fish were sacrificed. For each treatment group, plasma E_2 concentrations were measured in each of four fish, and plasma VTG concentrations were measured in the four remaining fish. In Ekman et al. (in review), 64 FHMs were exposed to TB in each treatment group. On the 1st, 2nd, 4th, and 8th day of exposure, for each treatment group, eight FHMs were sacrificed to measure plasma E_2 and VTG concentrations in each fish; on the 1st, 2nd, 4th, and 8th day of depuration (test days 9, 10, 12, and 16), for each treatment group, eight of the remaining 32 FHMs were sacrificed to measure plasma E_2 concentrations. Data from Ankley et al. (2003) were used to calibrate our model, and data from Garcia-Reyero et al (2009) and Ekman et al. (in review) were used to evaluate our model predictions.

VTG plasma concentrations in adult female FHMs exposed to EE_2 were obtained from three studies: (i) a flow-through water exposure to nominal concentrations of 10 or 100 ng EE_2/L in adult female FHMs for eight days, followed by an eight-day depuration (Ekman et al., 2008); (ii) a flow-through water exposure to a nominal concentration of 0.5, 1.5, and 4.5 ng EE_2/L in adult female FHMs for 21 days by Lazorchak et al. (manuscript in preparation); and (iii) a flow-through water exposure to a nominal concentration of 1.5 ng EE_2/L in adult female FHMs for 21 days by Brian et al. (2007). In Ekman et al. (2008)for each treatment group and each sampling time, eight FHMs were sacrificed to measure plasma VTG concentration in each fish. Sampling occurred on the 1st, 4th, and 8th day of exposure to EE_2, and the 8th day of EE_2 depuration (test day

16). In Lazorchak et al. (manuscript in preparation), 28 FHMs in each of the 0.5, 1.5, and 4.5 ng EE_2/L treatment groups were sacrificed to measure plasma VTG concentration in each fish on the 21st day. In Brian et al. (2007), four FHMs were sacrificed to measure plasma VTG concentration in each fish on the 21st day after exposure to 1.5 ng EE_2/L. As opposed to the three TB and other EE_2 studies which did not use carrier solvents, Brian et al. (2007) used N,N-dimethylformamide (DMF) as a chemical carrier for EE_2. Data from Ekman et al. (2007) were used to calibrate our model, and data from Lazorchak et al. (manuscript in preparation), and Brian et al. (2007) were used to evaluate our model predictions.

3.2.2 Model Formulation

We developed the HPG axis model for adult female FHM by modifying a computational model for male FHM described by Watanabe et al. (2009). In the following, we mainly focus on the unique formulations and/or assumptions in this model for adult female FHMs.

The model for female FHMs contains six tissue compartments which represent organs or tissues important for absorption, distribution, metabolism, and elimination of exogenous and endogenous chemicals of interest (Figure 3.1). The six compartments are gill, brain, gonad, liver, venous blood and "other". In arterial blood, for each chemical of interest, we set its concentrations in both free and bound forms equal to those in venous blood compartment, unless there is a water exposure of the chemical. When a water exposure of a chemical presents, we use equation 2 (see below) to calculate the concentration of the chemical in free form in arterial blood.

Based upon a mass balance for each chemical of interest, a set of coupled ordinary differential equations were formulated in each compartment following the principles of physiologically based pharmacokinetic modeling. A detailed description of the differential equations can be found in Section 3.5 Supplementary Information.

In brain, gonad, and liver compartments, we simulated both ER and AR dynamics. The AR component was not included in the model for male FHM published by

Watanabe et al. (2009). ER binds estrogens (e.g., E_2 and EE_2), and bound ER affects the production of VTG. AR binds androgens (e.g., T and TB), and subsequently regulates biochemical processes such as the production of gonadotropins (Heinlein and Chang, 2002). A general mathematical formulation of ligand-receptor binding is shown in Equation 1.

$$\frac{d(C_{\mathrm{iR},j}V_j)}{dt} = k_{1\_\mathrm{iR},j}C_{i,j}C_{R,j}V_j - K_{\mathrm{d\_iR},j}k_{1\_\mathrm{iR},j}C_{\mathrm{iR},j}V_j \quad (1)$$

where, $C_{\mathrm{iR},j}$ (nmol/L) is the concentration of compound i (e.g. T, TB, E_2 and EE_2) bound to its receptor in compartment j (e.g. brain, liver, gonad, and venous blood) ; V_j (L) is the volume of compartment j; $k_{1\_\mathrm{iR},j}$ (1/nM/hr) is the association rate constant of compound i with its receptor in compartment j; $C_{i,j}$ (nmol/L) is the concentration of free compound i in compartment j; $C_{R,j}$ (nmol/L) is the concentration of unbound receptor of compound i in compartment j; $K_{\mathrm{d\_iR},j}$ (nmol/L) is the equilibrium dissociation constant of compound i with its receptor in compartment j.

Gill. In this model, female FHMs can be exposed to TB and/or EE_2 in water, and the gill compartment is where the exogenous chemicals are absorbed. The concentration of each chemical in test water was represented as a function of time. Then, equilibrium partitioning was assumed, and the FHM arterial blood concentration was calculated from the water concentration using an equilibrium partition coefficient assigned for each chemical (Eq. 2). In addition, we assumed that the gill compartment did not accumulate any exogenous chemicals, nor did it express any genes related to the HPG axis (e.g., *vtg*, *er*, *ar*, and *lh*). Although *vtg* genes are transcribed in the gills of adult male FHMs exposed to EE_2, the transcription level is relatively low compared to that in the liver (Lattier et al., 2002). Furthermore, we do not have enough quantitative information to simulate any gene expression in FHM gills. As a result, in our model no hormone or protein is produced in the gill compartment.

$$\mathrm{CArt}_i = \frac{\mathrm{FW}_{\mathrm{gil}} \times C_{i,\mathrm{H20}} + F_{\mathrm{car}} \times \mathrm{CVen}_i}{\frac{\mathrm{FW}_{\mathrm{gil}}}{\lambda_{i,\mathrm{bld}}} + F_{\mathrm{car}}} \quad (2)$$

In equation 2, $\mathrm{FW}_{\mathrm{gil}}$ (L/hr) is the volumetric flow rate of water through the gills; $C_{i,\mathrm{H20}}$ (nmol/L) is the concentration of exogenous chemical *i* (e.g. TB and EE_2) in exposure water as a function of time; CArt_i (nmol/L) is the concentration of exogenous chemical *i* in arterial blood; $\lambda_{i,\mathrm{bld}}$ is the partition coefficient of exogenous chemical *i* between blood and water; F_{car} (L/hr) is cardiac output; and CVen_i (nmol/L) is the concentration of exogenous chemical *i* in venous blood.

Brain. In the brain compartment, three key assumptions were made: (i) the down-regulation of luteinizing hormone synthesis by bound AR; (ii) the up-regulation of LH synthesis by bound ER; (iii) the down-regulation of AR synthesis by free androgens.

In the brain, androgens have negative feedback on the synthesis and release of GnRH (Villeneuve et al., 2007), which in turn controls the synthesis of gonadotropins. To investigate how androgens may regulate GnRH, we searched for an ARE in the promoter regions of *gnrh* genes. Due to a lack of information on gene promoter sequences in FHM, we conducted the search in zebrafish (*Danio rerio*), a cyprinid fish closely related to FHM. We found that *gnrh* promoters contain several ARE half sites (tgttct) (Verrijdt et al., 2003). Thus, we postulated that androgens have a negative control on GnRH synthesis mainly through bound AR. However, we did not have any measurements of GnRH in FHM and GnRH was not included in the model, so we formulated a down-regulation of LH synthesis by bound AR in the model.

In our model, we also assumed an up-regulation of LH synthesis by bound ER in the brain compartment. The assumption was based upon observations of EREs in the promoter region of the *lh* gene and reports of estrogen stimulated LH production in fish (Yaron et al., 2003).

Equation 3 shows LH production rate in the brain compartment as a function of bound AR and ER. In the equation, $P_{\mathrm{LH,brn}}$ (nmol/hr) is the production rate of LH in brain; $P_{\mathrm{b\_LH,brn}}$ (nmol/hr) is the background production rate of LH in brain, which was formulated as a diurnal cycle; $C_{\mathrm{ER\_bd,brn}}$ (nmol/L) is the total concentration of bound ER in brain, which equals the sum of E_2- and EE_2- bound ER concentrations; $\rho_{\mathrm{u\_LH,brn}}$ (nmol/L) is an induction factor for LH production by bound ER; $C_{\mathrm{AR\_bd,brn}}$ (nmol/L) is the total concentration of bound AR in brain, which equals the sum of T- and TB- bound AR concentrations ; $\rho_{\mathrm{d\_LH,brn}}$ (nmol/L) is a factor for inhibition of LH production by bound AR.

$$P_{\mathrm{LH,brn}} = P_{\mathrm{b\_LH,brn}} \times \frac{1+\dfrac{C_{\mathrm{ER\_bd,brn}}}{\rho_{\mathrm{u\_LH,brn}}}}{1+\dfrac{C_{\mathrm{AR\_bd,brn}}}{\rho_{\mathrm{d\_LH,brn}}}} \tag{3}$$

The brain compartment is also very important for the regulation of AR production (Burgess and Handa, 1993; Kumar and Thakur, 2004). In mammals (e.g. rats, mice, and human), AR mRNA in brain is down-regulated by androgens, such as T and dihydrotestosterone (DHT) (Burgess and Handa, 1993; Kumar and Thakur, 2004), though little is known about the corresponding mechanisms. We searched for AREs in the promoter region of the *ar* gene in zebrafish, but did not find any match. Hence, we postulated that the down-regulation of AR mRNA by androgens is associated with a non-genomic pathway (Foradori et al., 2008), or associated with cell factors other than the soluble AR simulated in our model (Burnstein, 2005). Thus, we assumed a down-regulation of AR production by free androgens in the brain compartment. When ARs are produced, some bind androgens, some remain unbound, and others degrade. Based upon a mass balance for free AR, Equation 4 describes the processes of AR production, association and disassociation with T or TB, and degradation.

$$\frac{d(C_{\text{AR\_free,brn}})}{dt} = \frac{\text{Pbg}_{\text{AR,brn}}}{1+\frac{(C_{T,\text{brn}}+C_{\text{TB,brn}})}{K_{\text{AR,brn}}}} - (k_{\text{1\_TAR,brn}} \times C_{T,\text{brn}} \times C_{\text{AR\_free,brn}} - K_{\text{d\_TAR,brn}} \times k_{\text{1\_TAR,brn}} \times C_{\text{TAR,brn}}) - (k_{\text{1\_TBAR,brn}} \times C_{\text{TB,brn}} \times C_{\text{AR\_free,brn}} - K_{\text{d\_TBAR,brn}} \times k_{\text{1\_TBAR,brn}} \times C_{\text{TBAR,brn}}) - k_{\text{e\_AR,brn}} \times C_{\text{AR\_free,brn}} \quad (4)$$

where, $C_{\text{AR\_free,brn}}$ (nmol/L) is the free AR concentration in brain; $\text{Pbg}_{\text{AR,brn}}$ (nmol//L/hr) is the background production rate of AR in brain; $C_{T,\text{brn}}$ (nmol/L) is the free T concentration in brain; $C_{\text{TB,brn}}$ (nmol/L) is the free TB concentration in brain; $K_{\text{AR,brn}}$ (nmol/L) is an inhibition rate constant for AR production by free T and TB; $k_{\text{1\_TAR,brn}}$ (1/nM/hr) is the association rate constant for T and AR; $\text{K}_{\text{d\_TAR,brn}}$ (nM) is the disassociation rate constant for T bound to AR; $C_{\text{TAR,brn}}$ (nmol/L) is the concentration of the T-AR complex in brain; $k_{\text{1\_TBAR,brn}}$ (1/nM/hr) is the association rate of TB to AR; $\text{K}_{\text{d\_TBAR,brn}}$ (nM) is the disassociation rate constant for TB bound to AR; $C_{\text{TBAR,brn}}$ (nmol/L) is the concentration of the TB-AR complex in brain; and $k_{\text{e\_AR,brn}}$ (1/hr) is the elimination rate for free AR. We included the inhibition of LH by bound AR and the inhibition of AR by free androgens to account for the U-shaped concentration-response curves for E_2, T and VTG observed in female FHMs exposed to TB (Ankley et al., 2003).

Gonad. In the gonad compartment, in addition to the model formulations for male FHMs, we simulated two more processes: (i) absorption of VTG into oocytes; and (ii) up-regulation of E_2 production by bound LH. The absorption of VTG into oocytes was formulated as a first order kinetic process. VTG is synthesized in the liver (Flouriot et al., 1997), and circulates to the gonads where it is taken up via receptor-mediated endocytosis into oocytes, and then processed into yolk proteins (Nagahama et al., 1995). Although the molecular mechanism of VTG uptake is known, we did not have data to describe this process quantitatively. As a result, a first order kinetic equation with an assumed first order rate constant was formulated to represent the process (Eq. 5).

$$R_{\text{VTG,gon}} = k_{\text{VTG,gon}} \times C_{\text{VTG,gon}} \times V_{\text{gon}} \quad (5)$$

where, $R_{\text{VTG,gon}}$ (nmol/hr) is the absorption rate of VTG into oocytes in the gonad

compartment; $k_{VTG,gon}$ (1/hr) is the absorption rate constant for VTG into oocytes in the gonad compartment; $C_{VTG,gon}$ (nmol/L) is the concentration of VTG in the gonad compartment; and V_{gon} (1/L) is the volume of the gonad compartment.

Secondly, we simulated an up-regulation of E_2 production by bound LH in the gonad compartment. It was observed that LH stimulates the activity and gene expression of aromatase in the gonads of teleosts (Kagawa et al., 2003). In our model, we formulated the regulation of E_2 production as being proportional to the concentration of bound LH in the gonad compartment (Eq. 6).

$$P_{E2,gon} = \frac{\rho_{E2\_LHLRgon} \times C_{LHLRgon} \times \mathrm{Vmax}_{aro,gon} \times C_{T,gon}}{\mathrm{Km}_{aro,gon} + C_{T,gon}} \quad (6)$$

where, $P_{E2,\,gon}$ (nmol/hr) is the rate of E_2 production; $\rho_{E2\_LHLR,gon}$ (1/nM) is an induction factor of E_2 production by bound LH; $C_{LHLR,gon}$ (nM) is the concentration of bound LH; $\mathrm{Vmax}_{aro,gon}$ (nmol/hr) is the maximum rate of E_2 production by gonad aromatase; $\mathrm{Km}_{aro,gon}$ (nmol/L) is the Michaelis-Menten constant for gonad aromatase; $C_{T,gon}$ (nmol/L) is the concentration of T.

Liver. In the liver compartment, formulations including ER auto-regulation and bound-ER-stimulated VTG production are the same as those described by Watanabe et al. (2009), except that we added the ligand-receptor binding of T and TB to the AR.

Venous blood. Besides E_2 and T, we simulated the association and disassociation processes of EE_2 to SBPs in the venous blood compartment. There is contradictory information about the binding affinity (BA) of EE_2 to SBPs in fish. Compared to E_2, some fish species such as channel catfish (*Ictalurus punctatus*) and zebrafish (*Danio rerio*) have high BAs of EE_2 to SBPs (Gale et al., 2004; Miguel-Queralt and Hammond, 2008), while other fish species such as Arctic charr (*Salvelinus alpinus*) have a low BA (Tollefsen et al., 2004). To date, BA measurements of EE_2 to SBPs in FHM have not been made. Watanabe et al. (2009) did not include the binding process of EE_2 to SBPs in blood. In their modeling work for male FHMs, the total concentration of SBPs was

defined as 20 nM (Teeguarden and Barton, 2004), a relatively low value which would have little effect on free plasma EE_2 concentration or model performance. However, the blood SBP concentration in females is naturally higher than that in males, and in our model for female FHMs we defined the total concentration of SBPs as 400 nM (Laidley and Thomas, 1994; Teeguarden and Barton, 2004). Consequently, a large amount of EE_2 could be bound by SBPs in blood, which would affect the total concentration of EE_2 in the plasma. Therefore, we included the binding process of EE_2 to SBPs in this model, and formulated it using Equation 1.

Other. All tissues except for those defined as compartments above (i.e., Gill, Brain, Liver, and Gonad) are defined as 'Other' compartment. In our model, the 'Other' compartment is where elimination of exogenous and endogenous chemicals and proteins occur. Besides E_2, EE_2, T, VTG, and LH (included in Watanabe et al. (2009)), we added a first order kinetic equation to describe the elimination of TB, and the first order elimination rate constant was assumed to be the same as that of EE_2 (Eq. 7).

$$R_{\mathrm{TB,oth}} = k_{\mathrm{e\_TB,oth}} \times C_{\mathrm{TB,oth}} \times V_{\mathrm{oth}} \tag{7}$$

where $R_{\mathrm{TB,oth}}$ (nmol/hr) is the elimination rate of TB in the Other compartment; $k_{\mathrm{e\_TB,oth}}$ (1/hr) is the elimination rate constant for TB in the Other compartment; $C_{\mathrm{TB,oth}}$ (nmol/L) is the concentration of TB in the Other compartment; and V_{oth} (1/L) is the volume of the Other compartment.

3.2.3 Model Calibration

In total, our model contains 123 input parameters, such as volume and blood flow rates of each compartment, chemical equilibrium partition coefficients, ligand-receptor association and disassociation rate constants, and kinetic rate constants for each biochemical reaction. The parameters were fixed with known values, or calibrated using experimental data collected in adult female FHMs. In total, 97 model parameters were fixed with values obtained from published literature or measured for this study (Table 3.1). The remaining 26 model parameters were calibrated using MCMC simulation (Bois

et al., 1996b; Gelman et al., 1995; Lin et al., 2004; Watanabe et al., 2005), which requires the definition of prior distributions for each parameter being calibrated.

Of the 26 calibrated model parameters, 17 were sensitive model parameters with little or no information available in the open literature (Table 3.2). Vague prior distributions were used for these 17 model parameters. For example, we could not find a published value for the dissociation constant of E_2 binding to ER in FHM brain specifically ($K_{d\_E2ER,\ brn}$). Denny et al. (2005) reported that the dissociation constant of E_2 binding in female FHM liver cytosol is 8.6 nM. As a result, we assigned a lognormal distribution with a geometric mean of 8.6 and a geometric standard deviation of three, which corresponds to a coefficient of variation equal to 1.5. When no data were available in the open literature, we assigned a uniform or log-uniform prior distribution with a large range bounded by biological plausibility. For example, there were no published data for the blood to water TB partition coefficient ($\lambda_{TB,\ bld}$). But, we knew that the EE_2 partition coefficient for blood to water is around 300 (Watanabe et al., 2009). Therefore, we assigned a log-uniform distribution with a lower bound of one and an upper bound of 1000.

The remaining nine parameters were the variances of prediction errors for plasma E_2, T, and VTG concentrations in unexposed, TB-exposed, and EE_2-exposed FHMs. We assumed that our model predictions followed a lognormal distribution with the model prediction as the geometric mean. The variance of the assumed lognormal distribution was estimated by grouping the experimental data from unexposed, TB-exposed, and EE_2-exposed FHM into three different levels, and the error variances of the three reproductive endpoints for each group were estimated respectively (Bois et al., 1996b; Lin et al., 2004). For each of the nine error variances, we assigned an Inverse Gamma prior distribution based upon a natural logarithm transformation of the measured plasma E_2, T and VTG concentrations (Watanabe et al., 2009).

To perform the MCMC simulations, we used MCSim (Bois and Maszle, 1997), a software package freely available online (http://directory.fsf.org/math/mcsim.html). Four independent Markov chains with random seeds were run for 20,000 iterations. For

each of the four chains, we saved the last 10,000 iterations, and extracted one out of every 10. For each calibrated parameter, convergence was evaluated using the 1,000 iterations from each chain for all 26 calibrated parameters. A potential scale reduction method (Gelman et al., 1995) was used to compare the variances between and within the four chains. Potential scale reduction values between 1.0 and 1.2 were used as convergence criteria.

3.2.4 Model Evaluation

We evaluated the predictive ability of our model by simulating reproductive endpoints (i.e., plasma concentrations of E_2, T, or VTG) from independent studies. The 1,000 iterations thinned from the last 10,000 iteration calibrated model parameters of the four chains were pooled, and the 4,000 sets of parameter values were treated as a pool of adult female FHMs. We randomly sampled *n* (number of fish in a study) parameter sets to represent the *n* fish used in the study, and simulated the reproductive endpoints measured for each fish. The detailed simulation procedures followed the methods described by Watanabe et al. (2009).

After completing *n* simulations for a study, for each reproductive endpoint, we added the predictive error back based upon our lognormal error model. As described in the Model Calibration section, variances of predictive errors were estimated during model calibration. Using the model prediction and the estimated variance as two parameters, we randomly sampled from the lognormal distribution for each endpoint in each fish. The sampled values were compared with experimental measurements.

3.2.5 Prediction of Unmeasured Reproductive Endpoints

To observe the EDC effects on unmeasured components of the HPG axis (e.g., ER, AR, and LH), and to observe the effects on reproductive endpoints by a mixture of TB and EE_2, we did three extra simulations. We simulated liver ER concentration, brain AR concentration, and plasma E_2, T, VTG, and LH concentrations as a function of time in adult female FHMs exposed to 15 ng TB/L, 10 ng EE_2/L, or a mixture of 15 ng TB /L and 10 ng EE_2/L for 48 hours respectively. The concentrations of TB and EE_2 were set as 15

ng TB/L and 10 ng EE_2/L respectively, because they are environmentally relevant concentrations (Durhan et al., 2006; Ericson et al., 2002b; Schiffer et al., 2001). In all three simulations, we used the reported (Watanabe et al., 2007) median body weight, GSI, and HSI values in adult female FHMs as input parameters.

3.3 Results and Discussion

3.3.1 Model Calibration

A good fit of the experimental data was obtained by running four Markov chains using the MCMC simulations. For the 26 calibrated model parameters, the four Markov chains reached convergence within 20,000 iterations based upon a potential scale reduction method by Gelman (1995). The Rhat values of the 26 parameters were all less than 1.2, indicating acceptable convergence. Figure 3.2 plots the trajectories of the four Markov chains for the relative binding affinity of TB versus T (RBA_{TB_T}), which is one of the 26 calibrated model parameters. The four trajectories for the parameter mixed well and reached convergence within 20,000 iterations.

Table 3.2 includes the summary statistics of posterior distributions for the 26 calibrated parameters. The posterior distribution summary statistics are based on the 4,000 iterations, 1,000 iterations from each of the four chains. In brief, our model improved estimates of 23 model parameters. Of the 26 parameters, 21 had 95% CIs narrower than those of their prior distributions; three parameters (RBA_{EE2_E2}, error variances of E_2 and T for EE_2-exposed FHMs) had 95% CIs similar to their prior distribution CIs; and two parameters (error variances of VTG in unexposed and EE_2-exposed FHMs) had 95% CIs slightly different from their prior distribution CIs. For the error variance of VTG in unexposed FHMs, the upper confidence limit of the 95% CIs of the posterior distribution was 72% of the 2.5^{th} percentile of its prior distribution. For the error variances of VTG in EE_2-exposed FHMs, the 95% CIs of the prior and posterior distributions overlapped with each other. But the upper confidence limit of the 95% CIs of the posterior distribution was only 5% of the 97.5^{th} percentile of its prior distribution. These large differences occurred mainly because the assigned prior distributions for the

error variances were based upon the variances of experimental data, which does not represent the predictive errors, but were good starting points for parameter estimate.

It is important to note that the posterior distributions listed in Table 3.2 were conditional upon fixed model parameters (Table 3.1), prior distributions of calibrated parameters (Table 3.2), and the data sets used in calibration. Any change in these components may lead to different posterior distributions of the calibrated parameters. In this study, we carefully searched the literature to assign our model parameters with meaningful and physiologically based values or prior distributions. As additional data become available, our model could be re-calibrated to better define parameter posterior distributions.

3.3.2 Model Evaluation

3.3.2.1 Predictions for Plasma E_2, T, and VTG Concentrations in Unexposed FHMs

With the calibrated model parameters, we simulated plasma concentrations of E_2, T, and VTG in 95 unexposed adult female FHMs. Figure 3.3 shows a comparison of model predictions and experimental data. For all three endpoints, the mean and median model predictions were within 80 to 150% of the measured means and medians, respectively. Model-predicted 95% CIs encompassed the mean and median measurements, and model-predicted means and medians were within the 95% CIs of the measured data. Thus, in unexposed adult female FHMs, our model successfully predicted all three endpoints. This is an improvement compared to the model for male FHMs (Watanabe et al., 2009), which predicted the medians of the measured data, but under-predicted the variances for all the three endpoints. Adding back the predictive errors in this model enabled predicting both medians and variances of the measured data.

3.3.2.2 Predictions for plasma E_2 and VTG concentrations in TB-exposed FHMs

Figure 3.4 compares the measured and model-predicted plasma VTG (Figure 3.4A) and E_2 (Figure 3.4B) concentrations in female FHMs exposed to 0, 0.05, 0.5, and 5 µg TB/L for 48 hours (Garcia-Reyero et al., 2009). Our model predictions followed the

general trend of the measured data, and the model prediction range overlapped with the measured data range for both endpoints at each TB concentration. For plasma VTG concentrations, the median model predictions were within 96% to 579% of the median measurements. For plasma E_2 concentrations, the median model predictions were within 44 to 113% of the median measurements. Kolmogorov-Smirnov tests (α=0.05) showed that the model predictions were not significantly different from the measured data for both plasma VTG and E_2 concentrations.

To further evaluate the model's predictive ability for TB-exposed FHMs, we simulated plasma E_2 and VTG concentrations in FHMs exposed to 0, 0.05, and 0.5 µg TB/L for 8 days followed by an 8-day depuration (Ekman et al. in review). For plasma E_2 concentrations (Figure 3.5 A, B, and C), the 95% CIs of model predictions encompassed the medians of the measured data under 16 out of 24 experimental conditions (eight sampling times and three different TB concentrations). Generally, our model predicted the plasma E_2 concentrations better during the TB exposure phase than during the depuration phase. This is not surprising since we only calibrated the model with experimental data from a TB exposure (Ankley et al., 2003). In addition, it is interesting to see that the measured plasma E_2 concentrations declined from the t = P48 to P192 hours for both control FHMs and FHMs exposed to different concentrations of TB. However, the model predictions showed a different trend; that is, for control FHMs, the predicted plasma E_2 concentrations remained relatively stable throughout the experimental period (Figure 3.5A); for TB-exposed FHMs, after the exposure, the plasma E_2 concentrations increased and recovered to concentrations seen in unexposed FHMs. Since the measured plasma E_2 concentrations decreased in both control FHMs and FHMs exposed to TB, we suspect that there might be some factors that we have not accounted for during the depuration phase.

Figure 3.5 D, E, and F compare model-predicted plasma VTG concentrations with the measured data. The comparison was only for the TB exposure phase because no VTG concentrations were measured during the depuration phase. The median model predictions were within 0.6 to 2.5 fold of the measured median, and the 95% CIs of

model predictions encompassed all the measured medians at each sampling time. These results show that the model worked well for predicting the plasma E_2 and VTG concentrations in female FHMs exposed to 0, 0.05, and 0.5 µg TB/L for eight days.

After being calibrated with the experimental data from Ankley et al. (2003), our model accurately predicted the plasma E_2, T, and VTG concentrations in adult female FHMs exposed to TB. This feature was achieved by simulating AR related ligand-receptor binding processes, and by assuming two gene regulation pathways: i) down regulation of AR production by free androgens; and ii) down regulation of LH production by bound AR. It is noteworthy that the model was able to accurately fit not only the calibration data but also the VTG and E_2 data from Garcia-Reyero et al. (2009) and Ekman et al. (in review). These results indicate that our AR based modeling framework is plausible, and could be used in studies focused on regulatory aspects of the AR on HPG function.

The calibration and evaluation results showed that the model was able to predict the three HPG-related endpoints from different studies with variant experimental conditions. Although the data sets used to calibrate and validate the model were from studies with different experimental designs and analytic methods, the model accounted for the differences and predicted the endpoints well. For example, the calibration data were measured in FHMs exposed to TB for 21 days with a flow-through water exposure design, and the plasma VTG concentrations were measured by a polyclonal FHM-based ELISA (Ankley et al., 2003). In contrast, one validation data set was from FHMs exposed to TB for 48 hours with a static water exposure design, and plasma VTG concentrations measured using a monoclonal carp-based ELISA (Garcia-Reyero et al., 2009), while the other validation data set was from FHMs exposed to TB for 8 days followed by an 8 day depuration in a flow-through system, with plasma VTG concentrations measured using the polyclonal FHM-based ELISA. With the parameter set calibrated with the data from one study, our model predicted plasma E_2 and VTG concentrations comparable to the measurements from the other two studies. This indicates that the model not only fitted the data empirically, but also captured the major

features of the HPG axis in female FHMs exposed to TB. In addition, the two model evaluations also supported the point by Watanabe et al. (2009) that the VTG measurements by a polyclonal FHM-based ELISA and by a monoclonal carp-based ELISA were, in fact, consistent.

3.3.2.3 Predictions for plasma VTG concentrations in EE_2-exposed FHMs

Figure 3.6 compares model-predicted and measured plasma VTG concentrations in female FHMs exposed to three different concentrations of EE_2 for 21 days (Lazorchak et al., manuscript in preparation). For the 0.5, 1.5 and 4.5 ng/L exposures, respectively, the 90%, 80%, and 50% CIs of model predicted VTG concentrations encompassed the medians of the measured data. This trend suggests that the model predicts the endpoint better when the EE_2 exposure concentration is high and closer to the exposure concentrations used to calibrate the model (i.e., 10 and 100 ng EE_2/L). For FHMs exposed to 4.5 ng EE_2/L, the median of our model predictions was around 2 times higher than the measured data, and all measured data were within the 95% CIs of the model predictions. Considering that exposure concentrations less than 10 ng EE_2/L and exposure durations longer than 8 days are an extrapolation of the model, model predictions of plasma VTG concentrations for the 21-day 4.5 ng EE_2/L exposure were a surprisingly good fit. Actually, the low exposure concentration high time frame exposure is more environmentally relevant, because in the aquatic environmental, the EE_2 concentration ranges from 0.5 to 15 ng EE_2/L (Desbrow et al., 1998; Ericson et al., 2002a; Ribeiro et al., 2008; Ying et al., 2008), while aquatic animals may be exposed to the chemical throughout their lifetime.

Additionally, we simulated plasma VTG concentrations in FHMs exposed to 1.5 ng EE_2/L for 21 days as reported by Brian et al. (2007). In total, four control FHMs and four FHMs exposed to EE_2 were simulated. Brian et al. measured the VTG concentrations with a polyclonal carp VTG ELISA, which uses polyclonal antibodies prepared from carp VTG. In contrast, VTG data used to calibrate the model were measured with a homologous FHM VTG ELISA, which uses polyclonal antibodies prepared from FHM VTG. Direct comparison of the two methods have shown that

measurements of FHM plasma VTG concentrations can differ by several orders of magnitude (Mylchreest et al., 2003). As a result, instead of comparing the model predictions with the measured data directly, we compared the relative changes of plasma VTG concentrations. The results showed that the range of model-predicted relative change was 0.44 to 4.93, while the range of the measured data relative change was 0.78 to 0.82, all within the range of model predictions.

3.3.2.4 Predictions for reproductive endpoints in a mixture of TB and EE_2

In the next phase of our analysis, we predicted liver ER concentration, brain AR concentration, and plasma E_2, T, VTG, andLH concentrations in female FHMs exposed to 15 ng TB /L, 10 ng EE_2/L, and a mixture of 15 ng TB /L and 10 ng EE_2/L for 48 hours, respectively. Concentrations of both EDCs are within the range that has been reported in the environment. In panels A, B, and C of Figure 3.7, we plotted plasma E_2, T, and VTG concentrations as a function of time under the three exposure conditions. After exposure to TB alone, the plasma E_2, T, and VTG concentrations followed a trend consistent with the data used in the model calibration and validation. After exposure to EE_2 by itself, plasma E_2 and T concentrations decreased. We did not find any reports of plasma E_2 or T concentrations in female FHMs exposed to EE_2. However, in female zebrafish (a small cyprinid fish closely related to FHM) it was observed that both plasma E_2 and T concentrations decreased after exposure to 15 ng EE_2/L for 48 hours (Hoffmann et al., 2006), which agrees with our model predictions. In addition, plasma VTG concentrations increased after exposure to EE_2, consistent with the data used to calibrate and validate our model. Interestingly, after exposure to a mixture of TB and EE_2, our model predicted that the plasma E_2 and T concentrations decreased in an additive manner. In contrast, the plasma VTG concentration increased and followed the trend of an EE_2 exposure.

In panels D, E, and F of Figure 3.7, we plotted liver ER, brain AR, and plasma LH concentrations respectively as a function of time under the three different exposure conditions. Liver ER concentrations were predicted to decrease slightly after exposure to TB, increase dramatically after exposure to EE_2 (consistent with the gene expression data in female FHMs exposed to 10 ng EE_2/L (Filby et al., 2007)); predicted response to the

mixture was similar to the EE_2-exposure pattern. Brain AR concentrations were predicted to increase after exposure to TB, decrease slightly after exposure to EE_2, and followed the TB-exposure pattern in the mixture exposure. Plasma LH concentrations were predicted to decrease after exposure to TB, increase slightly after exposure to EE_2 (consistent with the observation in teleost exposed to EE_2 (Yaron et al., 2003)), and mimic the TB-exposure pattern in animals exposed to the EE_2/TB mixture.

To date, we do not have published data to validate model-predicted effects for a mixture of TB and EE_2; and, so far, three of the predicted endpoints (liver ER, brain AR, and plasma LH concentrations), have not been measured in FHM at a protein level because of technique limits. However, the predictions can be used to generate hypotheses and help explore possible mechanisms and pathways, which might be tested in the future.

3.4 Conclusions

The model represents the HPG axis in adult female FHM robustly, and predicts plasma E_2, T and VTG concentrations in female FHMs exposed to TB, EE_2, or a mixture of TB and EE_2. This study has shown that the model could predict reproductive endpoints from independent studies well. For more than 80% of the simulation results, the 95% CIs of model predictions encompassed the median of the experimental data. To further validate the model's predictive ability, more experimental data are needed, especially for the endpoints in FHMs exposed to a mixture of TB and EE_2.

Important features of this model include: (i) the simulation of AR in multiple tissue compartments (i.e., brain, liver, and gonad); (ii) AR binding and its effects upon the HPG axis; and (iii) free androgen effects on brain AR concentration. As a result, this model provides a computational framework for endocrine responses of EDCs functioning through AR.

The model can be used to generate hypotheses to facilitate studies of endocrine responses in female FHMs exposed to other estrogenic EDCs in addition to EE_2, or other androgenic EDCs in addition to TB. The application can be achieved through defining

chemical-specific parameters, such as binding affinity to ER and AR, blood to water and tissue to blood partitioning coefficients. Furthermore, the endpoints simulated in this study (i.e. plasma E_2, T and VTG concentrations) are important determinants affecting egg production in FHMs. In the future, the current modeling work could be linked to an oocyte dynamic model (Li et al. in review). The model integration would build a connection between EDC effects at a molecular level with effects upon an organism, and thus a population, which is an urgent need in ecotoxicological risk assessment.

3.5 Supplementary Information

Differential equations used in the HPG axis model

Brain

$$\frac{d(C_{\mathrm{TAR,brn}})}{dt} = k_{1\_\mathrm{TAR,brn}} C_{\mathrm{T,brn}} C_{\mathrm{AR,brn}} - K_{\mathrm{d\_TAR,brn}} k_{1\_\mathrm{TAR,brn}} C_{\mathrm{TAR,brn}}$$

$$\frac{d(C_{\mathrm{E2ER,brn}})}{dt} = k_{1\_\mathrm{E2ER,brn}} C_{\mathrm{E2,brn}} C_{\mathrm{ER,brn}} - K_{\mathrm{d\_E2ER,brn}} k_{1\_\mathrm{E2ER,brn}} C_{\mathrm{E2ER,brn}}$$

$$\frac{d(C_{\mathrm{TBAR,brn}})}{dt} = k_{1\_\mathrm{TBAR,brn}} C_{\mathrm{TB,brn}} C_{\mathrm{AR,brn}} - K_{\mathrm{d\_TBAR,brn}} k_{1\_\mathrm{TBAR,brn}} C_{\mathrm{TBAR,brn}}$$

$$\frac{d(C_{\mathrm{EE2ER,brn}})}{dt} = k_{1\_\mathrm{EE2ER,brn}} C_{\mathrm{EE2,brn}} C_{\mathrm{ER,brn}} - K_{\mathrm{d\_EE2ER,brn}} k_{1\_\mathrm{EE2ER,brn}} C_{\mathrm{EE2ER,brn}}$$

$$\frac{d(C_{\mathrm{AR\_free,brn}})}{dt} = \frac{\mathrm{Pbg}_{\mathrm{AR,brn}}}{1+\dfrac{(C_{\mathrm{T,brn}} + C_{\mathrm{TB,brn}})}{K_{\mathrm{AR,brn}}}} - (k_{1\_\mathrm{TAR,brn}} C_{\mathrm{T,brn}} C_{\mathrm{AR\_free,brn}} - K_{\mathrm{d\_TAR,brn}} k_{1\_\mathrm{TAR,brn}} C_{\mathrm{TAR,brn}})$$
$$-(k_{1\_\mathrm{TBAR,brn}} C_{\mathrm{TB,brn}} C_{\mathrm{AR\_free,brn}} - K_{\mathrm{d\_TBAR,brn}} k_{1\_\mathrm{TBAR,brn}} C_{\mathrm{TBAR,brn}}) - k_{\mathrm{e\_AR,brn}} C_{\mathrm{AR\_free,brn}}$$

$$\frac{d(C_{\mathrm{LH,brn}} V_{\mathrm{brn}})}{dt} = F_{\mathrm{brn}}(\mathrm{CArt}_{\mathrm{LH}} - \frac{C_{\mathrm{LH,brn}}}{\lambda_{\mathrm{LH,brn}}}) + P_{\mathrm{b\_LH,brn}} \times \frac{1+\dfrac{C_{\mathrm{ER\_bd,brn}}}{\rho_{\mathrm{u\_LH,brn}}}}{1+\dfrac{C_{\mathrm{AR\_bd,brn}}}{\rho_{\mathrm{d\_LH,brn}}}}$$

$$\frac{d(C_{\mathrm{T,brn}} V_{\mathrm{brn}})}{dt} = F_{\mathrm{brn}}(\mathrm{CArt}_{\mathrm{T}} - \frac{C_{\mathrm{T,brn}}}{\lambda_{\mathrm{T,brn}}}) - \frac{\mathrm{Vmax}_{\mathrm{aro,brn}} C_{\mathrm{T,brn}}}{\mathrm{Km}_{\mathrm{aro,brn}} + C_{\mathrm{T,brn}}}$$
$$-V_{\mathrm{brn}}(k_{1\_\mathrm{TAR,brn}} C_{\mathrm{T,brn}} C_{\mathrm{AR,brn}} - K_{\mathrm{d\_TAR,brn}} k_{1\_\mathrm{TAR,brn}} C_{\mathrm{TAR,brn}})$$

$$\frac{d(C_{\mathrm{E2,brn}} V_{\mathrm{brn}})}{dt} = F_{\mathrm{brn}}(\mathrm{CArt}_{\mathrm{E2}} - \frac{C_{\mathrm{E2,brn}}}{\lambda_{\mathrm{E2,brn}}}) + \frac{\mathrm{Vmax}_{\mathrm{aro,brn}} C_{\mathrm{T,brn}}}{\mathrm{Km}_{\mathrm{aro,brn}} + C_{\mathrm{T,brn}}}$$
$$-V_{\mathrm{brn}}(k_{1\_\mathrm{E2ER,brn}} C_{\mathrm{E2,brn}} C_{\mathrm{ER,brn}} - K_{\mathrm{d\_E2ER,brn}} k_{1\_\mathrm{E2ER,brn}} C_{\mathrm{E2ER,brn}})$$

$$\frac{d(C_{\mathrm{Vtg,brn}} V_{\mathrm{brn}})}{dt} = F_{\mathrm{brn}}(\mathrm{CAr}_{\mathrm{Vtg}} - \frac{C_{\mathrm{Vtg,brn}}}{\lambda_{\mathrm{Vtg,brn}}})$$

$$\frac{d(C_{\mathrm{TB,brn}} V_{\mathrm{brn}})}{dt} = F_{\mathrm{brn}}(\mathrm{CArt}_{\mathrm{TB}} - \frac{C_{\mathrm{TB,brn}}}{\lambda_{\mathrm{TB,brn}}}) - V_{\mathrm{brn}}(k_{1\_\mathrm{TBAR,brn}} C_{\mathrm{TB,brn}} C_{\mathrm{AR,brn}} - K_{\mathrm{d\_TBAR,brn}} k_{1\_\mathrm{TBAR,brn}} C_{\mathrm{TBAR,brn}})$$

$$\frac{d(C_{\mathrm{EE2,brn}} V_{\mathrm{brn}})}{dt} = F_{\mathrm{brn}}(\mathrm{CArt}_{\mathrm{EE2}} - \frac{C_{\mathrm{EE2,brn}}}{\lambda_{\mathrm{EE2,brn}}}) - V_{\mathrm{brn}}(k_{1\_\mathrm{EE2ER,brn}} C_{\mathrm{EE2,brn}} C_{\mathrm{ER,brn}} - K_{\mathrm{d\_EE2ER,brn}} k_{1\_\mathrm{EE2ER,brn}} C_{\mathrm{EE2ER,brn}})$$

Gonad

$$\frac{d(C_{\mathrm{LHLR,gon}})}{dt} = k_{1\_\mathrm{LHLR,gon}} C_{\mathrm{LH,gon}} C_{\mathrm{LR,gon}} - K_{\mathrm{d\_LHLR,gon}} k_{1\_\mathrm{LHLR,gon}} C_{\mathrm{LHLR,go}}$$

$$\frac{d(C_{\mathrm{TARgon}})}{dt} = k_{1\_\mathrm{TARgon}} C_{\mathrm{T,gon}} C_{\mathrm{ARgon}} - K_{\mathrm{d\_TARgon}} k_{1\_\mathrm{TARgon}} C_{\mathrm{TARgon}}$$

$$\frac{d(C_{\mathrm{E2ER,gon}})}{dt} = k_{1\_\mathrm{E2ER,gon}} C_{\mathrm{E2,gon}} C_{\mathrm{ER,gon}} - K_{\mathrm{d\_E2ER,gon}} k_{1\_\mathrm{E2ER,gon}} C_{\mathrm{E2ER,go}}$$

$$\frac{d(C_{\mathrm{TBAR,gon}})}{dt} = k_{1\_\mathrm{TBAR,gon}} C_{\mathrm{TB,gon}} C_{\mathrm{AR,gon}} - K_{\mathrm{d\_TBAR,gon}} k_{1\_\mathrm{TBAR,gon}} C_{\mathrm{TBAR,gon}}$$

$$\frac{d(C_{\mathrm{EE2ER,gon}})}{dt} = k_{1\_\mathrm{EE2ER,gon}} C_{\mathrm{EE2,gon}} C_{\mathrm{ER,gon}} - K_{\mathrm{d\_EE2ER,gon}} k_{1\_\mathrm{EE2ER,gon}} C_{\mathrm{EE2ER,go}}$$

$$\frac{d(C_{\mathrm{LH,gon}} V_{\mathrm{gon}})}{dt} = F_{\mathrm{gon}} (\mathrm{CArt}_{\mathrm{LH}} - \frac{C_{\mathrm{LH,gon}}}{\lambda_{\mathrm{LH,gon}}}) - V_{\mathrm{gon}} (k_{1\_\mathrm{LHLR,gon}} C_{\mathrm{LH,gon}} C_{\mathrm{LR,gon}} - K_{\mathrm{d\_LHLR,gon}} k_{1\_\mathrm{LHLR,gon}} C_{\mathrm{LHLR,gon}})$$

$$\frac{d(C_{\mathrm{T,gon}} V_{\mathrm{gon}})}{dt} = F_{\mathrm{gon}} (\mathrm{CArt}_{\mathrm{T}} - \frac{C_{\mathrm{T,gon}}}{\lambda_{\mathrm{T,gon}}}) - \frac{k_{\mathrm{E2\_LHLRgon}} C_{\mathrm{LHLR,gon}} \mathrm{Vmax}_{\mathrm{aro,gon}} C_{\mathrm{T,gon}}}{\mathrm{Km}_{\mathrm{aro,gon}} + C_{\mathrm{T,gon}}}$$

$$+ \frac{\mathrm{Vmax}_{\mathrm{Scc,gon}} C_{\mathrm{Chol,gon}}^{n_{\mathrm{T}}}}{\mathrm{K}_{0.5\mathrm{Scc,gon}}^{n_{\mathrm{T}}} + C_{\mathrm{Chol,gon}}^{n_{\mathrm{T}}}} \div (1 + \frac{C_{\mathrm{E2ER,gon}} + C_{\mathrm{EE2ER,gon}}}{K_{\mathrm{T}}})$$

$$- V_{\mathrm{gon}} (k_{1\_\mathrm{TAR,gon}} C_{\mathrm{T,gon}} C_{\mathrm{AR,gon}} - K_{\mathrm{d\_TAR,gon}} k_{1\_\mathrm{TAR,gon}} C_{\mathrm{TAR,gon}})$$

$$\frac{d(C_{\mathrm{E2,gon}} V_{\mathrm{gon}})}{dt} = F_{\mathrm{gon}} (\mathrm{CArt}_{\mathrm{E2}} - \frac{C_{\mathrm{E2,gon}}}{\lambda_{\mathrm{E2,gon}}}) + \frac{\rho_{\mathrm{E2\_LHLRgon}} C_{\mathrm{LHLR,gon}} \mathrm{Vmax}_{\mathrm{aro,gon}} C_{\mathrm{T,gon}}}{\mathrm{Km}_{\mathrm{aro,gon}} + C_{\mathrm{T,gon}}}$$

$$- V_{\mathrm{gon}} (k_{1\_\mathrm{E2ER,gon}} C_{\mathrm{E2,gon}} C_{\mathrm{ER,gon}} - K_{\mathrm{d\_E2ER,gon}} k_{1\_\mathrm{E2ER,gon}} C_{\mathrm{E2ER,gon}})$$

$$\frac{d(C_{\mathrm{Vtg,gon}} V_{\mathrm{gon}})}{dt} = F_{\mathrm{gon}} (\mathrm{CArt}_{\mathrm{Vtg}} - \frac{C_{\mathrm{Vtg,gon}}}{\lambda_{\mathrm{Vtg,gon}}}) - k_{\mathrm{VTG,gon}} C_{\mathrm{VTG,gon}} V_{\mathrm{gon}}$$

$$\frac{d(C_{\mathrm{TB,gon}} V_{\mathrm{gon}})}{dt} = F_{\mathrm{gon}} (\mathrm{CArt}_{\mathrm{KT}} - \frac{C_{\mathrm{TB,gon}}}{\lambda_{\mathrm{TB,gon}}}) - V_{\mathrm{gon}} (k_{1\_\mathrm{TBAR,gon}} C_{\mathrm{TB,gon}} C_{\mathrm{AR,gon}} - K_{\mathrm{d\_TBAR,gon}} k_{1\_\mathrm{TBAR,gon}} C_{\mathrm{TBAR,gon}})$$

$$\frac{d(C_{\mathrm{EE2,gon}} V_{\mathrm{gon}})}{dt} = F_{\mathrm{gon}} (\mathrm{CArt}_{\mathrm{EE2}} - \frac{C_{\mathrm{EE2,gon}}}{\lambda_{\mathrm{EE2,gon}}}) - V_{\mathrm{gon}} (k_{1\_\mathrm{EE2ER,gon}} C_{\mathrm{EE2,gon}} C_{\mathrm{ER,gon}} - K_{\mathrm{d\_EE2ER,gon}} k_{1\_\mathrm{EE2ER,gon}} C_{\mathrm{EE2ER,gon}})$$

Liver

$$\frac{d(C_{\mathrm{ER,liv}})}{dt} = \mathrm{Pbg}_{\mathrm{ER,liv}} + k_{\mathrm{ER,liv}} (C_{\mathrm{E2ER\_liv}} + C_{\mathrm{EE2ER\_liv}}) - (k_{1\_\mathrm{EE2ER,liv}} C_{\mathrm{EE2,liv}} C_{\mathrm{ER,liv}} - K_{\mathrm{d\_EE2ER,liv}} k_{1\_\mathrm{EE2ER,liv}} C_{\mathrm{EE2ER,liv}}$$

$$- (k_{1\_\mathrm{E2ER,liv}} C_{\mathrm{E2,liv}} C_{\mathrm{ER,liv}} - K_{\mathrm{d\_E2ER,liv}} k_{1\_\mathrm{E2ER,liv}} C_{\mathrm{E2ER,liv}}) - k_{\mathrm{e\_ER,liv}} C_{\mathrm{ER,liv}}$$

$$\frac{d(C_{\mathrm{TARliv}})}{dt} = k_{1\_\mathrm{TARliv}} C_{\mathrm{T,liv}} C_{\mathrm{ARliv}} - K_{\mathrm{d\_TARliv}} k_{1\_\mathrm{TARliv}} C_{\mathrm{TARliv}}$$

$$\frac{d(C_{\text{E2ER,liv}})}{dt} = k_{\text{1\_E2ER,liv}} C_{\text{E2,liv}} C_{\text{ER,liv}} - K_{\text{d\_E2ER,liv}} k_{\text{1\_E2ER,liv}} C_{\text{E2ER,liv}}$$

$$\frac{d(C_{\text{TBAR,liv}})}{dt} = k_{\text{1\_TBAR,liv}} C_{\text{TB,liv}} C_{\text{AR,liv}} - K_{\text{d\_TBAR,liv}} k_{\text{1\_TBAR,liv}} C_{\text{TBAR,liv}}$$

$$\frac{d(C_{\text{EE2ER,liv}})}{dt} = k_{\text{1\_EE2ER,liv}} C_{\text{EE2,liv}} C_{\text{ER,liv}} - K_{\text{d\_EE2ER,liv}} k_{\text{1\_EE2ER,liv}} C_{\text{EE2ER,liv}}$$

$$\frac{d(C_{\text{LH,liv}} V_{\text{liv}})}{dt} = F_{\text{liv}} (\text{CArt}_{\text{LH}} - \frac{C_{\text{LH,liv}}}{\lambda_{\text{LH,liv}}})$$

$$\frac{d(C_{\text{T,liv}} V_{\text{liv}})}{dt} = F_{\text{liv}} (\text{CArt}_{\text{T}} - \frac{C_{\text{T,liv}}}{\lambda_{\text{T,liv}}}) - V_{\text{liv}} (k_{\text{1\_TAR,liv}} C_{\text{T,liv}} C_{\text{AR,liv}} - K_{\text{d\_TAR,liv}} k_{\text{1\_TAR,liv}} C_{\text{TAR,liv}})$$

$$\frac{d(C_{\text{E2,liv}} V_{\text{liv}})}{dt} = F_{\text{liv}} (\text{CArt}_{\text{E2}} - \frac{C_{\text{E2,liv}}}{\lambda_{\text{E2,liv}}}) - V_{\text{liv}} (k_{\text{1\_E2ER,liv}} C_{\text{E2,liv}} C_{\text{ER,liv}} - K_{\text{d\_E2ER,liv}} k_{\text{1\_E2ER,liv}} C_{\text{E2ER,liv}})$$

$$\frac{d(C_{\text{Vtg,liv}} V_{\text{liv}})}{dt} = F_{\text{liv}} (\text{CArt}_{\text{Vtg}} - \frac{C_{\text{Vtg,liv}}}{\lambda_{\text{Vtg,liv}}}) + \frac{\text{Vmax}_{\text{Vtg,liv}} (C_{\text{E2ER,liv}} + C_{\text{EE2ER,liv}})^{n_{\text{Vtg}}}}{\text{K}_{0.5\text{Vtg,liv}}^{n_{\text{Vtg}}} + (C_{\text{E2ER,liv}} + C_{\text{EE2ER,liv}})^{n_{\text{Vtg}}}}$$

$$\frac{d(C_{\text{TB,liv}} V_{\text{liv}})}{dt} = F_{\text{liv}} (\text{CArt}_{\text{TB}} - \frac{C_{\text{TB,liv}}}{\lambda_{\text{TB,liv}}}) - V_{liv} (k_{\text{1\_TBAR,liv}} C_{\text{TB,liv}} C_{\text{AR,liv}} - K_{\text{d\_TBAR,liv}} k_{\text{1\_TBAR,liv}} C_{\text{TBAR,liv}})$$

$$\frac{d(C_{\text{EE2,liv}} V_{\text{liv}})}{dt} = F_{\text{liv}} (\text{CArt}_{\text{EE2}} - \frac{C_{\text{EE2,liv}}}{\lambda_{\text{EE2,liv}}}) - V_{\text{liv}} (k_{\text{1\_EE2ER,liv}} C_{\text{EE2,liv}} C_{\text{ER,liv}} - K_{\text{d\_EE2ER,liv}} k_{\text{1\_EE2ER,liv}} C_{\text{EE2ER,liv}})$$

Other

$$\frac{d(C_{\text{LH,oth}} V_{\text{oth}})}{dt} = F_{\text{oth}} (\text{CArt}_{\text{LH}} - \frac{C_{\text{LH,oth}}}{\lambda_{\text{LH,oth}}}) - k_{\text{e\_LH,oth}} C_{\text{LH,oth}} V_{\text{oth}}$$

$$\frac{d(C_{\text{T,oth}} V_{\text{oth}})}{dt} = F_{\text{oth}} (\text{CArt}_{\text{T}} - \frac{C_{\text{T,oth}}}{\lambda_{\text{T,oth}}}) - k_{\text{e\_T,oth}} C_{\text{T,oth}} V_{\text{oth}}$$

$$\frac{d(C_{\text{E2,oth}} V_{\text{oth}})}{dt} = F_{\text{oth}} (\text{CArt}_{\text{E2}} - \frac{C_{\text{E2,oth}}}{\lambda_{\text{E2,oth}}}) - k_{\text{e\_E2,oth}} C_{\text{E2,oth}} V_{\text{oth}}$$

$$\frac{d(C_{\text{Vtg,oth}} V_{\text{oth}})}{dt} = F_{\text{oth}} (\text{CArt}_{\text{Vtg}} - \frac{C_{\text{Vtg,oth}}}{\lambda_{\text{Vtg,oth}}}) - k_{\text{e\_Vtg,oth}} C_{\text{Vtg,oth}} V_{\text{oth}}$$

$$\frac{d(C_{\text{TB,oth}} V_{\text{oth}})}{dt} = F_{\text{oth}} (\text{CArt}_{\text{TB}} - \frac{C_{\text{TB,oth}}}{\lambda_{\text{TB,oth}}}) - k_{\text{e\_TB,oth}} C_{\text{TB,oth}} V_{\text{oth}}$$

$$\frac{d(C_{\text{EE2,oth}} V_{\text{oth}})}{dt} = F_{\text{oth}} (\text{CArt}_{\text{EE2}} - \frac{C_{\text{EE2,oth}}}{\lambda_{\text{EE2,oth}}}) - k_{\text{e\_EE2,oth}} C_{\text{EE2,oth}} V_{\text{oth}}$$

Venous blood

$$\frac{d(C_{\text{TSBP,ven}})}{dt} = k_{1\_\text{TSBP,ven}} C_{\text{T,ven}} C_{\text{SBP,ven}} - K_{\text{d\_TSBP,ven}} k_{1\_\text{TSBP,ven}} C_{\text{TSBP,ven}}$$

$$\frac{d(C_{\text{E2SBP,ven}})}{dt} = k_{1\_\text{E2SBP,ven}} C_{\text{E2,ven}} C_{\text{SBP,ven}} - K_{\text{d\_E2SBP,ven}} k_{1\_\text{E2SBP,ven}} C_{\text{E2SBP,ven}}$$

$$\frac{d(C_{\text{EE2SBP,ven}})}{dt} = k_{1\_\text{EE2SBP,ven}} C_{\text{EE2,ven}} C_{\text{SBP,ven}} - K_{\text{d\_EE2SBP,ven}} k_{1\_\text{EE2SBP,ven}} C_{\text{EE2SBP,ven}}$$

$$\frac{d(C_{\text{T,ven}} V_{\text{ven}})}{dt} = F_{\text{oth}} \frac{C_{\text{T,oth}}}{\lambda_{\text{T,oth}}} + F_{\text{liv}} \frac{C_{\text{T,liv}}}{\lambda_{\text{T,liv}}} + F_{\text{brn}} \frac{C_{\text{T,brn}}}{\lambda_{\text{T,brn}}} + F_{\text{gon}} \frac{C_{\text{T,gon}}}{\lambda_{\text{T,gon}}} - F_{\text{car}} C_{\text{T,ven}} - V_{\text{ven}} (k_{1\_\text{TSBP,ven}} C_{\text{T,ven}} C_{\text{SBP,ven}} - K_{\text{d\_TSBP,ven}} k_{1\_\text{TSBP,ven}} C_{\text{TSBP,ven}})$$

$$\frac{d(C_{\text{E2,ven}} V_{\text{ven}})}{dt} = F_{\text{oth}} \frac{C_{\text{E2,oth}}}{\lambda_{\text{E2,oth}}} + F_{\text{liv}} \frac{C_{\text{E2,liv}}}{\lambda_{\text{E2,liv}}} + F_{\text{brn}} \frac{C_{\text{E2,brn}}}{\lambda_{\text{E2,brn}}} + F_{\text{gon}} \frac{C_{\text{E2,gon}}}{\lambda_{\text{E2,gon}}} - F_{\text{car}} C_{\text{E2,ven}} - V_{\text{ven}} (k_{1\_\text{E2SBP,ven}} C_{\text{E2,ven}} C_{\text{SBP,ven}} - K_{\text{d\_E2SBP,ven}} k_{1\_\text{E2SBP,ven}} C_{\text{E2SBP,ven}})$$

CHAPTER 4

A Computational Model for Oocyte Dynamics in Asynchronous Spawning Fish (e.g., FHMs)

Adapted from a manuscript in preparation for publication: Li Z., Villeneuve D., Jensen K., Ankley G., Watanabe K.

4.1 Introduction

For several reasons it is important to understand mechanisms of oocyte development and regulation in asynchronous spawning fishes. For example, many asynchronous spawning small fish species (e.g., FHM) are used as ecotoxicological research models worldwide, and effects upon reproduction are a major concern. In recent years, molecular biomarkers have been used in ecotoxicology to evaluate chemical interactions with the HPG axis (Ankley et al., 2009a). In order to link chemical effects at a molecular level to effects at individual and ultimately population levels, it is important to explore the mechanisms regulating oocyte development both qualitatively and quantitatively. To date, most of the research on oocyte development and regulation has been conducted with synchronous-spawning fish species (Campbell et al., 2006; Kamei et al., 2006; Nagahama and Adachi, 1985; Nagahama et al., 1995; Tyler et al., 1997; Tyler et al., 1990), while comparatively few studies have been conducted with asynchronous-spawning fish species. Further, most studies that have been done with asynchronous-spawning fish have been from the perspective of basic reproduction (Jensen et al., 2001; Leino et al., 2005; Wolf et al., 2004). In this research context, computational models can be useful for combining knowledge from experimental studies and exploring possible underlying mechanisms.

Miller et al. (2007) found a linear relationship between relative fecundity and relative plasma VTG concentration (expressed as a proportion of the baseline measurements for each endpoint) for female FHMs exposed to five EDCs that reduce VTG synthesis. This relationship is consistent with previous knowledge that the majority of oocyte growth is associated with the accumulation of yolk proteins in the cytoplasm (Specker and Sullivan, 1994). Other than the work of Miller et al., we are not aware of any reports in the open literature of a computational model for oocyte growth and spawning in fishes. In this study, we developed a computational model to simulate oocyte growth and spawning in both unexposed FHMs and FHMs exposed to TB, one of the five EDCs used by Miller et al.

4.2 Materials and methods

4.2.1 Experimental data

Fathead minnow fecundity data were obtained from 13 studies conducted at the USEPA Mid-Continent Ecology Division Laboratory in Duluth, MN from 1999 to 2006 (Table 4.1). The experimental designs and corresponding data summaries were described by Watanabe et al. (2007). Among the 13 studies, one was a baseline reproduction study in unexposed FHMs (Jensen et al., 2001), and the remaining were reproduction studies in which FHMs were exposed to various EDCs (Ankley et al., 2005a; Ankley et al., 2001; Ankley et al., 2003; Ankley et al., 2002; Ankley et al., 2005b; Jensen et al., 2004; Jensen et al., 2006; Martinovic et al., 2008; Villeneuve et al., 2009a; Villeneuve et al., 2006). For modeling purposes, we used fecundity data from the baseline reproduction study, the control FHMs from the 12 EDC exposure experiments, and FHMs exposed to TB, a strong androgen receptor agonist that depresses VTG production (Ankley et al., 2003). The 13 studies were classified into two groups based upon experimental design: paired-spawning-design studies with one male and one female per tank (Ankley et al., 2005a; Ankley et al., 2005b; Jensen et al., 2001; Jensen et al., 2006; Martinovic et al., 2008; Villeneuve et al., 2009a; Villeneuve et al., 2006); and group-spawning-design studies with 2 males and 4 females per tank (Ankley et al., 2001; Ankley et al., 2003; Ankley et al., 2002; Jensen et al., 2004).

Figure 4.1 illustrates how we used these data in the model parameterization and evaluation. From paired-spawning-design studies, we had records of clutch sizes (i.e., number of eggs per spawn) and spawning intervals for 60 female FHMs. In total, there were 391 records for clutch sizes and 331 records for spawning intervals; both data sets were used to fit probability distributions (Table 4.2). The fitted distributions were used in our oocyte growth dynamics model to represent the distributions of oocyte recruitment size and oocyte recruitment interval, respectively. For 50 of the 60 female FHMs, we had records of plasma VTG concentration, clutch size, spawning interval, and average fecundity (eggs/female/day), and these data were used to evaluate our model predictions.

For control FHMs from group-spawning-design studies, we used records for 77 female FHMs which comprised 20 experimental units (in most cases there were four FHMs per group). For each individual FHM, we had a measurement of plasma VTG concentration, while for each group we had a record of average fecundity which was calculated as number of eggs per female per day based on the number of FHM females in the group.

In the TB exposure study, 71 female FHMs were from 18 experimental units (i.e., four FHMs per group, with data missing for one fish). The fish had been exposed to one of six TB concentrations (i.e., 0, 0.005, 0.05, 0.5, 5, 50 μg/L) for 21 days (three groups per concentration). All fecundity data from group-spawning-design studies were used to evaluate our model predictions

4.2.2 Model Development

Figure 4.2 is a conceptual model that describes how we simplified the processes of oocyte recruitment, growth, and spawning in FHM. Following the conceptual model, the computational model simulates oocyte recruitment, growth, and subsequent batch spawning. A free software package, MCSim (Bois and Maszle, 1997) (http://www.gnu.org/software/mcsim/) was used to develop the computational model, and the ordinary differential equations describing oocyte growth dynamics were integrated using Euler's method.

In our model, oogonia are periodically recruited into oocyte growth starting when FHMs are three months old (2160 hrs post-hatch) (Villeneuve et al., 2007). An oogonia, prior to being recruited into the growth phase, was defined as having a volume of 5.2×10^{-7}µL, a value calculated from the diameter of an oogonia in FHM (Leino et al., 2005). Because we do not know the detailed mechanisms controlling oocyte recruitment or fecundity in FHM, we assumed that the number of oogonia recruited into the growth phase and the recruitment interval between two consecutive batches followed the fitted distributions of clutch size and spawning interval with upper and lower bounds set at the maximum and minimum recorded values, respectively. In addition, although we know that atresia (i.e., oocyte degeneration) plays an important role in regulating the number of oocytes in many vertebrates, limited quantitative studies concerning this process have been done in teleosts (Tyler and Sumpter, 1996; Wallace and Selman, 1981). Hence, we assumed that once oocytes were recruited into the growth phase, their number would not change, and all eggs would be spawned.

In MCSim, we used a vector function to track oocyte batches, and each vector contained 100 elements representing 100 batches of oocytes; the size of this vector can be adjusted by the user. The clutch size distribution was sampled randomly to determine the number of oocytes (N_i) recruited into each batch i (i = 1, 2, … 100). Similarly, the spawning interval distribution was randomly sampled to determine oocyte recruitment intervals (T_i) between two batches of oocytes. To compute the number of oocytes per batch in MCSim, a rate of oocyte recruitment (number of eggs/hr) was defined using MCSim's PerDose function (eq. 1, Figure 4.3).

$$R_{\text{recruited}} = \text{PerDose}\ (N_i,\ T_{\text{exp}},\ T_i,\ 1), \qquad (1)$$

In eq. 1, $R_{\text{recruited}}$ is the number of eggs recruited per hr; T_{exp} (hr) is the total length of the experiment being simulated (= 4608 hrs in this study); and 1 (hr) represents the length of time over which oocytes are recruited into the growth phase. We calculated the number of oocytes in each batch (N_{Ooc}) by integrating $R_{\text{recruited}}$ over 1 hr (eq. 2).

$$\frac{d(N_{\text{Ooc}})}{dt} = R_{\text{recruited}}, \quad (2)$$

After being recruited into the growth phase, we simulated oocyte growth based upon the uptake of VTG. The rate of VTG uptake was formulated to be proportional to the plasma VTG concentration and the oocyte volume (eq. 3) because it was observed in rainbow trout that the rate of VTG uptake increased with oocyte diameter even when it was normalized to oocyte surface area (Charles et al., 1988; Specker and Sullivan, 1994), and that an increase in VTG or VTG degradation products in oocytes was associated with an increase in plasma VTG concentrations (Perazzolo et al., 1999). We assumed that VTG uptake into oocytes in FHM followed a similar pattern to that of trout, since we did not have data specific for FHMs.

$$\frac{d(M_{\text{VTG}})}{dt} = \rho_{\text{VTG\_Ooc}} \times C_{\text{VTG}} \times V_{\text{Ooc}}, \quad (3)$$

In eq. 3, M_{VTG} (nmol) is the amount of VTG absorbed into each oocyte in each batch; $\rho_{\text{VTG\_Ooc}}$ (1/hr) is the VTG absorption rate constant; C_{VTG} (nmol/µL) is the plasma VTG concentration; V_{Ooc} (µL) is the volume of each oocyte in each batch. For each batch of oocytes, we assumed that all oocytes grew equally, and their volumes were the same.

It is known that, in an optimized laboratory setting, the spawning interval of reproductively active unexposed FHMs ranges from 1 to 15 days, with most values falling in the range of 3 to 4 days (Jensen et al., 2001). In addition, at least four stages of oocytes have been observed in a FHM ovary at one time (Jensen et al., 2001; Villeneuve et al., 2007). As a result, it is reasonable to assume that there are at least four batches of oocytes developing simultaneously. Given that there are four batches of oocytes inside a FHM ovary, and that the spawning intervals are typically 3 to 4 days, the oocyte growth period in FHMs should be on the order of 12 to 16 days. In our model, we set $\rho_{\text{VTG\_Ooc}}$ at 1 hr^{-1}, which resulted in an average oocyte growth period of approximately 13 days. This

pattern agrees with oocyte growth mechanisms in many mammals, amphibians, and other fish species (Coward and Bromage, 1998; Hirao and Miyano, 2008; Scott, 2000).

Along with VTG, other molecules (e.g., water and minerals) enter oocytes (Specker and Sullivan, 1994; Tyler et al., 1990), and also contribute to the increase in oocyte volume. In our model, the volume of an oocyte is equal to its initial volume (volume of oogonia) plus the oocyte growth volume. We assumed that there was a proportional relationship between the uptake of VTG and other molecules during vitellogenesis, and therefore the oocyte growth volume was formulated to be proportional to the amount of VTG absorbed into the oocyte.

$$V_{Ooc} = V_{Oog} + 0.156 \times M_{VTG} \times r_{VTG\_Water}, \quad (4)$$

In eq. 4, V_{Oog}(μL) is the initial volume of an oocyte; 0.156 (mg/nmol) is the molecular weight of VTG; r_{VTG_Water} (μL/mg) is the ratio of the volume of oocyte growth to the amount of VTG absorbed. In this study, we set the value of r_{VTG_Water} to be three, an empirical value based upon the observation that fish oocytes are about 2/3 water (Milla et al., 2006), and the density of fish oocytes is around 1 mg/μL (unpublished data).

In our model, we used oocyte size as a criterion to determine when an oocyte will be spawned. The critical size was set to be 0.52 μL, a value calculated from the diameter of a mature oocyte reported in FHM (Leino et al., 2005). When oocytes in a batch reached the critical size, they were spawned, and the number of oocytes in the fish decreased.

4.2.3 Model Evaluation

To evaluate the predictive ability of our model, we simulated the number of eggs spawned as a function of time for unexposed FHMs with paired-spawning and group-spawning designs, respectively, and for FHMs exposed to TB for 21 days with a group-spawning design. For simulation of the three data types above, measured FHM plasma VTG concentration was input as a model parameter. For each unexposed FHM from

paired- or group-spawning-design studies, plasma VTG concentration was assumed to be a constant throughout the simulation, and its value was set to be the measured plasma VTG concentration recorded when the FHM was sacrificed. For FHMs exposed to TB, plasma VTG concentration before exposure was set to be the average plasma VTG concentration of the controls because we did not have pre-exposure plasma VTG data. At the actual start of a TB exposure, plasma VTG concentration in the FHM was set to be the value measured at conclusion of the test.

In total, we simulated 50 unexposed FHMs from paired-spawning studies. Predicted clutch sizes, spawning intervals, and average fecundities were compared to experimental data visually. In addition, for each reproductive endpoint, we used a non-parametric two-sample Kolmogorov-Smirnov test in MATLAB 7.1 to test whether the model predictions and the measured data were different at a significance level of 0.01 (α=0.01). The null hypothesis was that the two samples were drawn from the same distribution; the alternative hypothesis was that they were drawn from different distributions.

The distributions used in our model (i.e., the distributions of oocyte recruitment size and recruitment interval) were derived from experimental data of FHMs from paired-spawning-design studies, while the independent experimental data available to evaluate our model predictions were from experimental data of FHMs from group-spawning-design studies. To evaluate whether the model could be used to simulate average fecundity from a group-spawning design, we performed a non-parametric two-sample Kolmogorov-Smirnov test (α=0.01) to evaluate whether the measured average fecundity data from FHMs with a group-spawning design (number of fish =77, number of groups = 20, number of average fecundity data points= 20) differed significantly from the FHMs with a paired-spawning design (number of fish =50, number of average fecundity data points=50). We could not reject the hypothesis that the two average fecundity data sets were from the same distribution, i.e., the two data sets were not significantly different.

To determine whether our model could predict average fecundity in FHMs with a group-spawning design, we simulated spawning in 77 unexposed FHMs from group-

spawning-design studies. Model predictions for the 77 FHMs were divided into 20 groups according to the experimental design. The average fecundity of each group was calculated and compared to experimental data.

To evaluate whether our model could predict the average fecundity in FHMs exposed to TB, we simulated spawning in the 71 FHMs exposed to TB for 21 days. Model predictions for the 71 FHMs were divided into 18 groups according to the experimental design. The average fecundity of each group was calculated, grouped based on the different TB concentrations, and compared to experimental data.

Figure 4.4 illustrates a timeline for our model simulations. For all simulations, we set three months (2160 hrs post-hatch) as the time that female FHMs start to recruit oocytes. For unexposed FHMs we started tracking fecundity at five months (3600 hr) and continued tracking it for 21 days (3600 to 4104 hrs). This was intended to simulate the actual age of reproductive maturity, as well as the actual age of FHMs used in the studies providing experimental data. For the TB exposure study, we started tracking FHM fecundity at five months and continued for 21 days before the exposure. Then, we simulated the TB exposure starting at five months and 22 days, and tracked fecundity from 4104 to 4608 hrs.

To fully explore the sampling space of the distributions of oocyte recruitment size and spawning interval, all simulations were performed 1000 times using Monte Carlo simulation in MCSim. The MCSim output file was imported into MATLAB 7.1, and out of 1000 results we randomly sampled one set of results for each fish. Based upon the sampled results, we counted and calculated reproductive endpoints such as clutch size, spawning interval, and average fecundity. The estimated reproductive endpoints were then pooled, and visually compared to the measured data.

4.3 Results

4.3.1 Distribution Fitting

For the 60 unexposed FHMs from the paired-spawning-design studies, clutch sizes fit a lognormal distribution with geometric mean (GM, exponential of the mean in log-space) and geometric standard deviation (GSD, exponential of the standard deviation in log-space) equal to 4.11 and 0.96, respectively (Table 4.2). The spawning intervals fit a lognormal distribution with GM and GSD equal to 1.21 and 0.57, respectively (Table 4.2).

4.3.2 Model Predictions in Unexposed FHMs with a Paired-spawning Design

Figure 4.5 compares model predictions with the experimental data for the 50 unexposed female FHMs from paired-spawning-design studies over a 21-day period. The mean and median model predictions were within 0.5 to 2.0 fold of the mean and median measurements for clutch size (Figure 4.5A), spawning interval (Figure 4.5B), and average fecundity (Figure 4.5C), respectively. The 95% CIs of model predictions encompassed the mean and median measurements, and the mean and median model predictions were within the 95% CIs of experimental data for each endpoint. Using non-parametric two-sample Kolmogorov-Smirnov tests (α=0.01), we concluded that there was no significant difference between the model predictions and experimental data for the three reproductive endpoints.

4.3.3 Model Predictions in Unexposed FHMs with a Group-spawning Design

Figure 4.6 shows a comparison of model predictions with experimental data for the 77 unexposed female FHMs (20 groups) from group-spawning-design studies, which were not used in the model calibration. Although the model predictions had a variance (4.0) slightly smaller than that of the experimental data variance (7.1), the two data sets were generally comparable. The 95% CIs of model predictions (11.7, 24.7) encompassed the mean (16.7) and median (16.3) measurements, and the mean (18.3) and median (17.9) model predictions were within the 95% CIs (5.1, 28.0) of the experimental data. Using a

non-parametric two-sample Kolmogorov-Smirnov test (α=0.01), we concluded that there were no significant differences between the model predictions and experimental data.

4.3.4 Model Predictions in TB-exposed FHMs with a Group-spawning Design

Figure 4.7 shows a comparison of model-predicted average fecundity with experimental data for 71 female FHMs (18 groups) exposed to 0, 0.005, 0.05, 0.5, 5, 50 µg/L TB for 21 days. Predicted average fecundity followed the same trend as the experimental data, i.e., with increasing TB concentrations, the average fecundity of FHMs decreased, and the model predictions overlapped the experimental data. For each concentration of TB, the predicted medians were 20.5, 13.8, 9.6, 0, 0, and 1.5, respectively, and the medians of measured data were 11.5, 11.6, 6.8, 0.4, 0, and 0, respectively. It was interesting to see an increase in average fecundity predicted by the model for the highest TB exposure concentration (50 µg/L). At exposure concentrations equal to 0.5 and 5 µg/L, all three predicted average fecundity values were 0 whereas at an exposure concentration equal to 50 µg/L, two of the three predicted average fecundity values were greater than zero.

4.4 Discussion

4.4.1 Fecundity in Unexposed FHMs with a Group-spawning Design

For our modeling we used data from studies with two different experimental designs: paired- and group-spawning. In a paired-spawning-design experiment, it is clear that all eggs collected within a tank are spawned from a single female. However, in a group-spawning-design experiment, the eggs collected in one tank may be from one of four females, or even from more than one female in the tank because multiple females might spawn on the same day. This makes it difficult to determine individual fecundity, so only average fecundity can be compared between a group-spawning design and a paired-spawning design study.

In our model, the distributions of oocyte recruitment size and oocyte recruitment interval used to predict the average fecundity of FHMs with a group-spawning design

were exactly the same as those used for FHMs with a paired-spawning design. With the same distributions, our model successfully predicted the average fecundity of FHMs from studies with a group-spawning design. The simulation results showed that the average fecundity from two different experimental designs were not significantly different from each other. These results suggest that the clutch sizes and spawning intervals for individual fish are not affected by the two experimental designs evaluated in this study.

4.4.2 Predictions of Fecundity in EDC-exposed FHMs with Group-spawning Design

Model-predicted average fecundity in TB exposed FHMs followed the trend of the experimental data, which suggests that our model captured the relationship between VTG concentrations and oocyte growth dynamics. That is, the U-shaped curve in our model-predicted average fecundity (Figure 4.7) was influenced by the U-shaped curve in the plasma VTG measurements (Ankley et al., 2003). However, the predictions did not exactly match the experimental data, especially for the 50 µg/L TB treatment.

Atresia might be one possible explanation for the over-predictions at the 50 µg/L TB treatment. Atresia is a common event in many vertebrates, which plays an important role in regulating the number of oocytes that are eventually spawned (Tyler and Sumpter, 1996). While atresia occurs under ideal environmental conditions, exposure to environmental stressors may increase the rate of atresia (Wallace and Selman, 1981). In our model, we did not include the process of atresia because of a shortage of quantitative information. However, in the TB-exposed FHMs, atresia was indeed one of the major histological lesions noted by Ankley et al. (2003). As a result, our model may tend to predict higher fecundity in the exposed FHMs, especially for the FHMs exposed to high levels of TB.

An alternative explanation for the fecundity over-prediction in the exposed FHMs is that the plasma VTG concentrations used in the simulations were not a function of time, but were set as a constant prior to exposure and after the start of exposure, respectively. When we simulated the fecundity of an unexposed FHM from paired- or group-spawning-design studies, we input the plasma VTG concentration measured when the

FHM was sacrificed, and its value was set to a constant. Since it was observed that, in unexposed reproductively-active FHMs, the plasma VTG concentrations remained relatively constant over a spawning interval (Jensen et al., 2001), we assumed a constant plasma VTG concentration to predict the fecundity in an unexposed FHM was reasonable. However, when we simulated the fecundity of a TB exposed FHM, we set the plasma VTG concentration prior to exposure to the average plasma VTG concentration of the control FHMs, and the VTG concentration after the start of exposure to the one measured at the end of the 21-day test. As a result, prior to exposure, all FHMs had a uniform VTG concentration, and after the start of exposure, plasma VTG concentrations in each exposed FHM changed sharply. In reality, prior to exposure, different FHMs have different VTG concentrations (e.g., plasma VTG concentrations in the control FHMs ranged from 0.12 to 0.24 nmol/μL). Similarly, after the start of the exposure, VTG concentrations in reality probably changed as a function of time. For example, as shown by Seki et al. (2006), plasma VTG concentrations in spawning fish exposed to TB were lower on day 14 than on day 21. Similarly, time-course studies by Villeneuve et al. (2009b) and Ankley et al. (2009b) showed gradual declines, rather than an abrupt decrease, in average plasma VTG concentrations occurring over the first 4-8 d of exposure to EDCs that inhibit aromatase activity. Hence, the fixed VTG concentration for each exposed FHM in our simulations may overestimate or underestimate the plasma concentration of VTG available for oocyte growth. Thus, having a time course of plasma VTG concentrations would likely improve the model predictions, which could be achieved by connecting the oocyte growth dynamics model to other models predicting plasma VTG concentrations as a function a time (Murphy et al., 2009).

4.4.3 Future Work

In vertebrates, such as fish, oocyte development is under the regulation of multiple hormones (e.g., follicle-stimulating hormone, luteinizing hormone, 17β-estradiol, and 17α, 20β-dihydroxy-4-pregnen-3-one), and oocytes at different developmental stages provide different feedback signals to the regulatory system (Kim et al., 2006; Schulz et al., 2001). In synchronous spawners, hormone levels and feedback signals are based

upon the state of one oocyte batch (Yaron et al., 2003). However, in asynchronous spawners, hormone levels must meet the combined requirements of multiple oocyte batches, and these different batches may provide different biochemical feedback signals, making the regulation more complicated. Thus far, in asynchronous spawning fish the regulatory hormone dynamics are not understood fully.

Our oocyte growth dynamics model simplifies the mechanisms controlling oocyte development in FHMs leaving hormonal regulations to future work. For example, we do not know the mechanism controlling oocyte recruitment in FHMs, and assumed that oocyte recruitment size and interval followed the distributions of clutch size and spawning interval, respectively. Similarly, we did not include atresia because of a shortage of quantitative information. In the future, once quantitative information on these processes are available, we should be able to substitute the present elements (e.g., the distributions of clutch size and spawning interval) or add in new factors (e.g., the mechanism controlling atresia) that interact with oocyte growth and development dynamically.

A study by Murphy et al. (2009) linked a physiologically-based model in Atlantic croaker to a linear statistical model relating fecundity to relative VTG concentration in FHMs (Miller et al., 2007). That study represents a very good example of connecting two computational models. However, as stated by Murphy et al., "*VTG concentration is in a state of flux"*, so assuming a simple direct relationship between fecundity and VTG concentration measured or predicted at a certain time point might introduce extra errors into model predictions. Furthermore, we speculate that there might be a delay in the effects of changes in VTG on fecundity because both VTG uptake and oocyte spawning are dynamic processes, i.e., the present plasma VTG concentration may not affect a clutch of oocytes currently being spawned. If our oocyte growth dynamics model was linked to the model, VTG concentrations would be input as a continuous function of time, and the effects of VTG on fecundity could be predicted dynamically.

It would be valuable to connect our oocyte dynamics model to the physiologically-based computational model for the HPG axis in female FHMs described

in chapter 3. The HPG axis model predicts plasma VTG concentrations as a function a time in both unexposed and EDC-exposed female FHMs. The plasma VTG concentrations can serve as connectors, which can be outputs from the HPG axis model and inputs to the oocyte growth dynamics model. As a result, the model connection would allow us to predict the EDC effects on fecundity directly. It is a part of our research plan to integrate the physiologically based model in female FHMs with the oocyte dynamics model in the future.

The algorithm developed to simulate oocyte growth in FHMs can be adapted and applied to other asynchronous and synchronous spawning fish. For asynchronous spawning fish, the fish-specific parameters (e.g., oocyte recruitment size, oocyte recruitment interval, and critical size for spawning) would need to be modified for the fish species of interest. For synchronous spawning fish, after assigning fish-specific values to oocyte recruitment size and critical size for oocytes to spawn, the model algorithm can be used to simulate one batch of oocytes.

In summary, our oocyte growth dynamics model links plasma VTG concentration to fecundity in FHMs, which connects a molecular biomarker of EDC exposure with reproductive effects in individuals and populations. This is important, because a greater number of toxicological studies are evaluating changes in molecular-level endpoints, whereas ecological risk assessments focus on endpoints (e.g., fecundity) that affect a population (Forbes et al., 2006). In addition, our oocyte growth dynamics model presents a novel algorithm for oocyte growth and spawning that can be adapted and applied to other fish species including both asynchronous and synchronous spawners. Linking the model to a physiologically-based model of the HPG axis would enable research on hormone regulation of oocyte development, and provide additional connections between EDC effects at a molecular level and effects at the individual level in order to contribute to ecological risk assessment.

REFERENCE

Amano, M, Ikuta, K, Kitamura, S, Aida, K (1997) The maturation of the salmon GnRH system and its regulation by gonadal steroids in masu salmon. *Fish Physiol Biochem,* 17(1): 63.

Ankley, GT, Bencic, DC, Breen, MS, Collette, TW, Conolly, RB, Denslow, ND, Edwards, SW, Ekman, DR, Garcia-Reyero, N, Jensen, KM, Lazorchak, JM, Martinovic, D, Miller, DH, Perkins, EJ, Orlando, EF, Villeneuve, DL, Wang, R-L, Watanabe, KH (2009a) Endocrine disrupting chemicals in fish: Developing exposure indicators and predictive models of effects based on mechanism of action. *Aquat Toxicol,* 92(3): 168.

Ankley, GT, Bencic, DC, Cavallin, JE, Jensen, KM, Kahl, MD, Makynen, EA, Martinovic, D, Mueller, ND, Wehmas, LC, Villeneuve, DL (2009b) Dynamic nature of alterations in the endocrine system of fathead minnows exposed to the fungicide prochloraz. *Toxicol Sci*, 112(2): 344-353.

Ankley, GT, Jensen, KM, Durhan, EJ, Makynen, EA, Butterworth, BC, Kahl, MD, Villeneuve, DL, Linnum, A, Gray, LE, Cardon, M, Wilson, VS (2005a) Effects of two fungicides with multiple modes of action on reproductive endocrine function in the fathead minnow (*Pimephales promelas*). *Toxicol Sci,* 86(2): 300-308.

Ankley, GT, Kahl, MD, Jensen, KM, Hornung, MW, Korte, JJ, Makynen, EA, Leino, RL (2002) Evaluation of the aromatase inhibitor fadrozole in a short-term reproduction assay with the fathead minnow (*Pimephales promelas*). *Toxicol Sci,* 67(1): 121-130.

Ankley, GT, Jensen, KM, Kahl, MD, Korte, JJ, Makynen, EA (2001) Description and evaluation of a short-term reproduction test with the fathead minnow (*Pimephales promelas*). *Environ Toxicol Chem,* 20(6): 1276-1290.

Ankley, GT, Jensen, KM, Makynen, EA, Kahl, MD, Korte, JJ, Hornung, MW, Henry, TR, Denny, JS, Leino, RL, Wilson, VS, Cardon, MC, Hartig, PC, Gray, LE (2003) Effects of the androgenic growth promoter 17-beta-trenbolone on fecundity and reproductive endocrinology of the fathead minnow. *Environ Toxicol Chem,* 22(6): 1350-1360.

Ankley, GT, Johnson, RD (2004) Small fish models for identifying and assessing the effects of endocrine-disrupting chemicals. *Ilar J,* 45(4): 469-483.

Ankley, GT, Kuehl, DW, Kahl, MD, Jensen, KM, Linnum, A, Leino, RL, Villeneuvet, DA (2005b) Reproductive and developmental toxicity and bioconcentration of perfluorooctanesulfonate in a partial life-cycle test with the fathead minnow (*Pimephales promelas*). *Environ Toxicol Chem,* 24(9): 2316-2324.

Ankley, GT, Villeneuve, DL (2006) The fathead minnow in aquatic toxicology: past, present and future. *Aquat Toxicol,* 78(1): 91-102.

Artemenko, IP, Zhao, D, Hales, DB, Hales, KH, Jefcoate, CR (2001) Mitochondrial processing of newly synthesized steroidogenic acute regulatory protein (StAR), but not total StAR, mediates cholesterol transfer to cytochrome P450 side chain cleavage enzyme in adrenal cells. *J Biol Chem,* 276(49): 46583-46596.

Antonopoulou, E, Swanson, P, Mayer, I, Borg, B (1999) Feedback control of gonadotropins in Atlantic salmon, Salmo salar, male parr.II. Aromatase inhibitor and androgen effects. *Gen Comp Endocrinol,* 114(1): 142-150.

Arukwe, A (2008) Steroidogenic acute regulatory (StAR) protein and cholesterol side-chain cleavage (P450scc)-regulated steroidogenesis as an organ-specific

molecular and cellular target for endocrine disrupting chemicals in fish. *Cell Biol Toxicol,* 24(6): 527.

Artemenko, IP, Zhao, D, Hales, DB, Hales, KH, Jefcoate, CR (2001) Mitochondrial processing of newly synthesized steroidogenic acute regulatory protein (StAR), but not total StAR, mediates cholesterol transfer to cytochrome P450 side chain cleavage enzyme in adrenal cells. *J Biol Chem,* 276(49): 46583-46596.

Barton, HA, Andersen, ME (1998) A model for pharmacokinetics and physiological feedback among hormones of the testicular-pituitary axis in adult male rats: A framework for evaluating effects of endocrine active compounds. *Toxicol Sci,* 45(2): 174-187.

Blom, MJ, Wassink, MG, Kloosterboer, HJ, Ederveen, AG, Lambert, JG, Goos, HJ (2001) Metabolism of estradiol, ethynylestradiol, and moxestrol in rat uterus, vagina, and aorta: influence of sex steroid treatment. *Drug Metab Dispos,* 29(1): 76-81.

Bois, FY, Maszle, DR (1997) MCSim: A Monte Carlo Simulation Program. *J Stat Softw,* 2(9): 1-56.

Bois, FY, Gelman, A, Jiang, J, Maszle, DR, Zeise, L, Alexeef, G (1996a) Population toxicokinetics of tetrachloroethylene. *Arch Toxicol,* 70: 347-355.

Bois, FY, Jackson, ET, Pekari, K, Smith, MT (1996b) Population toxicokinetics of benzene. *Environ Health Perspect,* 104(Supplement 6): 1405-1411.

Breen, MS, Villeneuve, DL, Breen, M, Ankley, GT, Conolly, RB (2007) Mechanistic computational model of ovarian steroidogenesis to predict biochemical responses to endocrine active compounds. *Ann Biomed Eng,* 35(6): 970-981.

Bretveld, R, Thomas, C, Scheepers, P, Zielhuis, G, Roeleveld, N (2006) Pesticide exposure: the hormonal function of the female reproductive system disrupted? *Reprod Biol Endocrinol,* 4(1): 30.

Brian, JV, Harris, CA, Scholze, M, Backhaus, T, Booy, P, Lamoree, M, Pojana, G, Jonkers, N, Runnalls, T, Bonfa, A, Marcomini, A, Sumpter, JP (2005b) Accurate prediction of the response of freshwater fish to a mixture of estrogenic chemicals. *Environ Health Perspect,* 113(6): 721-728.

Brian, JV, Harris, CA, Scholze, M, Kortenkamp, A, Booy, P, Lamoree, M, Pojana, G, Jonkers, N, Marcomini, A, Sumpter, JP (2007) Evidence of estrogenic mixture effects on the reproductive performance of fish. *Environ Sci Technol,* 41(1): 337-344.

Brill, R, Cousins, K, Jones, D (1998) Blood volume, plasma volume and circulation time in a high-energy-demand teleost, the yellowfin tuna (*Thunnus albacares*). *J Exp Biol,* 201(12): 647-654.

Brion, F, Tyler, CR, Palazzi, X, Laillet, B, Porcher, JM, Garric, J, Flammarion, P (2004) Impacts of 17 beta-estradiol, including environmentally relevant concentrations, on reproduction after exposure during embryo-larval-, juvenile- and adult-life stages in zebrafish (*Danio rerio*). *Aquat Toxicol,* 68(3): 193-217.

Burgess, LH, Handa, RJ (1993) Hormonal regulation of androgen receptor mRNA in the brain and anterior pituitary gland of the male rat. *Brain Res Mol Brain Res,* 19(1-2): 31-38.

Burnstein, KL (2005) Regulation of androgen receptor levels: implications for prostate cancer progression and therapy. *J Cell Biochem,* 95(4): 657-669.

Butala, H, Metzger, C, Rimoldi, J, Willett, KL (2004) Microsomal estrogen metabolism in channel catfish. *Mar Environ Res,* 58(2-5): 489.

Callard, GV (1992) Autocrine and paracrine role of steroids during spermatogenesis: Studies in *Squalus acanthias* and *Necturus maculosus*. *J Exp Zool,* 261(2): 132-142.

Callard, GV, Tchoudakova, AV, Kishida, M, Wood, E (2001) Differential tissue distribution, developmental programming, estrogen regulation and promoter characteristics of cyp19 genes in teleost fish. *J Steroid Biochem Mol Biol,* 79(1-5): 305-314.

Campbell, B, Dickey, J, Beckman, B, Young, G, Pierce, A, Fukada, H, Swanson, P (2006) Previtellogenic oocyte growth in salmon: relationships among body growth, plasma insulin-like growth factor-1, estradiol-17beta, follicle-stimulating hormone and expression of ovarian genes for insulin-like growth factors, steroidogenic-acute regulatory protein and receptors for gonadotropins, growth hormone, and somatolactin. *Biol Reprod,* 75(1): 34-44.

Carson, R (1962) *Silent Spring.* Houghton Mifflin Harcourt.

Charles, RT, John, PS, Niall, RB (1988) In vivo ovarian uptake and processing of vitellogenin in the rainbow trout, *Salmo gairdneri*. *J Exp Zool,* 246(2): 171-179.

Colborn, T, vom Saal, FS, Soto, AM (1993) Developmental effects of endocrine-disrupting chemicals in wildlife and humans. *Environ Health Perspect,* 101(5): 378-384.

Coward, K, Bromage, NR (1998) Histological classification of oocyte growth and the dynamics of ovarian recrudescence in Tilapia zillii. *J Fish Biol,* 53(2): 285-302.

Crain, DA, Janssen, SJ, Edwards, TM, Heindel, J, Ho, S-m, Hunt, P, Iguchi, T, Juul, A, McLachlan, JA, Schwartz, J, Skakkebaek, N, Soto, AM, Swan, S, Walker, C, Woodruff, TK, Woodruff, TJ, Giudice, LC, Guillette Jr, LJ (2008) Female reproductive disorders: the roles of endocrine-disrupting compounds and developmental timing. *Fertil Steril,* 90(4): 911.

Crim, LW, Arnaud, RS, Lavoie, M, Labrie, F (1988) A study of LH-RH receptors in the pituitary gland of the winter flounder (*Pseudopleuronectes americanus Walbaum*). *Gen Comp Endocrinol,* 69(3): 372-377.

Crisp, TM, Clegg, ED, Cooper, RL, Wood, WP, Anderson, DG, Baetcke, KP, Hoffmann, JL, Morrow, MS, Rodier, DJ, Schaeffer, JE, Touart, LW, Zeeman, MG, Patel, YM (1998) Environmental endocrine disruption: an effects assessment and analysis. *Environ Health Perspect,* 106 Suppl 1: 11-56.

Denny, JS, Tapper, MA, Schmieder, PK, Hornung, MW, Jensen, KM, Ankley, GT, Henry, TR (2005) Comparison of relative binding affinities of endocrine active compounds to fathead minnow and rainbow trout estrogen receptors. *Environ Toxicol Chem,* 24(11): 2948.

Desbrow, C, Routledge, EJ, Brighty, GC, Sumpter, JP, Waldock, M (1998) Identification of estrogenic chemicals in STW effluent. 1. Chemical fractionation and in vitro biological screening. *Environl Sci Tech,* 32(11): 1549-1558.

Durhan, EJ, Lambright, CS, Makynen, EA, Lazorchak, J, Hartig, PC, Wilson, VS, Gray, LE, Ankley, GT (2006) Identification of metabolites of trenbolone acetate in androgenic runoff from a beef feedlot. *Environ Health Perspect,* 114 Suppl 1: 65-68.

Ekman, DR, Collette, TW, Teng, Q, Ankley, GT, Jensen, KM, Kahl, MD, Villeneuve, DL (2006) A metabolomic approach to understanding endocrine disruption in fathead minnow. *Second Scientific Meeting of the Metabolomics Society* Boston, MA: Second Scientific Meeting of the Metabolomics Society.

Ekman, DR, Teng, Q, Villeneuve, DL, Kahl, MD, Jensen, KM, Durhan, EJ, Ankley, GT, Collette, TW (2008) Investigating compensation and recovery of fathead minnow (*Pimephales promelas*) exposed to 17α-ethynylestradiol with metabolite profiling. *Environ Sci Technol,* 42(11): 4188-4194.

Enciso, G, Sontag, ED (2004) On the stability of a model of testosterone dynamics. *J Math Biol,* 49(6): 627-634.

Ericson, JF, Laenge, R, Sullivan, DE (2002a) Comment on "Pharmaceuticals, Hormones, and Other Organic Wastewater Contaminants in U.S. Streams, 1999-2000: A National Reconnaissance". *Environ Sci Technol,* 36(18): 4005-4006.

Ericson, JF, Laenge, R, Sullivan, DE (2002b) Comment on "Pharmaceuticals, hormones, and other organic wastewater contaminants in U.S. streams, 1999-2000: a national reconnaissance". *Environ Sci Technol,* 36(18): 4005-4006; author reply 4007-4008.

Fenton, SE (2006) Endocrine-disrupting compounds and mammary gland development: early exposure and later life consequences. *Endocrinology,* 147(6 Suppl): S18-24.

Filby, AL, Neuparth, T, Thorpe, KL, Owen, R, Galloway, TS, Tyler, CR (2007a) Health impacts of estrogens in the environment, considering complex mixture effects. *Environ Health Perspect,* 115(12): 1704-1710.

Filby, AL, Thorpe, KL, Maack, G, Tyler, CR (2007b) Gene expression profiles revealing the mechanisms of anti-androgen-and estrogen-induced feminization in fish. *Aquat Toxicol,* 81(2): 219-231.

Filby, AL, Tyler, CR (2005) Molecular characterization of estrogen receptors 1, 2a, and 2b and their tissue and ontogenic expression profiles in fathead minnow (*Pimephales promelas*). *Biol Reprod,* 73(4): 648-662.

Flouriot, G, Pakdel, F, Ducouret, B, Ledrean, Y, Valotaire, Y (1997) Differential regulation of two genes implicated in fish reproduction: vitellogenin and estrogen receptor genes. *Mol Reprod Dev,* 48(3): 317-323.

Flouriot, G, Pakdel, F, Valotaire, Y (1996) Transcriptional and post-transcriptional regulation of rainbow trout estrogen receptor and vitellogenin gene expression. *Mol Cell Endocrinol,* 124(1-2): 173-183.

Folmar, LC, Hemmer, MJ, Denslow, ND, Kroll, K, Chen, J, Cheek, A, Richman, H, Meredith, H, Grau, EG (2002) A comparison of the estrogenic potencies of

estradiol, ethynylestradiol, diethylstilbestrol, nonylphenol and methoxychlor in vivo and in vitro. *Aquat Toxicol,* 60(1-2): 101-110.

Foradori, CD, Weiser, MJ, Handa, RJ (2008) Non-genomic actions of androgens. *Front Neuroendocrinol,* 29(2): 169-181.

Forbes, VE, Palmqvist, A, Bach, L (2006) The use and misuse of biomarkers in ecotoxicology. *Environ Toxicol Chem,* 25(1): 272-280.

Gale, WF, Buynak, GL (1982) Fecundity and Spawning Frequency of the Fathead Minnow--A Fractional Spawner. *Trans Am Fish Soc,* 111(1): 35-40.

Gale, WL, Patino, R, Maule, AG (2004b) Interaction of xenobiotics with estrogen receptors alpha and beta and a putative plasma sex hormone-binding globulin from channel catfish (*Ictalurus punctatus*). *Gen Comp Endocrinol,* 136(3): 338-345.

Garcia-Reyero, N, Kroll, K, Liu, L, Orlando, E, Watanabe, K, Sepulveda, M, Villeneuve, D, Perkins, E, Ankley, G, Denslow, N (2009) Gene expression responses in male fathead minnows exposed to binary mixtures of an estrogen and antiestrogen. *BMC Genomics,* 10(1): 308.

Garcia-Reyero, N, Villeneuve, DL, Kroll, KJ, Liu, L, Orlando, EF, Watanabe, KH, Sepulveda, MS, Ankley, GT, Denslow, ND (2009) Expression signatures for a model androgen and antiandrogen in the fathead minnow (*Pimephales promelas*) ovary. *Environ Sci Technol,* 43(7): 2614-2619.

Ge, R-S, Gao, H-B, Nacharaju, VL, Gunsalus, GL, Hardy, MP (1997) Identification of a kinetically distinct activity of 11β-hydroxysteroid dehydrogenase in rat Leydig cells. *Endocrinology,* 138(6): 2435-2442.

Gelman, AJ, Carlin, JB, Stern, HS, Rubin, DB (1995) *Bayesian Data Analysis.* Boca Raton, FL: Chapman & Hall/CRC.

Giusti, RM, Iwamoto, K, Hatch, EE (1995) Diethylstilbestrol revisited: a review of the long-term health effects. *Ann Intern Med,* 122(10): 778-788.

Halm, S, Pounds, N, Maddix, S, Rand-Weaver, M, Sumpter, JP, Hutchinson, TH, Tyler, CR (2002) Exposure to exogenous 17beta-oestradiol disrupts p450aromB mRNA expression in the brain and gonad of adult fathead minnows (*Pimephales promelas*). *Aqua Toxicol,* 60(3-4): 285-299.

Halm, S, Rand-Weaver, M, Sumpter, JP, Tyler, CR (2001) Cloning and molecular characterization of an ovarian-derived (brain-like) P450 aromatase cDNA and development of a competitive RT-PCR assay to quantify its expression in the fathead minnow (*Pimephales promelas*). *Fish Physiol Biochem,* 24(1): 49-62.

Hansson, T, Rafter, J (1983) In vitro metabolism of estradiol-17[beta] by liver microsomes from juvenile rainbow trout, *Salmo gairdneri*. *Gen Comp Endocrinol,* 49(3): 490.

Heinlein, CA, Chang, C (2002) Androgen receptor (AR) coregulators: an overview. *Endocr Rev,* 23(2): 175-200.

Hemmer, MJ, Bowman, CJ, Hemmer, BL, Friedman, SD, Marcovich, D, Kroll, KJ, Denslow, ND (2002) Vitellogenin mRNA regulation and plasma clearance in male sheepshead minnows, (Cyprinodon variegatus) after cessation of exposure to 17 beta-estradiol and p-nonylphenol. *Aquat Toxicol,* 58(1-2): 99-112.

Hemming, JM, Waller, WT, Chow, MC, Denslow, ND, Venables, B (2001) Assessment of the estrogenicity and toxicity of a domestic wastewater effluent flowing through a constructed wetland system using biomarkers in male fathead minnows (*Pimephales promelas* rafinesque, 1820). *Environ Toxicol Chem,* 20(10): 2268-2275.

Hirao, Y, Miyano, T (2008) In vitro growth of mouse oocytes: oocyte size at the beginning of culture influences the appropriate length of culture period. *J Mamm Ova Res,* 25(1): 56-62.

Hoffmann, JL, Torontali, SP, Thomason, RG, Lee, DM, Brill, JL, Price, BB, Carr, GJ, Versteeg, DJ (2006) Hepatic gene expression profiling using Genechips in zebrafish exposed to 17alpha-ethynylestradiol. *Aquat Toxicol,* 79(3): 233-246.

Inoue, S, Nakamura, T, Sekiguchi, T (1970) A theoretical approach to the regulatory mechanism in the brain-hypophyseal-gonadal system with reference to its mathematical modeling and computer simulation. *Endocrinol. Japon.,* 17(6): 567-583.

Jensen, KM, Kahl, MD, Makynen, EA, Korte, JJ, Leino, RL, Butterworth, BC, Ankley, GT (2004) Characterization of responses to the antiandrogen flutamide in a short-term reproduction assay with the fathead minnow. *Aquat Toxicol,* 70(2): 99-110.

Jensen, KM, Korte, JJ, Kahl, MD, Pasha, MS, Ankley, GT (2001) Aspects of basic reproductive biology and endocrinology in the fathead minnow (*Pimephales promelas*). *Comp Biochem Physiol C Toxicol Pharmacol,* 128(1): 127-141.

Jensen, KM, Makynen, EA, Kahl, MD, Ankley, GT (2006) Effects of the feedlot contaminant 17alpha-trenbolone on reproductive endocrinology of the fathead minnow. *Environ Sci Technol,* 40(9): 3112-3117.

Jobling, S, Beresford, N, Nolan, M, Rodgers-Gray, T, Brighty, GC, Sumpter, JP, Tyler, CR (2002a) Altered sexual maturation and gamete production in wild roach (*Rutilus rutilus*) living in rivers that receive treated sewage effluents. *Biol Reprod,* 66(2): 272-281.

Jobling, S, Coey, S, Whitmore, JG, Kime, DE, Van Look, KJW, McAllister, BG, Beresford, N, Henshaw, AC, Brighty, G, Tyler, CR, Sumpter, JP (2002b) Wild intersex roach (*Rutilus rutilus*) have reduced fertility. *Biol Reprod,* 67(2): 515-524.

Jobling, S, Nolan, M, Tyler, CR, Brighty, G, Sumpter, JP (1998) Widespread Sexual Disruption in Wild Fish. *Environ Sci Technol,* 32(17): 2498.

Kagawa, H, Gen, K, Okuzawa, K, Tanaka, H (2003) Effects of luteinizing hormone and follicle-stimulating hormone and insulin-like growth factor-I on aromatase activity and P450 aromatase gene expression in the ovarian follicles of red seabream, Pagrus major. *Biol Reprod,* 68(5): 1562-1568.

Kamei, H, Kaneko, T, Aida, K (2006) Steroidogenic activities of follicle-stimulating hormone in the ovary of Japanese eel, *Anguilla japonica*. *Gen Comp Endocrinol,* 146(2): 83-90.

Kang, IJ, Yokota, H, Oshima, Y, Tsuruda, Y, Yamaguchi, T, Maeda, M, Imada, N, Tadokoro, H, Honjo, T (2002) Effect of 17 beta-estradiol on the reproduction of Japanese medaka (*Oryzias latipes*). *Chemosphere,* 47(1): 71-80.

Kashiwagi, K, Dafeldecker, W, Salhanick, H (1980) Purification and characterization of mitochondrial cytochrome P-450 associated with cholesterol side chain cleavage from bovine corpus luteum. *J Biol Chem,* 255(6): 2606-2611.

Khan, MN, Renaud, RL, Leatherland, JF (1997) Metabolism of Estrogens and Androgens by Embryonic Tissues of Arctic Charr, *Salvelinus alpinus*. *Gen Comp Endocrinol,* 107(1): 118.

Kidd, KA, Blanchfield, PJ, Mills, KH, Palace, VP, Evans, RE, Lazorchak, JM, Flick, RW (2007) Collapse of a fish population after exposure to a synthetic estrogen. *Proc Natl Acad Sci U S A,* 104(21): 8897-8901.

Kim, J (2004) Pharmacokinetics and Pharmacodynamics of Protein Turnover and Production in vivo. *Division of Pharmaceutics, College of Pharmacy* (pp. 225) Columbus: The Ohio State University.

Kim, J, Hayton, WL, Schultz, IR (2006) Modeling the brain-pituitary-gonad axis in salmon. *Mar Environ Res,* 62 Suppl: S426-432.

Korte, JJ, Kahl, MD, Jensen, KM, Pasha, MS, Parks, LG, LeBlanc, GA, Ankley, GT (2000) Fathead minnow vitellogenin: Complementary DNA sequence and messenger RNA and protein expression after 17β-estradiol treatment. *Environ Toxicol Chem,* 19(4): 972-981.

Korte, JJ, Mylchreest, E, Ankley, GT (2004) Comparative evaluation of ELISAs for detecting vitellogenin in the fathead minnow (*Pimephales promelas*) - a response to Tyler et al. *Comp Biochem Physiol C Toxicol Pharmacol,* 138(4): 533-536.

Kumar, RC, Thakur, MK (2004) Androgen receptor mRNA is inversely regulated by testosterone and estradiol in adult mouse brain. *Neurobiol Aging,* 25(7): 925-933.

Labadie, P, Budzinski, H (2005) Determination of steroidal hormone profiles along the Jalle d'Eysines river (near Bordeaux, France). *Environ Sci Tech,* 39(14): 5113-5120.

Laidley, CW, Thomas, P (1994) Partial characterization of a sex-steroid binding-protein in the spotted sea-trout (*Cynoscion nebulosus*). *Biol Reprod,* 51(5): 982-992.

Lange, IG, Daxenberger, A, Meyer, HH (2001) Hormone contents in peripheral tissues after correct and off-label use of growth promoting hormones in cattle: effect of the implant preparations Filaplix-H, Raglo, Synovex-H and Synovex Plus. *Apmis,* 109(1): 53-65.

Lattier, DL, Reddy, TV, Gordon, DA, Lazorchak, JM, Smith, ME, Williams, DE, Wiechman, B, Flick, RW, Miracle, AL, Toth, GP (2002) 17alpha-ethynylestradiol-induced vitellogenin gene transcription quantified in livers of adult males, larvae, and gills of fathead minnows (*Pimephales promelas*). *Environ Toxicol Chem,* 21(11): 2385-2393.

Lazier, CB, Lonergan, K, Mommsen, TP (1985) Hepatic estrogen receptors and plasma estrogen-binding activity in the Atlantic salmon. *Gen Comp Endocrinol,* 57(2): 234-245.

Leino, RL, Jensen, KM, Ankley, GT (2005) Gonadal histology and characteristic histopathology associated with endocrine disruption in the adult fathead minnow (*Pimephales promelas*). *Environ Toxicol Pharmacol,* 19(1): 85.

Li, AP, Hartman, NR, Lu, C, Collins, JM, Strong, JM (1999) Effects of cytochrome P450 inducers on 17alpha-ethinyloestradiol (EE2) conjugation by primary human hepatocytes. *Br J Clin Pharmacol,* 48(5): 733-742.

Lin, H, Berzins, DW, Myers, L, George, WJ, Abdelghani, A, Watanabe, KH (2004) A Bayesian bioaccumulation model of polycyclic aromatic hydrocarbons in crayfish (*Procambarus spp.*). *Environ Toxicol Chem,* 23(9): 2259-2266.

Liney, KE, Hagger, JA, Tyler, CR, Depledge, MH, Galloway, TS, Jobling, S (2006) Health effects in fish of long-term exposure to effluents from wastewater treatment works. *Environ Health Perspect Suppl,* 114(Suppl 1): 81-89.

Markey, CM, Rubin, BS, Soto, AM, Sonnenschein, C (2002) Endocrine disruptors: from Wingspread to environmental developmental biology. *J Steroid Biochem Mol Biol,* 83(1-5): 235-244.

Martinovic, D, Blake, LS, Durhan, EJ, Greene, KJ, Kahl, MD, Jensen, KM, Makynen, EA, Villeneuve, DL, Ankley, GT (2008) Reproductive toxicity of vinclozolin in the fathead minnow: confirming an anti-androgenic mode of action. *Environ Toxicol Chem,* 27(2): 478-488.

Matta, SL, Vilela, DA, Godinho, HP, Franca, LR (2002) The goitrogen 6-n-propyl-2-thiouracil (PTU) given during testis development increases Sertoli and germ cell numbers per cyst in fish: the tilapia (*Oreochromis niloticus*) model. *Endocrinology,* 143(3): 970-978.

Matthews, J, Celius, T, Halgren, R, Zacharewski, T (2000) Differential estrogen receptor binding of estrogenic substances: a species comparison. *J Steroid Biochem Mol Biol,* 74(4): 223-234.

McMillan, D (2007) *Fish Histology: Female Reproductive Systems.* Springer.

Melamed, P, Rosenfeld, H, Elizur, A, Yaron, Z (1998) Endocrine regulation of gonadotropin and growth hormone gene transcription in fish. *Comp Biochem Physiol C Pharmacol Toxicol Endocrinol,* 119(3): 325-338.

Metzler, M, Blaich, G, Tritscher, AM (1990) Role of metabolic activation in the carcinogenicity of estrogens: studies in an animal liver tumor model. *Environ Health Perspect,* 88: 117-121.

Miguel-Queralt, S, Hammond, GL (2008) Sex hormone-binding globulin in fish gills is a portal for sex steroids breached by xenobiotics. *Endocrinology,* 149(9): 4269-4275.

Milla, S, Jalabert, B, Rime, H, Prunet, P, Bobe, J (2006) Hydration of rainbow trout oocyte during meiotic maturation and in vitro regulation by 17,20{beta}-dihydroxy-4-pregnen-3-one and cortisol. *J Exp Biol*, 209(Pt 6): 1147-1156.

Miller, DH, Jensen, KM, Villeneuve, DL, Kahl, MD, Makynen, EA, Durhan, EJ, Ankley, GT (2007) Linkage of biochemical responses to population-level effects: a case study with vitellogenin in the fathead minnow (*Pimephales promelas*). *Environ Toxicol Chem,* 26(3): 521-527.

Miller, WL (1988) Molecular biology of steroid hormone synthesis. *Endocr Rev,* 9(3): 295-318.

Miracle, A, Ankley, G, Lattier, D (2006) Expression of two vitellogenin genes (vg1 and vg3) in fathead minnow (*Pimephales promelas*) liver in response to exposure to steroidal estrogens and androgens. *Ecotoxicol Environ Saf,* 63(3): 337-342.

Miwa, S, Yan, L, Swanson, P (1994) Localization of two gonadotropin receptors in the salmon gonad by in vitro ligand autoradiography. *Biol Reprod,* 50(3): 629-642.

Murphy, CA, Rose, KA, Thomas, P (2005) Modeling vitellogenesis in female fish exposed to environmental stressors: predicting the effects of endocrine disturbance due to exposure to a PCB mixture and cadmium. *Reprod Toxicol,* 19(3): 395-409.

Murphy, CA, Rose, KA, Rahman, MS, Thomas, P (2009) Testing and applying a fish vitellogenesis model to evaluate laboratory and field biomarkers of endocrine disruption in atlantic croaker (*Micropogonias undulatus*) exposed to hypoxia. *Environ Toxicol Chem,* 28(6): 1288-1303.

Myers, SF, Avila, VL (1980) Tritiated 17[beta]-estradiol uptake by the brain and other tissues of the cichlid jewel fish, Hemichromis bimaculatus. *Gen Comp Endocrinol,* 42(2): 203.

Mylchreest, E, Snajdr, S, Korte, JJ, Ankley, GT (2003) Comparison of ELISAs for detecting vitellogenin in the fathead minnow (*Pimephales promelas*). *Comp Biochem Physiol C Toxicol Pharmacol,* 134(2): 251-257.

Nagahama, Y (1994) Endocrine regulation of gametogenesis in fish. *Int J Dev Biol,* 38(2): 217-229.

Nagahama, Y, Adachi, S (1985) Identification of maturation-inducing steroid in a teleost, the amago salmon (*Oncorhynchus rhodurus*). *Dev Biol,* 109(2): 428-435.

Nagahama, Y, Yoshikuni, M, Yamashita, M, Tanaka, M (1994) Regulation of oocyte maturation in fish. In: Sherwood, NM, Hew, CL (Eds.) *Mol Endocrinol Fish* (pp. 393-439) San Diego: Academic Press.

Nagahama, Y, Yoshikuni, M, Yamashita, M, Tokumoto, T, Katsu, Y (1995) Regulation of oocyte growth and maturation in fish. *Curr Top Dev Biol,* 30: 103-145.

Nagahama, Y (1997) 17 alpha,20 beta-dihydroxy-4-pregnen-3-one, a maturation-inducing hormone in fish oocytes: mechanisms of synthesis and action. *Steroids,* 62(1): 190-196.

Nagahama, Y, Yamashita, M (2008) Regulation of oocyte maturation in fish. *Dev, Growth Differ,* 50(s1): S195-S219.

Nichols, JW, Fitzsimmons, PN, Whiteman, FW, Dawson, TD, Babeu, L, Juenemann, J (2004) A physiologically based toxicokinetic model for dietary uptake of hydrophobic organic compounds by fish: I. Feeding studies with 2,2',5,5'-tetrachlorobiphenyl. *Toxicol Sci,* 77(2): 206-218.

Nichols, JW, McKim, JM, Andersen, ME, Gargas, ML, Clewell, HJ, 3rd, Erickson, RJ (1990) A physiologically based toxicokinetic model for the uptake and disposition of waterborne organic chemicals in fish. *Toxicol Appl Pharmacol,* 106(3): 433-447.

Nichols, JW, McKim, JM, Lien, GJ, Hoffman, AD, Bertelsen, SL, Elonen, CM (1996) A physiologically based toxicokinetic model for dermal absorption of organic chemicals by fish. *Fundam Appl Toxicol,* 31(2): 229-242.

Norris, DO (1997) *Vertebrate Endocrinology.* San Diego: Academic Press.

Nunez, BS, Evans, AN (2007) Hormonal regulation of the steroidogenic acute regulatory protein (StAR) in gonadal tissues of the Atlantic croaker (*Micropogonias undulatus*). *Gen Comp Endocr,* 150(3): 495-504.

Ohkimoto, K, Sugahara, T, Sakakibara, Y, Suiko, M, Liu, MY, Carter, G, Liu, MC (2003) Sulfonation of environmental estrogens by zebrafish cytosolic sulfotransferases. *Biochem Biophys Res Commun,* 309(1): 7-11.

Orlando, EF, Kolok, AS, Binzcik, GA, Gates, JL, Horton, MK, Lambright, CS, Gray, LE, Jr., Soto, AM, Guillette, LJ, Jr. (2004) Endocrine-disrupting effects of cattle

feedlot effluent on an aquatic sentinel species, the fathead minnow. *Environ Health Perspect,* 112(3): 353-358.

Orn, S, Yamani, S, Norrgren, L (2006) Comparison of vitellogenin induction, sex ratio, and gonad morphology between zebrafish and Japanese medaka after exposure to 17alpha-ethinylestradiol and 17beta-trenbolone. *Arch Environ Contam Toxicol,* 51(2): 237-243.

Panter, GH, Thompson, RS, Sumpter, JP (2000) Intermittent exposure of fish to estradiol. *Environ Sci Tech,* 34(13): 2756-2760.

Parks, LG, Cheek, AO, Denslow, ND, Heppell, SA, McLachlan, JA, LeBlanc, GA, Sullivan, CV (1999) Fathead minnow (*Pimephales promelas*) vitellogenin: purification, characterization and quantitative immunoassay for the detection of estrogenic compounds. *Comp Biochem Physiol C Pharmacol Toxicol Endocrinol,* 123(2): 113-125.

Parks, LG, LeBlanc, GA (1998a) Involvement of Multiple Biotransformation Processes in the Metabolic Elimination of Testosterone by Juvenile and Adult Fathead Minnows (*Pimephales promelas*). *Gen Comp Endocrinol,* 112(1): 69.

Parks, LG, LeBlanc, GA (1998b) Involvement of multiple biotransformation processes in the metabolic elimination of testosterone by juvenile and adult fathead minnows (Pimephales promelas). *Gen Comp Endocrinol,* 112(1): 69-79.

Parrott, JL, Blunt, BR (2005) Life-cycle exposure of fathead minnows (*Pimephales promelas*) to an ethinylestradiol concentration below 1 ng/L reduces egg fertilization success and demasculinizes males. *Environ Toxicol,* 20(2): 131-141.

Parsons, HM, Ekman, DR, Collette, TW, Viant, MR (2008) Spectral relative standard deviation: A practical benchmark in metabolomics. *The Analyst,* submitted.

Pasmanik, M, Callard, G (1986) Characteristics of a testosterone-estradiol binding globulin (TEBG) in goldfish serum. *Biol Reprod,* 35(4): 838-845.

Patino, R, Yoshizaki, G, Thomas, P, Kagawa, H (2001) Gonadotropic control of ovarian follicle maturation: the two-stage concept and its mechanisms. *Comp Biochem Physiol B Biochem Mol Biol,* 129(2-3): 427-439.

Pawlowski, S, van Aerle, R, Tyler, CR, Braunbeck, T (2004) Effects of 17alpha-ethinylestradiol in a fathead minnow (Pimephales promelas) gonadal recrudescence assay. *Ecotoxicol Environ Saf,* 57(3): 330-345.

Perazzolo, LM, Coward, K, Davail, B, Normand, E, Tyler, CR, Pakdel, F, Schneider, WJ, Le Menn, F (1999) Expression and localization of messenger ribonucleic acid for the vitellogenin receptor in ovarian follicles throughout oogenesis in the rainbow trout, *Oncorhynchus mykiss*. *Biol Reprod,* 60(5): 1057-1068.

Petkam, R, Renaud, RL, Freitas, AMMS, Canario, AVM, Leatherland, JF (2002) In vitro metabolism of progesterone, androgens and estrogens by rainbow trout embryos. *Fish Physiol Biochem,* 27(1): 117.

Plouffe, L, Luxenberg, SN (1992) Biological modeling on a microcomputer using standard spreadsheet and equation solver programs - the hypothalamic pituitary ovarian axis as an example. *Comput Biomed Res,* 25(2): 117-130.

Plowchalk, DR, Teeguarden, J (2002) Development of a physiologically based pharmacokinetic model for estradiol in rats and humans: a biologically motivated quantitative framework for evaluating responses to estradiol and other endocrine-active compounds. *Toxicol Sci,* 69(1): 60-78.

Ribeiro, C, Pardal, M, Martinho, F, Margalho, R, Tiritan, M, Rocha, E, Rocha, M (2008) Distribution of endocrine disruptors in the Mondego River estuary, Portugal. *Environ Monit Assess,* ePub.

Robinson, DE, Balter, NJ, Schwartz, SL (1992) A physiologically based pharmacokinetic model for nicotine and cotinine in man. *J Pharmacokinet and Biopharm,* 20(6): 591-609.

Purdom, CE, Hardiman, PA, Bye, VVJ, Eno, NC, Tyler, CR, Sumpter, JP (1994) Estrogenic Effects of Effluents from Sewage Treatment Works. *Chem Ecol,* 8(4): 275 - 285.

Safe, S (2004) Endocrine disruptors and human health: is there a problem. *Toxicol,* 205(1-2): 3.

Sawyer, SJ, Gerstner, KA, Callard, GV (2006) Real-time PCR analysis of cytochrome P450 aromatase expression in zebrafish: Gene specific tissue distribution, sex differences, developmental programming, and estrogen regulation. *Gen Comp Endocrinol,* 147(2): 108-117.

Schiffer, B, Daxenberger, A, Meyer, K, Meyer, HH (2001) The fate of trenbolone acetate and melengestrol acetate after application as growth promoters in cattle: environmental studies. *Environ Health Perspect,* 109(11): 1145-1151.

Schlosser, PM, Borghoff, SJ, Coldham, NG, David, JA, Ghosh, SK (2006) Physiologically-based pharmacokinetic modeling of genistein in rats, part I: Model development. *Risk Anal,* 26(2): 483-500.

Schmid, T, Gonzalez-Valero, J, Rufli, H, Dietrich, DR (2002) Determination of vitellogenin kinetics in male fathead minnows (*Pimephales promelas*). *Toxicol Lett,* 131(1-2): 65-74.

Schultz, IR, Orner, G, Merdink, JL, Skillman, A (2001) Dose-response relationships and pharmacokinetics of vitellogenin in rainbow trout after intravascular administration of 17 alpha-ethynylestradiol. *Aquat Toxicol,* 51(3): 305-318.

Schulz, R, Bosma, P, Zandbergen, M, Van der Sanden, M, Van Dijk, W, Peute, J, Bogerd, J, Goos, H (1993) Two gonadotropin-releasing hormones in the African catfish, *Clarias gariepinus*: localization, pituitary receptor binding, and gonadotropin release activity. *Endocrinology,* 133(4): 1569-1577.

Schulz, RW, de Franca, LR, Lareyre, JJ, LeGac, F, Chiarini-Garcia, H, Nobrega, RH, Miura, T (2010) Spermatogenesis in fish. *Gen Comp Endocrinol,* 165(3): 390-411.

Schulz, RW, Vischer, HF, Cavaco, JE, Santos, EM, Tyler, CR, Goos, HJ, Bogerd, J (2001) Gonadotropins, their receptors, and the regulation of testicular functions in fish. *Comp Biochem Physiol B Biochem Mol Biol,* 129(2-3): 407-417.

Scott, E, Gilbert (2000) *Developmental Biology.* Sinauer Associates, Inc.

Seki, M, Fujishima, S, Nozaka, T, Maeda, M, Kobayashi, K (2006) Comparison of response to 17 beta-estradiol and 17 beta-trenbolone among three small fish species. *Environ Toxicol Chem,* 25(10): 2742-2752.

Seki, M, Yokota, H, Matsubara, H, Tsuruda, Y, Maeda, M, Tadokoro, H, Kobayashi, K (2002) Effect of ethinylestradiol on the reproduction and induction of vitellogenin and testis-ova in medaka (*Oryzias latipes*). *Environ Toxicol Chem,* 21(8): 1692-1698.

Senthilkumaran, B, Yoshikuni, M, Nagahama, Y (2004) A shift in steroidogenesis occurring in ovarian follicles prior to oocyte maturation. *Mol Cell Endocrinol,* 215(1-2): 11-18.

Shikita, M, Hall, PF (1973) Cytochrome P-450 from bovine adrenocortical mitochondria: an enzyme for the side chain cleavage of cholesterol. I. Purification and properties. *J Biol Chem,* 248(16): 5598-5604.

Snowberger, EA, Stegeman, JJ (1987) Patterns and regulation of estradiol metabolism by hepatic microsomes from two species of marine teleosts. *Gen Comp Endocrinol,* 66(2): 256-265.

So, YP, Idler, DR, Truscott, B, Walsh, JM (1985) Progestogens, androgens and their glucuronides in the terminal stages of oocyte maturation in landlocked Atlantic salmon. *J Steroid Biochem,* 23(5A): 583-591.

Sone, K, Hinago, M, Itamoto, M, Katsu, Y, Watanabe, H, Urushitani, H, Tooi, O, Guillette, LJ, Iguchi, T (2005) Effects of an androgenic growth promoter 17 beta-trenbolone on masculinization of mosquitofish (Gambusia affinis affinis). *Gen Comp Endocrinol,* 143(2): 151.

Specker, JL, Sullivan, CV (1994) Vitellogenesis in fishes: status and perspectives. *Perspect Comp Endocrinol*: 304-315.

Sperry, TS, Thomas, P (1999) Characterization of two nuclear androgen receptors in Atlantic croaker: comparison of their biochemical properties and binding specificities. *Endocrinology,* 140(4): 1602-1611.

Stifani, S, Le Menn, F, Rodriguez, JN, Schneider, WJ (1990) Regulation of oogenesis: the piscine receptor for vitellogenin. *Biochim Biophys Acta,* 1045(3): 271-279.

Sumpter, JP, Jobling, S (1995) Vitellogenesis as a biomarker for estrogenic contamination of the aquatic environment. *Environ Health Perspect,* 103 Suppl 7: 173-178.

Sumpter, JP, Johnson, AC (2005) Lessons from endocrine disruption and their application to other issues concerning trace organics in the aquatic environment. *Environ Sci Tech,* 39(12): 4321-4332.

Swanson, P, Dickey, JT, Campbell, B (2003) Biochemistry and physiology of fish gonadotropins. *Fish Physiol Biochem,* 28(1): 53.

Teeguarden, JG, Barton, HA (2004) Computational modeling of serum-binding proteins and clearance in extrapolations across life stages and species for endocrine active compounds. *Risk Anal,* 24(3): 751-770.

Tollefsen, KE, Ovrevik, J, Stenersen, J (2004) Binding of xenoestrogens to the sex steroid-binding protein in plasma from Arctic charr (*Salvelinus alpinus L.*). *Comp Biochem Physiol C Toxicol Pharmacol,* 139(1-3): 127-133.

Tyler, CR, van Aerle, R, Santos, EM (2004) ELISAs for detecting vitellogenin in the fathead minnow (Pimephales promelas)--a critical analysis. Response to Mylchreest et al., Comp Biochem Physiol C 134: 251-257, 2003. *Comp Biochem Physiol C Toxicol Pharmaco,* 138(4): 531.

Tyler, CR, Pottinger, TG, Coward, K, Prat, F, Beresford, N, Maddix, S (1997) Salmonid follicle-stimulating hormone (GtH I) mediates vitellogenic development of oocytes in the rainbow trout, *Oncorhynchus mykiss*. *Biol Reprod,* 57(5): 1238-1244.

Tyler, CR, Pottinger, TG, Santos, E, Sumpter, JP, Price, SA, Brooks, S, Nagler, JJ (1996) Mechanisms controlling egg size and number in the rainbow trout, Oncorhynchus mykiss. *Biol Reprod,* 54(1): 8-15.

Tyler, CR, Sumpter, JP (1996) Oocyte growth and development in teleosts. *Rev Fish Biol Fish,* 6(3): 287-318.

Tyler, CR, Sumpter, JP, Kawauchi, H, Swanson, P (1991) Involvement of gonadotropin in the uptake of vitellogenin into vitellogenic oocytes of the rainbow trout, *Oncorhynchus mykiss*. *Gen Comp Endocrinol,* 84(2): 291-299.

Tyler, CR, Sumpter, JP, Witthames, PR (1990) The dynamics of oocyte growth during vitellogenesis in the rainbow trout (*Oncorhynchus mykiss*). *Biol Reprod,* 43(2): 202-209.

Vajda, AM, Barber, LB, Gray, JL, Lopez, EM, Woodling, JD, Norris, DO (2008) Reproductive disruption in fish downstream from an estrogenic wastewater effluent. *Environ Sci Technol,* 42(9): 3407-3414.

Van den Belt, K, Verheyen, R, Witters, H (2003) Effects of 17 alpha-ethynylestradiol in a partial life-cycle test with zebrafish (*Danio rerio*): effects on growth, gonads and female reproductive success. *Sci Total Environ,* 309(1-3): 127-137.

Venkatesh, B, Tan, CH, Kime, DE, Loy, GL, Lam, TJ (1992) Steroid metabolism by ovarian follicles and extrafollicular tissue of the guppy (Poecilia reticulata) during oocyte growth and gestation. *Gen Comp Endocrinol,* 86(3): 378-394.

Verrijdt, G, Haelens, A, Claessens, F (2003) Selective DNA recognition by the androgen receptor as a mechanism for hormone-specific regulation of gene expression. *Mol Genet Metabol,* 78(3): 175-185.

Versonnen, BJ, Janssen, CR (2004) Xenoestrogenic effects of ethinylestradiol in zebrafish (*Danio rerio*). *Environ Toxicol,* 19(3): 198-206.

Villeneuve, DL, Garcia-Reyero, N, Martinovic, D, Mueller, ND, Cavallin, JE, Durhan, EJ, Makynen, EA, Jensen, KM, Kahl, MD, Blake, LS, Perkins, EJ, Ankley, GT (2009a) I. Effects of a dopamine receptor antagonist on fathead minnow, *Pimephales promelas,* reproduction. *Ecotoxicol Environ Saf,* in press.

Villeneuve, DL, Knoebl, I, Kahl, MD, Jensen, KM, Hammermeister, DE, Greene, KJ, Blake, LS, Ankley, GT (2006) Relationship between brain and ovary aromatase activity and isoform-specific aromatase mRNA expression in the fathead minnow (Pimephales promelas). *Aquat Toxicol,* 76(3-4): 353-368.

Villeneuve, DL, Larkin, P, Knoebl, I, Miracle, AL, Kahl, MD, Jensen, KM, Makynen, EA, Durhan, EJ, Carter, BJ, Denslow, ND, Ankley, GT (2007a) A graphical systems model to facilitate hypothesis-driven ecotoxicogenomics research on the teleost brain-pituitary-gonadal axis. *Environ Sci Technol,* 41(1): 321-330.

Villeneuve, DL, Miracle, AL, Jensen, KM, Degitz, SJ, Kahl, MD, Korte, JJ, Greene, KJ, Blake, LS, Linnum, AL, Ankley, GT (2007b) Development of quantitative real-time PCR assays for fathead minnow (*Pimephales promelas*) gonadotropin beta subunit mRNAs to support endocrine disruptor research. *Comp Biochem Physiol C Toxicol Pharmacol,* 145(2): 171-183.

Villeneuve, DL, Mueller, ND, Martinovic, D, Makynen, EA, Kahl, MD, Jensen, KM, Durhan, EJ, Cavallin, JE, Bencic, D, Ankley, GT (2009b) Direct effects, compensation, and recovery in female fathead minnows exposed to a model aromatase inhibitor. *Environ Health Perspect,* 117(4): 624-631.

Villeneuve, DL, Murphy, MB, Kahl, MD, Jensen, KM, Butterworth, BC, Makynen, EA, Durhan, EJ, Linnum, A, Leino, RL, Curtis, LR, Giesy, JP, Ankley, GT (2006) Evaluation of the methoxytriazine herbicide prometon using a short-term fathead minnow reproduction test and a suite of in vitro bioassays. *Environ Toxicol Chem,* 25(8): 2143-2153.

Wallace, RA, Selman, K (1981) Cellular and dynamic aspects of oocyte growth in teleosts. *Amer. Zool.,* 21(2): 325-343.

Watanabe, KH, Jensen, KM, Orlando, EF, Ankley, GT (2007) What is normal? Biological variability in reproductive parameters of unexposed fathead minnows (*Pimephales promelas*). *Comp Biochem Physiol C Toxicol Pharmacol,* 146: 348-356.

Watanabe, KH, Li, Z, Kroll, KJ, Villeneuve, DL, Garcia-Reyero, N, Orlando, EF, Sepulveda, MS, Collette, TW, Ekman, DR, Ankley, GT, Denslow, ND (2009) A computational model of the hypothalamic-pituitary-gonadal axis in male fathead minnows exposed to 17alpha-ethinylestradiol and 17beta-estradiol. *Toxicol Sci,* 109(2): 180-192.

Watanabe, KH, Lin, H, Bart Jr., HL, Martinat, P, Means, JC, Kunas, ML, Grimm, DA (2005) Bayesian estimation of kinetic rate constants in a food web model of polycyclic aromatic hydrocarbon bioaccumulation. *Ecol Model,* 181(2-3): 229-246.

Wilson, VS, Cardon, MC, Gray, LE, Jr., Hartig, PC (2007) Competitive binding comparison of endocrine-disrupting compounds to recombinant androgen receptor

from fathead minnow, rainbow trout, and human. *Environ Toxicol Chem*, 26(9): 1793-1802.

Wilson, VS, Cardon, MC, Thornton, J, Korte, JJ, Ankley, GT, Welch, J, Gray, LE, Jr., Hartig, PC (2004) Cloning and in vitro expression and characterization of the androgen receptor and isolation of estrogen receptor alpha from the fathead Minnow (Pimephales promelas). *Environ Sci Technol*, 38(23): 6314-6321.

Wolf, JC, Dietrich, DR, Friederich, U, Caunter, J, Brown, AR (2004) Qualitative and quantitative histomorphologic assessment of fathead minnow *Pimephales promelas* gonads as an endpoint for evaluating endocrine-active compounds: a pilot methodology study. *Toxicol Pathol*, 32(5): 600-612.

Woodling, JD, Lopez, EM, Maldonado, TA, Norris, DO, Vajda, AM (2006) Intersex and other reproductive disruption of fish in wastewater effluent dominated Colorado streams. *Comp Biochem Physiol C Toxicol Pharmacol*, 144(1): 10-15.

Yaron, Z, Gur, G, Melamed, P, Rosenfeld, H, Elizur, A, Levavi-Sivan, B (2003) Regulation of fish gonadotropins. *Int Rev Cytol*, 225: 131-185.

Ying, GG, Kookana, RS, Kumar, A (2008) Fate of estrogens and xenoestrogens in four sewage treatment plants with different technologies. *Environ Toxicol Chem*, 27(1): 87-94.

Zhao, J, Mak, P, Tchoudakova, A, Callard, G, Chen, S (2001) Different catalytic properties and inhibitor responses of the goldfish brain and ovary aromatase isozymes. *Gen Comp Endocrinol*, 123(2): 180-191.

TABLES

Table 2.1 Summary statistics of baseline data from male fathead minnow (*n* = 70) used in model calibration. SD = standard deviation; GSI = gonadosomatic index, equal to (gonad weight / body weight) × 100; HSI = hepatosomatic index, equal to (liver weight / body weight) × 100; T = plasma testosterone concentration; KT = plasma 11keto-testosterone concentration; E_2 = plasma 17β-estradiol concentration; and VTG = plasma vitellogenin concentration.

Statistics	Body Weight (g)	Gonad Weight (mg)	GSI	Liver Weight (mg)	HSI	T (ng/ml)	KT (ng/ml)	E_2 (ng/ml)	VTG (mg/ml)
Mean	3.80	44	1.15	38	1.39	9.38	33.08	0.50	0.0052
SD	0.85	20	0.38	11	0.21	5.00	20.66	0.37	0.0049
Median	3.78	41	1.06	38	1.44	8.84	29.65	0.40	0.0048
Maximum	5.48	110	2.19	54	1.63	24.12	70.05	1.60	0.0215
Minimum	1.91	11	0.35	20	1.05	2.82	2.49	0.10	0.0004

Table 2.2 Plasma T and VTG concentrations measured in male fathead minnows exposed to nominal water concentrations of 10 or 50 ng EE_2/L for 48 hrs (Garcia-Reyero et al., 2009). T = plasma testosterone concentration; VTG = plasma vitellogenin concentration; SD = standard deviation. The body weight of each fish was measured at the end of the exposure.

Fish ID	Body Weight (g)	T (ng/ml)	VTG (mg/ml)
Nominal water concentration = 50 ng EE_2/L;			
Average measured concentration = 41 ng EE_2/L			
129	3.4	2.5	29
139	3.9	2.2	33
146	5.0	2.3	28
153	3.3	1.9	26
Mean	3.9	2.2	29
SD	0.78	0.2	3.1
Nominal water concentration = 10 ng EE_2/L;			
Average measured concentration = 5.3 ng EE_2/L			
102	2.2	-	12
108	2.8	-	16
115	4.1	-	7.7
124	3.1	-	14
Mean	3.1	-	13
SD	0.79	-	4.3

Table 2.3 Calibrated model input parameters: Prior distributions and posterior distribution summary statistics. * Definition of prior distribution parameters P1 and P2. Lognormal: P1 = geometric mean (exponential of the mean in log-space); P2 = geometric standard deviation (exponential of the standard deviation in log-space, strictly superior to 1). Loguniform: P1 = minimum of the sampling range (real number) in natural space; P2 = maximum of the sampling range in natural space. Uniform: P1 = minimum of the sampling range (real number) in natural space. P2 = maximum of the sampling range in natural space. Inverse gamma: P1 = shape; P2 = scale (both of the parameters are strictly positive).

Parameter description	Symbols	Prior Distribution (P1, P2)*	Reference	Posterior Distribution		
				Mean	Median	95% CIs
Magnitude of LH production (nmol/hr)	Mag_{LH}	Loguniform (5.0e-06, 5.0e-04)	Schulz *et al.* (1993)	2.6e-5	2.6e-5	(9.2 e-6, 4.0e-5)
Dissociation constant of E_2 binding to ER in brain (nM)	$K_{d\_E2ER,\ brn}$	Lognormal (2.5, 3)	Murphy *et al.* (2005)	7.3	2.8	(0.24, 57)
Association rate of E_2 binding to ER in brain (1/nM/hr)	$k_{1\_E2ER,\ brn}$	Lognormal (0.743, 3)	Murphy *et al.* (2005)	1.7	0.84	(0.094, 10)
Association rate of LH binding to LH receptor in gonad (1/nM/hr)	$k_{1\_LHLR,\ gon}$	Lognormal (0.1, 3)	assumed	0.20	0.12	(0.015, 0.87)

Parameter description	Symbols	Prior Distribution (P1, P2)*	Reference	Posterior Distribution		
				Mean	Median	95% CIs
ER background production rate (nM/hr)	$Pbg_{ER,liv}$	Loguniform (5.0e-5, 5.0e-1)	assumed	2.1e-3	2.1e-3	(1.4e-3, 3.1e-3)
Induction rate of LH production by E_2 (1/hr)	$\rho_{LH,brn}$	Loguniform (0.0005, 0.5)	assumed	0.19	0.18	(7.4e-4, 0.47)
Proportionality constant relating bound LH receptor to StAR	$\rho_{STAR,gon}$	Loguniform (1, 100)	assumed	30	22	(1.3, 91)
Proportionality constant relating cholesterol to StAR	$\rho_{Chol,gon}$	Loguniform (10, 10000)	Artemenko *et al.* (2001)	2.6e+3	1.5e+3	(57, 9.0e+3)
Elimination rate constant for E_2 in the "other" compartment (1/hr)	$Kelim_{E2,oth}$	Lognormal (0.1, 3)	Teeguarden and Barton (2004)	0.28	0.28	(0.21, 0.36)
First order rate constant for ER induction in liver (1/hr)	$k_{ER,liv}$	Uniform (0.001, 0.1)	assumed	0.082	0.083	(0.068, 0.096)

Parameter description	Symbols	Prior Distribution (P1, P2)*	Reference	Posterior Distribution		
				Mean	Median	95% CIs
Inhibition constant for T production (nM)	K_T	Loguniform (0.001, 0.5)	assumed	0.014	0.014	(8.8e-3, 0.020)
Concentration of microsomal protein in gonad (mg/L)	D_m_mp_gon	Loguniform (3.1e+1, 3.1e+5)	Measured by D. Villeneuve in female FHM	868	915	(76, 1.6e+3)
Concentration of microsomal protein in brain (mg/L)	D_m_mp_brn	Loguniform (1.8e+2, 1.8e+6)	Measured by D. Villeneuve in female FHM	469	412	(198, 1.0e+3)
Scaling coefficient of Vmax for Vtg production in liver (= Vmax/BodyWeight$^{0.75}$) (nmol/hr/kg$^{0.75}$)	$sc\_Vmax_{Vtg,\ liv}$	Loguniform (1, 1.0e+5)	assumed	216	200	(103, 406)
Hill coefficient of Vtg production in liver	n_{vtg}	Loguniform (2, 10)	based on ER dimerization	3.2	3.2	(2.8, 3.7)

Parameter description	Symbols	Prior Distribution (P1, P2)*	Reference	Posterior Distribution		
				Mean	Median	95% CIs
Partition coefficient of EE_2 (blood to water)	$\lambda_{EE2, bld}$	Lognormal (600, 3)	Kim (2004)	283	238	(103, 740)
Partition coefficient of EE_2 (liver to blood)	$\lambda_{EE2, liv}$	Loguniform (1, 100)	Plowchalk and Teeguarden (2002)	2.8	2.5	(1.0, 6.7)
Scaling coefficient of Vmax for KT production in gonad (= Vmax/number of leydig cells per gonad) (nmol/hr/cell)	sc_Vmax $_{11bHSD, gon}$	Loguniform (4.3e-9, 4.3e-6)	Ge *et al.* (1997)	5.3e-8	5.3e-8	(3.7e-8, 7.0e-8)
Variance of plasma E_2 concentration in natural log space	Var_Ln_CE2tot_pla_ngml	Inverse Gamma (2, 0.56)	Bois *et al.* (1996a)	9.1	9.0	(7.3, 12)
Variance of plasma T concentration in natural log space	Var_Ln_CTtot_pla_ngml	Inverse Gamma (2, 0.41)	Bois *et al.* (1996a)	0.31	0.30	(0.22, 0.42)

Table 2.4 Measured reproductive endpoints (Watanabe *et al.*, 2007) and model predictions for unexposed male fathead minnows. Measured data include 73 male fathead minnows. Model predictions include 8000 values generated using 8000 Markov chain Monte Carlo calibrated parameter sets. T = plasma testosterone concentration; KT = plasma 11-ketotestosterone concentration; E_2 = plasma 17β-estradiol concentration; VTG = plasma vitellogenin concentration; SD = standard deviation.

Reproductive Endpoint (Plasma Concentration)	Measured Data			**Model Predictions**			
	Mean	Median	SD	Mean	Median	SD	95% CI
T (ng/ml)	13	12	7.2	8.6	8.6	0.57	(7.6, 9.9)
KT (ng/ml)	37	35	26	35	35	4.7	(26, 44)
E_2 (ng/ml)	0.38	0.37	0.23	0.20	0.19	0.033	(0.14, 0.27)
VTG (mg/ml)	0.0036	0.0022	0.0038	0.0017	0.0016	0.00061	(0.00080, 0.0032)

Table 2.5 Model parameters treated as constants (n = 62). Default values listed are used by the model unless another value is set by the user.

Parameter description	Symbols	Value	Reference
Volumetric water flowing through gills	FW_{gil}	0.085 (L/hr)	Nichols *et al.* (2004)
Cardiac output	F_{car}	0.016 (L/hr)	Nichols *et al.* (2004)
Body weight	BodyWt	0.0041 (kg)	Watanabe *et al.* (2007)
Percentage of brain to body weight (BSI)	Pct_{brn}	0.9343	Measured by D. Villeneuve
Percentage of gonads to body weight (GSI)	Pct_{gon}	1.33	Watanabe *et al.* (2007)
Percentage of liver to body weight (HSI)	Pct_{liv}	1.8	Watanabe *et al.* (2007)
Percentage of gills to body weight	Pct_{gil}	1.67	Nichols *et al.* (1996)
Percentage of venous blood to body weight	Pct_{ven}	2.59	Robinson *et al.* (1992); Nichols *et al.* (1996)
Fraction of blood flow in brain to cardiac output	$\frac{F_{brn}}{F_{car}}$	0.036*BSI	Nichols *et al.* (1990)
Fraction of blood flow in gonad to cardiac output	$\frac{F_{gon}}{F_{car}}$	0.036*GSI	Nichols *et al.* (1990)
Fraction of blood flow in liver to cardiac output	$\frac{F_{liv}}{F_{car}}$	0.024*HSI	Nichols *et al.* (1990)

Parameter description	Symbols	Value	Reference
Fraction of plasma in venous blood	$Fct_{plasma, ven}$	0.7	Brill *et al.* (1998)
Total concentration of estrogen receptors in brain	$C_{ER, brn}$	14.3 (nmol/L tissue)	Plowchalk and Teaguarden (2002)
Total concentration of estrogen receptors in gonad	$C_{ER, gon}$	29 (nmol/L tissue)	Plowchalk and Teaguarden (2002)
Total concentration of LH receptors in gonad	$C_{LR, gon}$	2.0 (nmol/L tissue)	Miwa *et al.* (1994)
Total concentration of SBP in blood	$C_{SBP, ven}$	20 (nmol/L blood)	Teeguarden and Barton (2004)
Dissociation constant of E_2 to estrogen receptor in gonad	$K_{d\_E2ER, gon}$	$= K_{d\_E2ER, brn}$	assumed
Association rate of E_2 to estrogen receptor in gonad	$k_{1\_E2ER, gon}$	$= k_{1\_E2ER, brn}$	assumed
Dissociation constant of E_2 to estrogen receptor in liver	$K_{d\_E2ER, liv}$	$= K_{d\_E2ER, brn}$	assumed
Association rate of E_2 to estrogen receptor in liver	$K_{1\_E2ER, liv}$	$= k_{1\_E2ER, brn}$	assumed
Dissociation constant of EE_2 to estrogen receptor in brain	$K_{d\_EE2ER, brn}$	$= 0.2 * K_{d\_E2ER, brn}$	Gale *et al.* (2004)
Association rate of EE_2 to estrogen receptor in brain	$k_{1\_EE2ER, brn}$	$= k_{1\_E2ER, brn}$	assumed
Dissociation constant of EE_2	$K_{d\_EE2ER, gon}$	$= K_{d\_EE2ER, brn}$	assumed

Parameter description	Symbols	Value	Reference
to estrogen receptor in gonad			
Association rate of EE_2 to estrogen receptor in gonad	$k_{1\_EE2ER,\ gon}$	= $k_{1\_EE2ER,\ brn}$	assumed
Dissociation constant of EE_2 to estrogen receptor in liver	$K_{d\_EE2ER,\ liv}$	= $K_{d\_EE2ER,brn}$	assumed
Association rate of EE_2 to estrogen receptor in liver	$k_{1\_EE2ER,liv}$	= $k_{1\_EE2ER,brn}$	assumed
Dissociation constant of E_2 to SBP in blood	$K_{d\_E2SBP,ven}$	3.13 (nM)	Murphy *et al.* (2005)
Association rate of E_2 to SBP in blood	$k_{1\_E2SBP,ven}$	5.6687 (1/nM/hr)	Murphy *et al.* (2005)
Dissociation constant of T to SBP in blood	$K_{d\_TSBP,ven}$	4.89 (nM)	Murphy *et al.* (2005)
Association rate of T to SBP in blood	$K_{1\_TSBP,ven}$	5.6687 (1/nM/hr)	Murphy *et al.* (2005)
Dissociation constant of LH to LH receptor in gonad	$K_{d\_LHLR,\ gon}$	0.15 (nM)	Crim *et al.* (1988)
Scaling coefficient of Vmax of T production in gonad (=Vmax/bodyweight $^{0.75}$)	$sc\_Vmax_{Scc,gon}$	1.1e+05 (nmol/hr/kg body weight)	Kashiwagi *et al.* (1980); Shikita and Hall (1973)
$K_{0.5}$ of T production in gonad	$K_{0.5Scc,gon}$	190 (nM)	Shikita and Hall (1973)
Hill coefficient for T production in gonad	n_T	1.8	Murphy *et al.* (2005)

Parameter description	Symbols	Value	Reference
Scaling coefficient of Vmax of E_2 production in brain (=Vmax/ mass of microsomal protein in brain)	$sc\_Vmax_{aro,brn}$	1.05E-2 (nmol/hr/mg microsomal protein)	Zhao *et al.* (2001)
Km of E_2 production in brain	$Km_{aro,brn}$	9.6 (nM)	Zhao *et al.* (2001)
Scaling coefficient of Vmax of E_2 production in gonad (=Vmax/ mass of microsomal protein in gonad)	$sc\_Vmax_{aro,gon}$	2.3E-3 (nmol/hr/mg microsomal protein)	Zhao *et al.* (2001)
Km of E_2 production in gonad	$Km_{aro,gon}$	9.6 (nM)	Zhao *et al.* (2001)
Km of KT production in gonad	$Km_{11bHSD,gon}$	41.5 (nM)	Ge *et al.* (1997)
Number of leydig cells per mg testis	$sc\_N_{leydigcell,\ gon}$	4.4E+4 (1/mg testis)	Matta *et al.* (2002)
$K_{0.5}$ of Vtg production in liver production	$K_{0.5\ Vtg,\ liv}$	1 (nM)	assumed
Degradation rate constant of ER in liver	$Kelim_{ER,liv}$	0.01 (1/hr)	Murphy *et al.* (2005)
Elimination rate constant for LH in the "other" compartment	$Kelim_{LH,oth}$	0.1 (1/hr)	Teeguarden and Barton (2004)
Elimination rate constant for	$Kelim_{T,oth}$	0.1 (1/hr)	Teeguarden and Barton

Parameter description	Symbols	Value	Reference
T in the "other" compartment			(2004)
Elimination rate constant for EE_2 in the "other" compartment	$Kelim_{EE2,oth}$	0.1 (1/hr)	Teeguarden and Barton (2004)
Elimination rate constant for KT in the "other" compartment	$Kelim_{KT,oth}$	0.1 (1/hr)	Teeguarden and Barton (2004)
Elimination rate constant for Vtg in the "other" compartment	$Kelim_{Vtg,oth}$	0.001 (1/hr)	Teeguarden and Barton (2004)
Partition coefficient of EE_2 (brain to blood)	$\lambda_{EE2,\ brn}$	1	Teeguarden and Barton (2004)
Partition coefficient of EE_2 (gonad to blood)	$\lambda_{EE2,\ gon}$	1	Teeguarden and Barton (2004)
Partition coefficient of EE_2 ("other" to blood)	$\lambda_{EE2,\ oth}$	1	Teeguarden and Barton (2004)
Partition coefficient of E_2 (brain to blood)	$\lambda_{E2,\ brn}$	1	Teeguarden and Barton (2004)
Partition coefficient of E_2 (gonad to blood)	$\lambda_{E2,\ gon}$	1	Plowchalk and Teeguarden (2002)
Partition coefficient of E_2 (liver to blood)	$\lambda_{E2,\ liv}$	1	Teeguarden and Barton (2004)
Partition coefficient of E_2	$\lambda_{E2,\ oth}$	1	Plowchalk and Teeguarden

Parameter description	Symbols	Value	Reference
("other" to blood)			(2002)
Partition coefficient of T (brain to blood)	$\lambda_{T, brn}$	1	Barton and Andersen (1998)
Partition coefficient of T (gonad to blood)	$\lambda_{T, gon}$	1	Barton and Andersen (1998)
Partition coefficient of T (liver to blood)	$\lambda_{T, liv}$	1	Barton and Andersen (1998)
Partition coefficient of T ("other" to blood)	$\lambda_{T, oth}$	1	Barton and Andersen (1998)
Partition coefficient of KT (brain to blood)	$\lambda_{KT, brn}$	1	Barton and Andersen (1998)
Partition coefficient of KT (gonad to blood)	$\lambda_{KT, gon}$	1	Barton and Andersen (1998)
Partition coefficient of KT (liver to blood)	$\lambda_{KT, liv}$	1	Barton and Andersen (1998)
Partition coefficient of KT ("other" to blood)	$\lambda_{KT, oth}$	1	Barton and Andersen (1998)

Table 3.1 Model parameters treated as constants (n = 97). [a], [b], and [c] were assigned with measured values in each fish; the default values were used only when measured data were missing.

Parameter description	Symbols	Value	Reference
Body weight[a]	BodyWt	0.0016 (kg)	Watanabe et al. (2007)
Volumetric water flowing through gills	FW_{gil}	10.6× BodyWt $^{0.75}$ (L/hr)	Nichols et al. (2004)
Cardiac output	F_{car}	2.06× BodyWt $^{0.75}$ (L/hr)	Nichols et al. (2004)
Percentage of brain to body weight (BSI)	P_{brn}	1.18	Measured by D. Villeneuve
Percentage of gonads to body weight (GSI)[b]	P_{gon}	11	Watanabe et al. (2007)
Percentage of liver to body weight (HSI)[c]	P_{liv}	3.0	Watanabe et al. (2007)
Percentage of gills to body weight	P_{gil}	1.67	Nichols et al. (1996)
Percentage of venous blood to body weight	P_{ven}	2.59	Robinson et al. (1992) Nichols et al. (1996)

Parameter description	Symbols	Value	Reference
Percentage of "other" to body weight	P_{oth}	=100- P_{brn}- P_{gon}- P_{liv}- P_{gil}- P_{ven}	Watanabe et al. (2009)
Fraction of blood flow in brain to cardiac output	$\frac{F_{brn}}{F_{car}}$	$\frac{0.036 \times P_{brn}}{0.036 \times P_{brn} + 0.036 \times P_{gon} + 0.024 \times P_{liv} + 0.007 \times P_{oth}}$	Nichols et al. (1996)
Fraction of blood flow in gonad to cardiac output	$\frac{F_{gon}}{F_{car}}$	$\frac{0.036 \times P_{gon}}{0.036 \times P_{brn} + 0.036 \times P_{gon} + 0.024 \times P_{liv} + 0.007 \times P_{oth}}$	Nichols et al. (1996)
Fraction of blood flow in liver to cardiac output	$\frac{F_{liv}}{F_{car}}$	$\frac{0.024 \times P_{liv}}{0.036 \times P_{brn} + 0.036 \times P_{gon} + 0.024 \times P_{liv} + 0.007 \times P_{oth}}$	Nichols et al. (1996)
Fraction of blood flow in "other" to cardiac output	$\frac{F_{oth}}{F_{car}}$	$\frac{0.007 \times P_{oth}}{0.036 \times P_{brn} + 0.036 \times P_{gon} + 0.024 \times P_{liv} + 0.007 \times P_{oth}}$	Nichols et al. (1996)
Fraction of plasma in venous blood	$F_{plasma, ven}$	0.45	Measured by K. Kroll
Total concentration of estrogen receptors in brain	$C_{ER, brn}$	14.3 (nmol/L tissue)	Plowchalk and Teaguarden (2002)
Total concentration of estrogen receptors in gonad	$C_{ER, gon}$	29 (nmol/L tissue)	Plowchalk and Teaguarden (2002)

Parameter description	Symbols	Value	Reference
Total concentration of LH receptors in gonad	$C_{LR,\ gon}$	2.0 (nmol/L tissue)	Miwa et al. (1994)
Total concentration of SBP in blood	$C_{SBP,\ ven}$	400 (nmol/L blood)	Laidley and Thomas(1994) Teeguarden and Barton (2004)
Total concentration of AR in gonad	$C_{AR,\ gon}$	1.05 (nmol/L tissue)	Sperry and Thomas (1999)
Total concentration of AR in liver	$C_{AR,\ liv}$	= $C_{AR,\ gon}$	assumed
Association rate of E_2 to estrogen receptor in brain	$k_{1\_E2ER,\ brn}$	0.743	Murphy et al. (2005)
Dissociation constant of E_2 to estrogen receptor in gonad	$K_{d\_E2ER,\ gon}$	= $K_{d\_E2ER,\ brn}$	assumed
Association rate of E_2 to estrogen receptor in gonad	$k_{1\_E2ER,\ gon}$	= $k_{1\_E2ER,\ brn}$	assumed
Dissociation constant of E_2 to estrogen receptor in liver	$K_{d\_E2ER,\ liv}$	= $K_{d\_E2ER,\ brn}$	assumed

Parameter description	Symbols	Value	Reference
Association rate of E_2 to estrogen receptor in liver	$K_{1\_E2ER,\ liv}$	$= k_{1\_E2ER,\ brn}$	assumed
Dissociation constant of EE_2 to estrogen receptor in brain	$K_{d\_EE2ER,\ brn}$	$= K_{d\_E2ER,\ brn}/RBA_{EE2\_E2}$	Denny et al. (2005)
Association rate of EE_2 to estrogen receptor in brain	$k_{1\_EE2ER,\ brn}$	$= k_{1\_E2ER,\ brn}$	assumed
Dissociation constant of EE_2 to estrogen receptor in gonad	$K_{d\_EE2ER,\ gon}$	$= K_{d\_EE2ER,\ brn}$	assumed
Association rate of EE_2 to estrogen receptor in gonad	$k_{1\_EE2ER,\ gon}$	$= k_{1\_EE2ER,\ brn}$	assumed
Dissociation constant of EE_2 to estrogen receptor in liver	$K_{d\_EE2ER,\ liv}$	$= K_{d\_EE2ER,brn}$	assumed
Association rate of EE_2 to estrogen receptor in liver	$k_{1\_EE2ER,liv}$	$= k_{1\_EE2ER,brn}$	assumed
Dissociation constant of T to androgen	$K_{d\_TAR,\ brn}$	3 (nM)	Sperry and Thomas (1999)

Parameter description	Symbols	Value	Reference
receptor in brain			
Association rate of T to androgen receptor in brain	$k_{1\_TAR,\ brn}$	0.08 (1/nM/hr)	Sperry and Thomas (1999)
Dissociation constant of T to androgen receptor in gonad	$K_{d\_TAR,\ gon}$	= $K_{d\_TAR,\ brn}$	assumed
Association rate of T to androgen receptor in gonad	$k_{1\_TAR,\ gon}$	= $k_{1\_TAR,\ brn}$	assumed
Dissociation constant of T to androgen receptor in liver	$K_{d\_TAR,\ liv}$	= $K_{d\_TAR,\ brn}$	assumed
Association rate of T to androgen receptor in liver	$k_{1\_TAR,\ liv}$	= $k_{1\_TAR,\ brn}$	assumed
Dissociation constant of TB to androgen receptor in brain	$K_{d\_TBAR,\ brn}$	= $K_{d\_TAR,\ brn}$/ RBA_{TB_T}	Wilson et al. (2007)
Association rate of TB to androgen receptor in brain	$k_{1\_TBAR,\ brn}$	= $k_{1\_TAR,\ brn}$	assumed

Parameter description	Symbols	Value	Reference
Dissociation constant of TB to androgen receptor in gonad	$K_{\text{d\_TBAR, gon}}$	= $K_{d\_\text{TBAR, brn}}$	assumed
Association rate of TB to androgen receptor in gonad	$k_{1\_\text{TBAR, gon}}$	= $k_{1\_\text{TBAR, brn}}$	assumed
Dissociation constant of TB to androgen receptor in liver	$K_{\text{d\_TBAR, liv}}$	= $K_{d\_\text{TBAR, brn}}$	assumed
Association rate of TB to androgen receptor in liver	$k_{1\_\text{TBAR, liv}}$	= $k_{1\_\text{TBAR, brn}}$	assumed
Dissociation constant of E_2 to SBP in blood	$K_{\text{d\_E2SBP,ven}}$	3.13 (nM)	Murphy et al. (2005)
Association rate of E_2 to SBP in blood	$k_{1\_\text{E2SBP,ven}}$	5.6687 (1/nM/hr)	Murphy et al. (2005)
Dissociation constant of T to SBP in blood	$K_{\text{d\_TSBP,ven}}$	4.89 (nM)	Murphy et al. (2005)
Association rate of T to SBP in blood	$K_{1\_\text{TSBP,ven}}$	5.6687 (1/nM/hr)	Murphy et al. (2005)
Dissociation constant of EE_2 to SBP in	$K_{\text{d\_EE2SBP,ven}}$	0.58 (nM)	Miguel-Queralt and Hammond

Parameter description	Symbols	Value	Reference
blood			(2008)
Association rate of EE_2 to SBP in blood	$k_{1\_EE2SBP,ven}$	5.6687 (1/nM/hr)	Murphy et al. (2005)
Dissociation constant of LH to LH receptor in gonad	$K_{d\_LHLR,\ gon}$	2.9 (nM)	Crim et al. (1988)
Association rate of LH to LH receptor in gonad	$k_{1\_LHLR,\ gon}$	0.2 (1/nM/hr)	Watanabe et al. (2009)
Scaling coefficient of Vmax of T production in gonad (=Vmax/bodyweight $^{0.75}$)	$sc\_Vmax_{Scc,gon}$	1.1e+05 (nmol/hr/kg body weight)	Kashiwagi et al. (1980); Shikita and Hall (1973)
$K_{0.5}$ of T production in gonad	$K_{0.5Scc,gon}$	190 (nM)	Shikita and Hall (1973)
Inhibition constant of T production by bound ER	K_T	0.016	Watanabe et al. (2009)
Km of E_2 production in gonad	$Km_{aro,gon}$	9.6 (nM)	Zhao et al. (2001)
Concentration of microsomal protein in gonads	$D_{mp,gon}$	3100 (mg/L)	Measured by D. Villeneuve

Parameter description	Symbols	Value	Reference
Ratio between the concentrations of microsoaml protein in gonads and brain	Rho_{mp}	0.174	Measured by D. Villeneuve
Scaling coefficient of Vmax of E_2 production in brain (=Vmax/ mass of microsomal protein in brain)	$sc\_Vmax_{aro,brn}$	$=4.6\times sc\_Vmax_{aro,gon}$	Zhao et al. (2001)
Km of E_2 production in brain	$Km_{aro,brn}$	9.6 (nM)	Zhao et al. (2001)
Concentration of microsomal protein in brain	$D_{mp,brn}$	$= D_{mp,gon}/ Rho_{mp}$	Measured by D. Villeneuve
Ratio between concentrations of STAR and bound LR in gonads	$Rho_{STAR,gon}$	1	assumed
Rate constant for Vtg uptake into oocytes	$k_{vtg,gon}$	0.05	assumed
$K_{0.5}$ of Vtg production in liver production	$K_{0.5Vtg,\ liv}$	1.0 (nM)	Watanabe et al. (2009)
Elimination rate constant for ER in the liver compartment	$k_{e\_ER,liv}$	0.01 (1/hr)	Murphy et al. (2005)

Parameter description	Symbols	Value	Reference
Elimination rate constant for AR in the brain compartment	$k_{e\_AR,brn}$	0.01 (1/hr)	Assumed
Elimination rate constant for LH in the "other" compartment	$k_{e\_LH,oth}$	0.1 (1/hr)	Teeguarden and Barton (2004)
Elimination rate constant for E_2 in the "other" compartment	$k_{e\_E2,oth}$	0.1 (1/hr)	Teeguarden and Barton (2004)
Elimination rate constant for T in the "other" compartment	$k_{e\_T,oth}$	0.1 (1/hr)	Teeguarden and Barton (2004)
Elimination rate constant for EE_2 in the "other" compartment	$k_{e\_EE2,oth}$	0.1 (1/hr)	Teeguarden and Barton (2004)
Elimination rate constant for TB in the "other" compartment	$k_{e\_TB,oth}$	0.1 (1/hr)	Teeguarden and Barton (2004)
Elimination rate constant for Vtg in the "other" compartment	$k_{e\_Vtg,oth}$	0.001 (1/hr)	Teeguarden and Barton (2004)

Parameter description	Symbols	Value	Reference
Partition coefficient of LH (brain to blood)	$\lambda_{LH,\ brn}$	1	Teeguarden and Barton (2004)
Partition coefficient of LH (gonad to blood)	$\lambda_{LH,\ gon}$	1	Teeguarden and Barton (2004)
Partition coefficient of LH (liver to blood)	$\lambda_{LH,\ liv}$	1	Teeguarden and Barton (2004)
Partition coefficient of LH ("other" to blood)	$\lambda_{LH,\ oth}$	1	Teeguarden and Barton (2004)
Partition coefficient of VTG (brain to blood)	$\lambda_{VTG,\ brn}$	1	Teeguarden and Barton (2004)
Partition coefficient of VTG (gonad to blood)	$\lambda_{VTG,\ gon}$	1	Teeguarden and Barton (2004)
Partition coefficient of VTG (liver to blood)	$\lambda_{VTG,\ liv}$	1	Teeguarden and Barton (2004)

Parameter description	Symbols	Value	Reference
Partition coefficient of VTG ("other" to blood)	$\lambda_{VTG, oth}$	1	Teeguarden and Barton (2004)
Partition coefficient of EE_2 (blood to water)	$\lambda_{EE2, bld}$	300	Watanabe et al. (2009)
Partition coefficient of EE_2 (brain to blood)	$\lambda_{EE2, brn}$	1	Teeguarden and Barton (2004)
Partition coefficient of EE_2 (gonad to blood)	$\lambda_{EE2, gon}$	1	Teeguarden and Barton (2004)
Partition coefficient of EE_2 (liver to blood)	$\lambda_{EE2, liv}$	3	Watanabe et al. (2009)
Partition coefficient of EE_2 ("other" to blood)	$\lambda_{EE2, oth}$	1	Teeguarden and Barton (2004)
Partition coefficient of E_2 (blood to water)	$\lambda_{E2, bld}$	300	Watanabe et al. (2009)

Parameter description	Symbols	Value	Reference
Partition coefficient of E_2 (brain to blood)	$\lambda_{E2, brn}$	1	Teeguarden and Barton (2004)
Partition coefficient of E_2 (gonad to blood)	$\lambda_{E2, gon}$	1	Plowchalk and Teeguarden (2002)
Partition coefficient of E_2 (liver to blood)	$\lambda_{E2, liv}$	3	Watanabe et al. (2009)
Partition coefficient of E_2 ("other" to blood)	$\lambda_{E2, oth}$	1	Plowchalk and Teeguarden (2002)
Partition coefficient of T (brain to blood)	$\lambda_{T, brn}$	1	Barton and Andersen (1998)
Partition coefficient of T (gonad to blood)	$\lambda_{T, gon}$	1	Barton and Andersen (1998)
Partition coefficient of T (liver to blood)	$\lambda_{T, liv}$	1	Barton and Andersen (1998)

Parameter description	Symbols	Value	Reference
Partition coefficient of T ("other" to blood)	$\lambda_{T,\ oth}$	1	Barton and Andersen (1998)
Partition coefficient of TB (brain to blood)	$\lambda_{TB,\ brn}$	1	Barton and Andersen (1998)
Partition coefficient of TB (gonad to blood)	$\lambda_{TB,\ gon}$	1	Barton and Andersen (1998)
Partition coefficient of TB (liver to blood)	$\lambda_{TB,\ liv}$	1	Barton and Andersen (1998)
Partition coefficient of TB ("other" to blood)	$\lambda_{TB,\ oth}$	1	Barton and Andersen (1998)

Table 3.2 Summary statistics for prior and posterior distributions of calibrated model parameters (n = 26)

[a]Definition of P1 and P2 of prior distributions. Loguniform: P1 = minimum of the sampling range in natural space; P2 = maximum of the sampling range in natural space. Lognormal: P1 = geometric mean (exponential of the mean in log-space); P2 = geometric standard deviation (exponential of the standard deviation in log-space, strictly superior to 1). Uniform: P1 = minimum of the sampling range in natural space; P2 = maximum of the sampling range in natural space. Inverse gamma: P1 = shape; P2 = scale (both of the parameters are strictly positive).

Parameter description	Symbols	Prior Distribution (P1, P2)[a]	Reference	Posterior Distribution		
				Mean	Median	95% Confidence Interval
Partition coefficient of TB (blood to water)	$\lambda_{TB,\,bld}$	Loguniform (1, 1.0E+3)	Assumed	7.47	7.47	(5.96, 8.93)
Dissociation constant of E_2 binding to ER in brain (nM)	$K_{d\_E2ER,\,brn}$	Lognormal (8.6, 3)	Denny et al. (2005)	1.12	1.08	(0.71, 1.87)
Relative binding affinity of EE_2 to E_2 for ER binding	RBA_{EE2_E2}	Lognormal (1.66, 3)	Denny et al. (2005) Gale et al. (2004)	3.24	1.64	(0.030, 16.79)
Relative binding affinity of TB to T for AR binding	RBA_{TB_T}	Lognormal (6.03, 3)	Wilson et al. (2007)	5.25	4.84	(2.29, 10.76)
Inhibition factor for LH production by bound AR (nM)	$\rho_{d\_LH,brn}$	LogUniform (0.01, 1.0E+3)	Assumed	0.11	0.10	(0.042, 0.21)

Parameter description	Symbols	Prior Distribution (P1, P2)[a]	Reference	Posterior Distribution		
				Mean	Median	95% Confidence Interval
Induction factor for LH production by bound ER (nM)	$\rho_{u\_LH,brn}$	LogUniform (0.01, 1.0E+3)	Assumed	238	138	(4.23, 864)
Hill coefficient for T production	n_T	Lognormal (1.8, 3)	Murphy et al. (2005)	1.03	1.01	(0.93, 1.19)
Proportionality constant relating cholesterol to StAR	$\rho_{Chol,gon}$	Loguniform (1, 5.0E+3)	Artemenk et al. (2001)	2.37	1.83	(1.04, 6.69)
Scaling coefficient of Vmax for E_2 production in gonad (nmol/hr/mg micro-protein)	$sc\_Vmax_{aro,\ gon}$	Loguniform (2.3E-5, 0.23)	Zhao et al. (1997)	1.56E-3	1.53E-3	(1.15E-3, 2.12E-3)
Induction factor of E_2 production by bound LH (1/nM)	$\rho_{E2\_LHLR,gon}$	Loguniform (0.1, 100)	assumed	79.84	82.79	(42.61, 99.15)
Scaling coefficient of Vmax for Vtg production in liver (=Vmax/BodyWeight$^{0.75}$) (nmol/hr/kg$^{0.75}$)	$sc\_Vmax_{Vtg,\ liv}$	Loguniform (1, 1.0E+4)	Watanabe et al. (2009)	175	169	(121, 271)
Hill coefficient of Vtg production in liver	n_{VTG}	Uniform (1, 10)	Assumed	2.88	2.87	(1.97, 3.87)

Parameter description	Symbols	Prior Distribution (P1, P2)[a]	Reference	Posterior Distribution		
				Mean	Median	95% Confidence Interval
ER background production rate in liver (nM/hr)	$Pbg_{ER,liv}$	Loguniform (5.0E-5, 0.5)	assumed	0.12	0.12	(0.084, 0.17)
Induction rate constant for ER production in liver (1/hr)	$k_{ER,liv}$	Lognormal (0.08, 3)	Watanabe et al. (2009)	0.027	0.025	(5.73E-3, 0.065)
AR background production rate in brain (nM/hr)	$Pbg_{AR,brn}$	Loguniform (5.0E-5, 0.5)	assumed	0.012	0.012	(9.1E-3, 0.015)
Inhibition factor of AR production by free androgens (nM)	$K_{AR,brn}$	Loguniform (5E-4, 5)	assumed	3.95	4.08	(2.15, 4.95)
Magnitude of LH production (nmol/hr)	Mag_{LH}	Loguniform (2.7E-7, 2.7E-3)	Schulz et al. (1993)	8.86E-6	8.75E-6	(6.29E-6, 1.20E-5)
Error variance of plasma E_2 concentration in natural log space for unexposed female FHMs	Var_Ln_CE2tot_pla_ngml	Inverse Gamma (2, 1.19)	Bois et al. (1996a)	0.52	0.51	(0.38, 0.73)

Parameter description	Symbols	Prior Distribution (P1, P2)[a]	Reference	Posterior Distribution		
				Mean	Median	95% Confidence Interval
Error variance of plasma T concentration in natural log space for unexposed female FHMs	Var_Ln_CTtot_pla_ngml	Inverse Gamma (2, 0.53)	Bois et al. (1996a)	0.48	0.47	(0.34, 0.69)
Error variance of plasma VTG concentration in natural log space for unexposed female FHMs	Var_Ln_CVTG_pla_mgml	Inverse Gamma (2, 5.31)	Bois et al. (1996a)	0.49	0.48	(0.35, 0.68)
Error variance of plasma E_2 concentration in natural log space for TB-exposed female FHMs	Var_Ln_CE2tot_pla_ngml	Inverse Gamma (2, 1.19)	Bois et al. (1996a)	0.70	0.69	(0.48, 1.03)
Error variance of plasma T concentration in natural log space for TB-exposed female FHMs	Var_Ln_CTtot_pla_ngml	Inverse Gamma (2, 0.53)	Bois et al. (1996a)	0.40	0.39	(0.27, 0.60)
Error variance of plasma VTG concentration in natural log space for TB-exposed female FHMs	Var_Ln_CVTG_pla_mgml	Inverse Gamma (2, 5.31)	Bois et al. (1996a)	5.86	5.72	(3.98, 8.60)

Parameter description	Symbols	Prior Distribution (P1, P2)[a]	Reference	Posterior Distribution		
				Mean	Median	95% Confidence Interval
Error variance of plasma E_2 concentration in natural log space for EE_2-exposed female FHMs	Var_Ln_CE2tot_pla_ngml	Inverse Gamma (2, 1.19)	Bois et al. (1996a)	1.43	0.81	(0.22, 6.31)
Error variance of plasma T concentration in natural log space for EE_2-exposed female FHMs	Var_Ln_CTtot_pla_ngml	Inverse Gamma (2, 0.53)	Bois et al. (1996a)	0.59	0.34	(0.10, 2.76)
Error variance of plasma VTG concentration in natural log space for EE_2-exposed female FHMs	Var_Ln_CVTG_pla_mgml	Inverse Gamma (2, 5.31)	Bois et al. (1996a)	0.73	0.71	(0.51, 1.03)

Table 4.1 Summary of data used in model parameterization, calibration test, and model evaluation. TB = 17β-trenbolone; EL = exposure length; PSD = paired-spawning design; GSD= group-spawning design; # = number; CS = clutch size; SI = spawning interval; AF = average fecundity; VTG = plasma vitellogenin concentration.

Data	EDC	Dose (µg/L)	EL (days)	Designs	Female FHM #	Group #	Endpoints	Application	
I	None	0	0	PSD	50	50	CS, SI, AF, VTG	Parameterize the model (Table 2)	Calibration test (Fig. 4)
					10	10	CS, SI, AF		-
II	None	0	0	GSD	77	20	AF, VTG	Model evaluation (Fig. 5)	
III	TB	0.005, 0.05, 0.5, 5, and 50	21	GSD	71	18	AF, VTG	Model evaluation (Fig. 6)	

Table 4.2 Summary statistics of fecundity data from unexposed female FHMs (n = 60) with a paired-spawning experimental design (Ankley et al. 2005a, Ankley et al. 2005b, Jensen et al. 2001, Jensen et al. 2006, Martinovic et al. 2008, Villeneuve et al. 2009a, Villeneuve et al. 2006). Data were used to obtain probability distributions for clutch size and spawning interval. SD = standard deviation; Min = minimum; Max = maximum.

	Number of Records	Mean	Median	SD	Min	Max	Distribution Fitting	Distribution Used in Model Simulations
Clutch Size	391	88	75	68	1	317	Lognormal (4.11, 0.96)	Truncated Lognormal (4.11, 0.96, 1, 137)
Spawning Interval	331	3.9	3.0	2.5	1.0	25.0	Lognormal (1.21, 0.57)	Truncated Lognormal (1.21, 0.57, 1, 25)

FIGURES

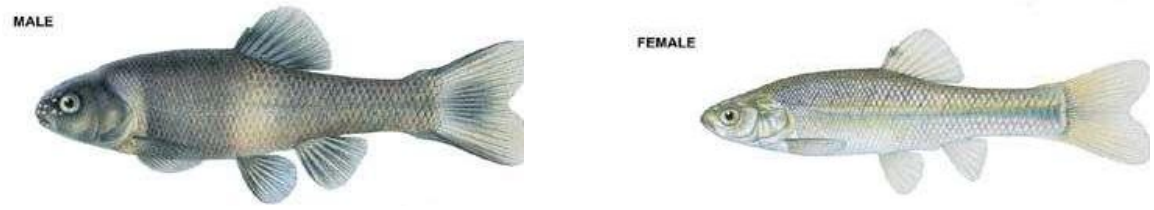

Figure 1.1: Male and female fathead minnows (FHMs, *Pimephales promelas)* illustrated by Joseph Tomelleri (http://www.dcswcd.org/SWCD/fatheadmale.jpg). Sexually mature FHMs are dimorphic. Adult males usually weigh three to five grams with large nuptial tubercles on the snout and elongated dorsal pad extending from the nape to the dorsal fin. The adult females usually weigh two to three grams, and have a fleshy ovipositor. The color of adult males is usually black on the sides with bright vertical bars, while the females have a lighter coloration.

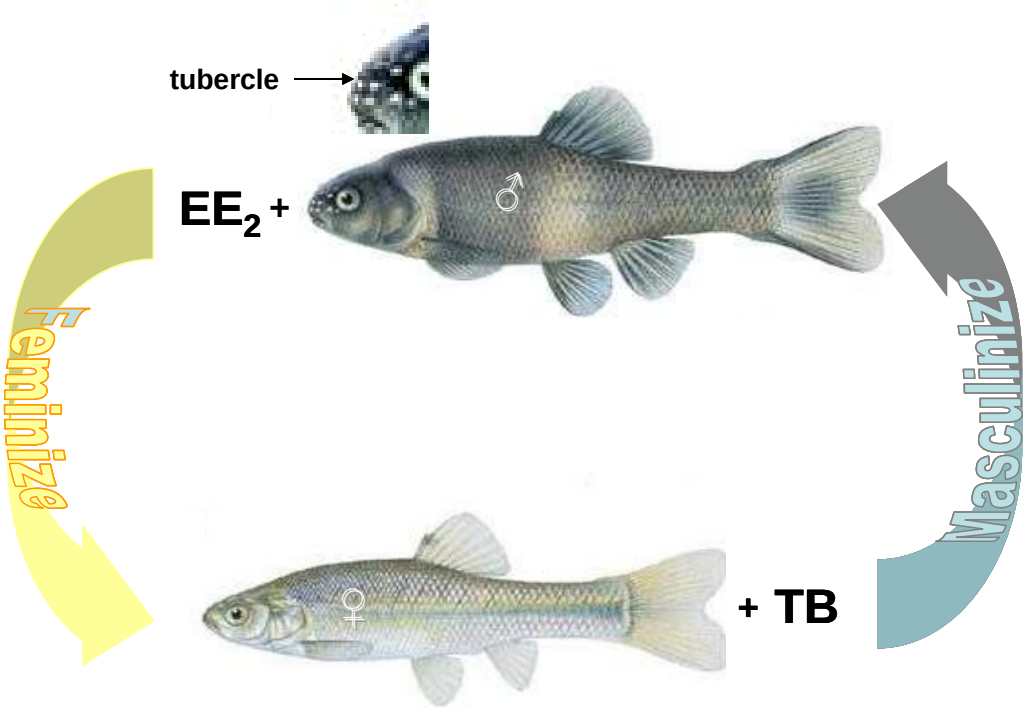

Figure 1.2: Feminization and masculinization of fathead minnows (FHMs, *Pimephales promelas)*. Exposure to estrogenic compounds (e.g., 17α-ethynylestradiol, EE_2) leads to feminization of male FHMs. The nuptial tubercles on the mouth of male FHMs disappear after an EE_2 exposure and their body weight decreases, which make males look like females. Exposure to androgenic compounds (e.g., 17β-trenbolone, TB) leads to masculinization of female FHMs. After exposure to TB, nuptial tubercles appear on female FHM mouths and their body weight increases, which make females look like males.

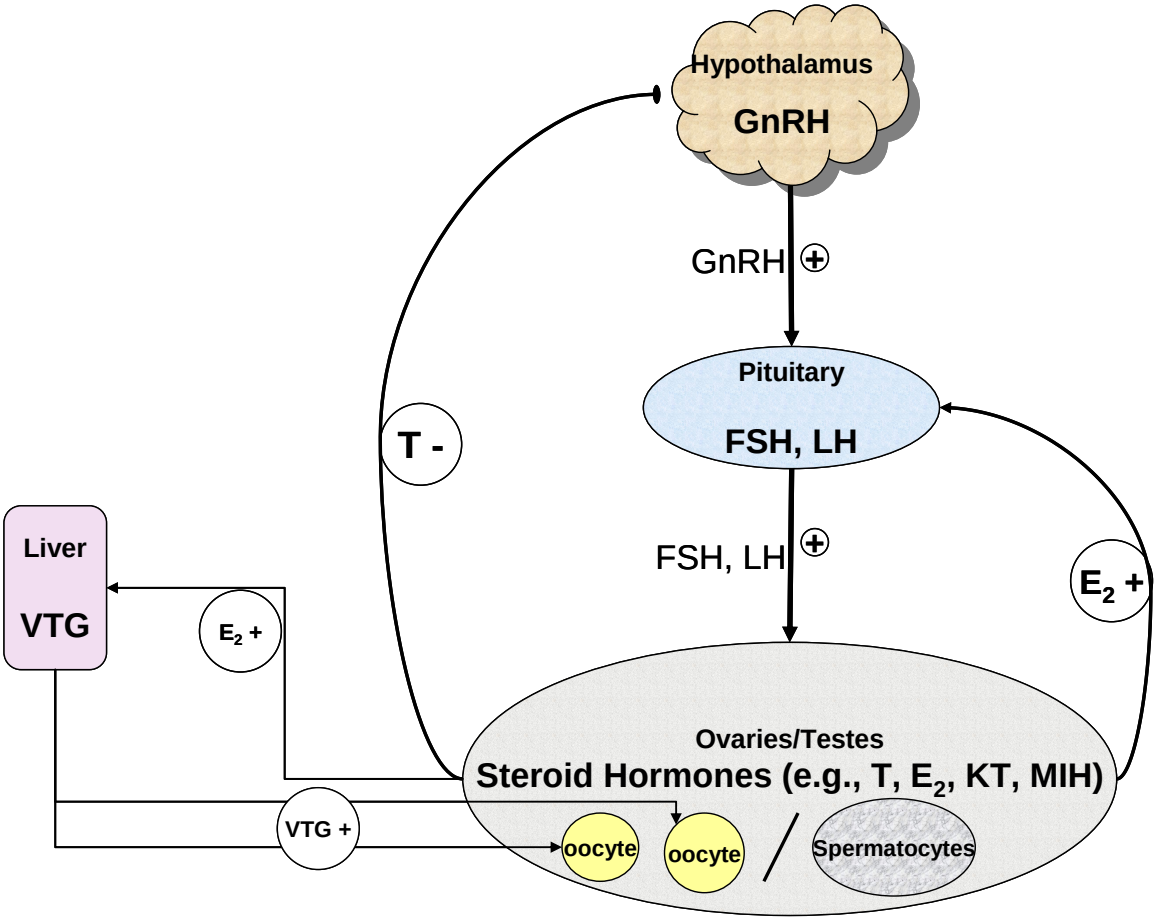

Figure 1.3: A schema of the hypothalamic-pituitary-gonadal (HPG) axis and its communication with the liver. GnRH = gonadotropin-releasing hormone; FSH = follicle-stimulating hormone; LH = luteinizing hormone; E_2 = 17β-estradiol; T = testosterone; KT = 11keto-testosterone; MIH = maturation-inducing hormone. The HPG axis is composed of the hypothalamus, the pituitary, and the ovaries (female) or testes (male). GnRH is produced and released by hypothalamus. The released GnRH goes to the pituitary gland and binds to GnRH receptors to stimulate the synthesis of FSH and LH. FSH and LH are released into the bloodstream and circulate to the gonads, where they bind to receptors to regulate gonadal functions by stimulating steroid production and gametogenesis. E_2, one of the steroid hormones produced in the gonads, is released into the bloodstream, circulates to the liver, and then stimulates VTG production. The VTG is then released, and circulates to the gonads. In females VTG is absorbed into oocytes, and processed to become egg yolk proteins.

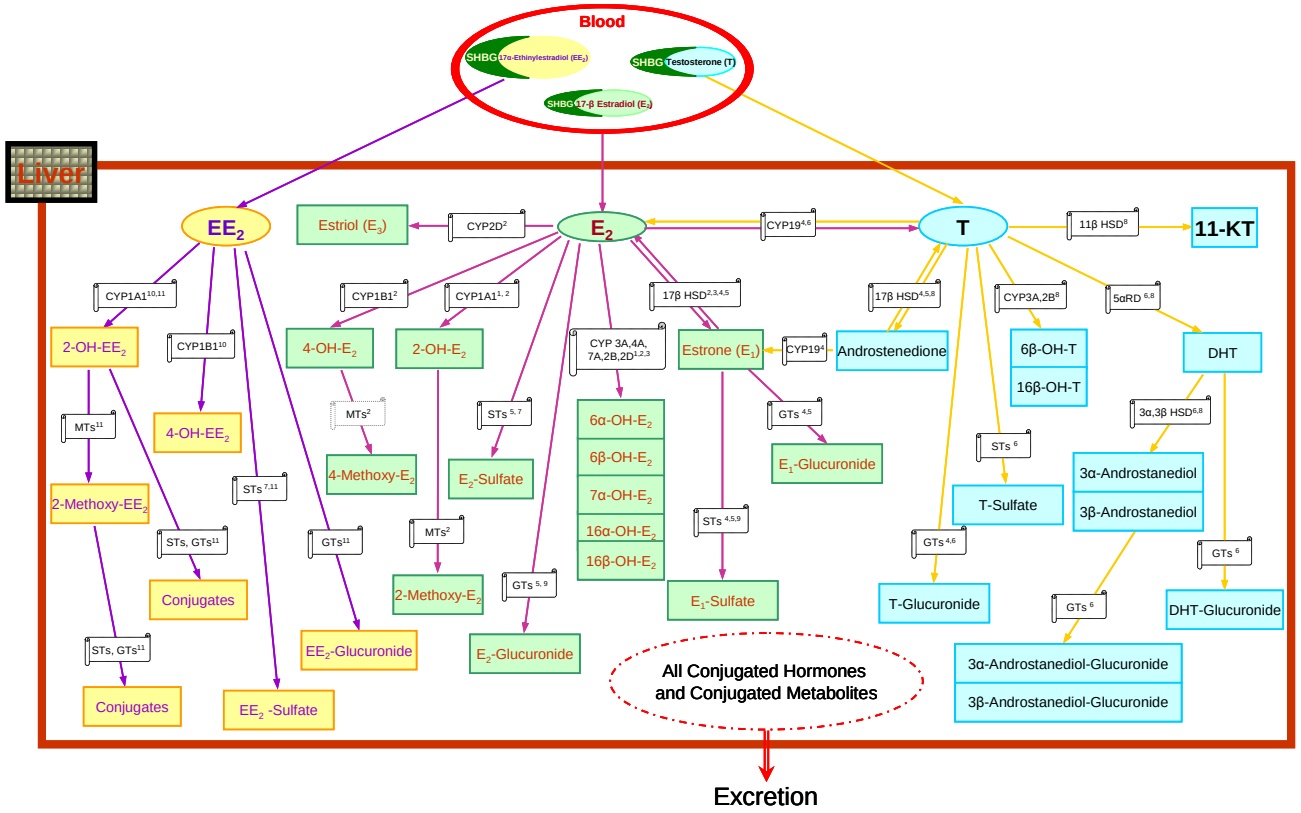

Figure 1.4. Steroid hormone metabolism pathways. Abbreviations: CYP1A1 = P450 2-hydroxylase; CYP1B1 = P450 4-hydroxylase; CYP 2D = P450 16α-hydroxylase; CYP4A = P450 6α–hydroxylase; CYP3A = P450 6β–hydroxylase; CYP7A = P450 7α–hydroxylase; CYP2B = P450 16β–hydroxylase; CYP19 = P450 Aromatase; MTs = methyltransferase; GTs = glucuronosyltransferase; STs = sulfotransferases; 17β HSD = 17β-hydroxysteroid dehydrogenase; 11β HSD = 11β-hydroxysteroid dehydrogenase; 5α RD = 5α-reductase; 3α-HSD = 3α-hydroxysteroid-dehydrogenase; 3β-HSD = 3β-hydroxysteroid-dehydrogenase. References: [1](Snowberger and Stegeman, 1987); [2](Butala et al., 2004); [3](Hansson and Rafter, 1983); [4](Khan et al., 1997); [5](Petkam et al., 2002); [6](Venkatesh et al., 1992); [7](Ohkimoto et al., 2003); [8](Parks and LeBlanc, 1998b); [9](Blom et al., 2001); [10](Metzler et al., 1990); [11](Li et al., 1999).

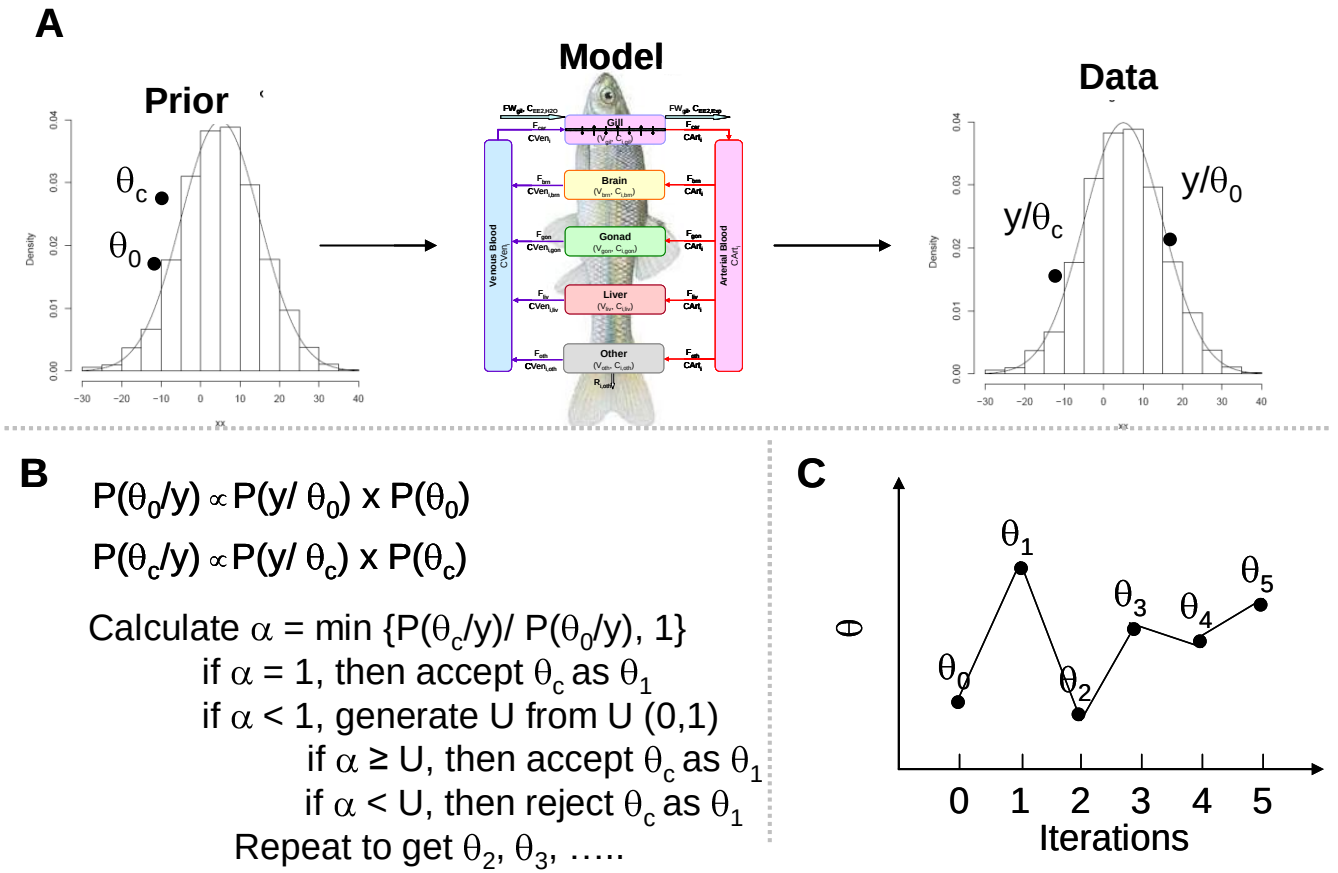

Figure 1.5. An illustration of Markov chain Monte Carlo method. (A): At each step of the MCMC simulation, for each model parameter, a value (e.g. θ_0, θ_c) is randomly sampled from its prior distribution. Then the value is input into the model to calculate model predictions that are compared to experimental data; (B): The Metropolis-Hastings algorithm core that is used to evaluate whether the sample parameter value, θ_c, should be accepted or not; (C): The trajectory of the parameter values that are accepted during MCMC simulation.

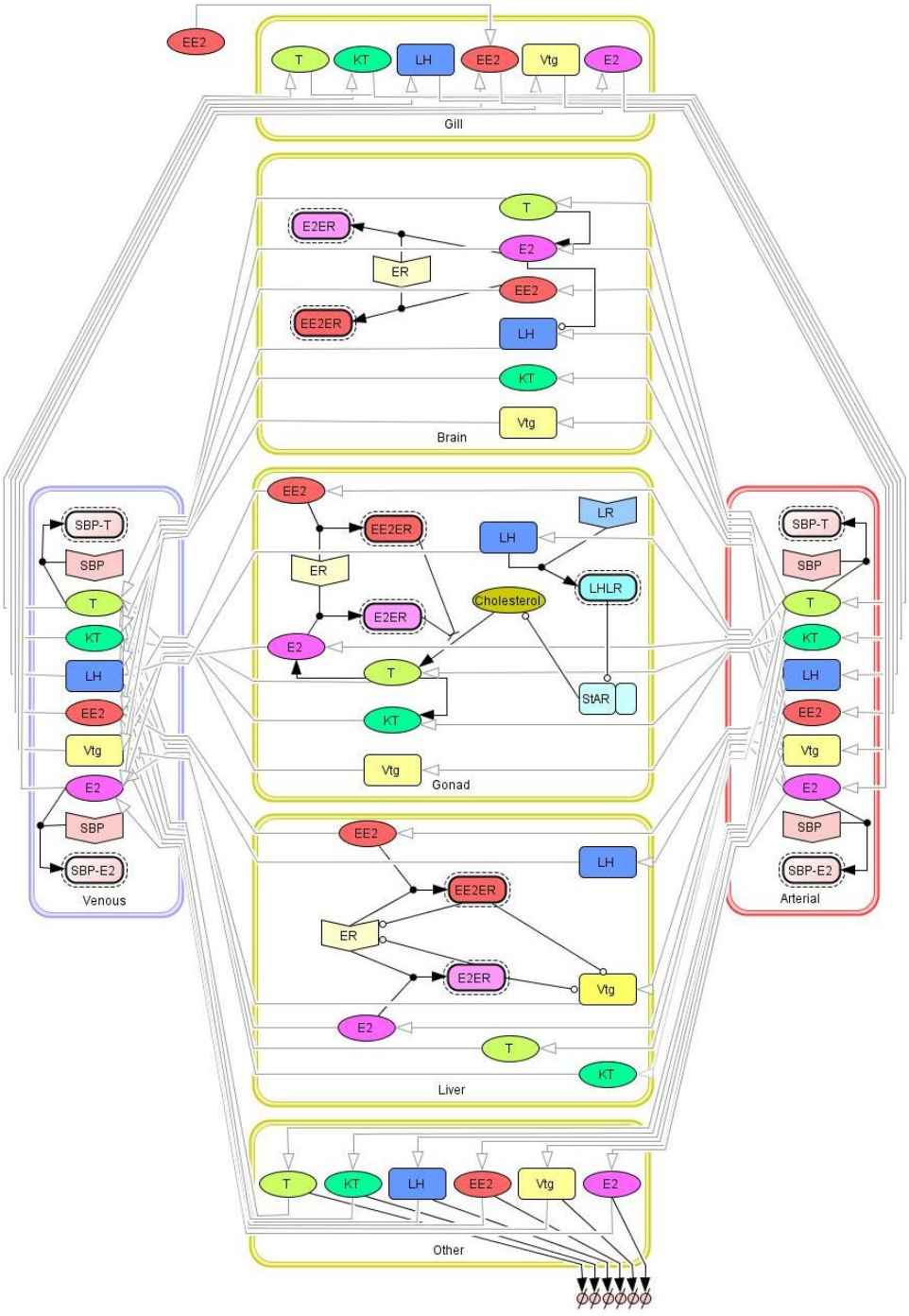
EE2
T
KT
LH
EE2
Vtg
E2
Gill
E2ER
ER
EE2ER
T
E2
EE2
LH
KT
Vtg
Brain
SBP-T
SBP
T
KT
LH
EE2
Vtg
E2
SBP
SBP-E2
Venous
EE2
EE2ER
ER
E2ER
E2
T
KT
Vtg
LR
LH
LHLR
Cholesterol
StAR
Gonad
EE2
LH
EE2ER
ER
E2ER
Vtg
E2
T
KT
Liver
T
KT
LH
EE2
Vtg
E2
Other
SBP-T
SBP
T
KT
LH
EE2
Vtg
E2
SBP
SBP-E2
Arterial

Figure 2.1: Schema of physiologically based model in male FHM. Tissues in male FHM are categorized into six compartments: gill, brain, gonad, liver, venous blood, and other. Each compartment is defined by volume, blood flow, and partition coefficient.

Figure 2.1 (continued)

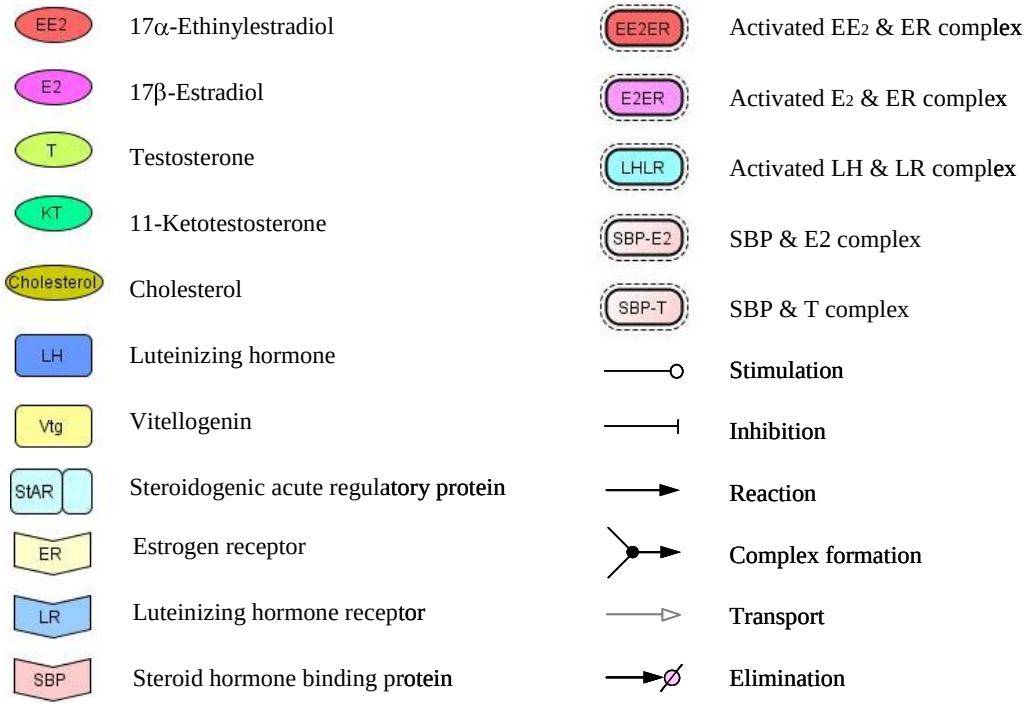

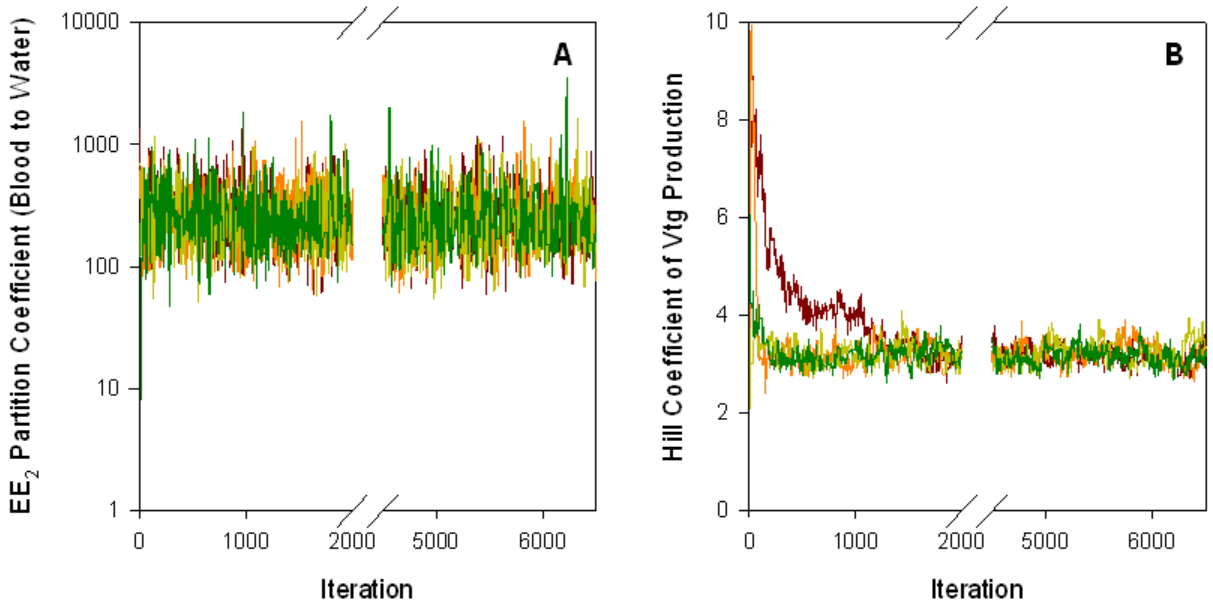

Figure 2.2: Parameter values from Markov chain Monte Carlo simulations: (A) 17α-ethinylestradiol blood to water partition coefficient ($\lambda_{EE2,\,bld}$); and (B) Hill coefficient for vitellogenin production (n_{vtg}).

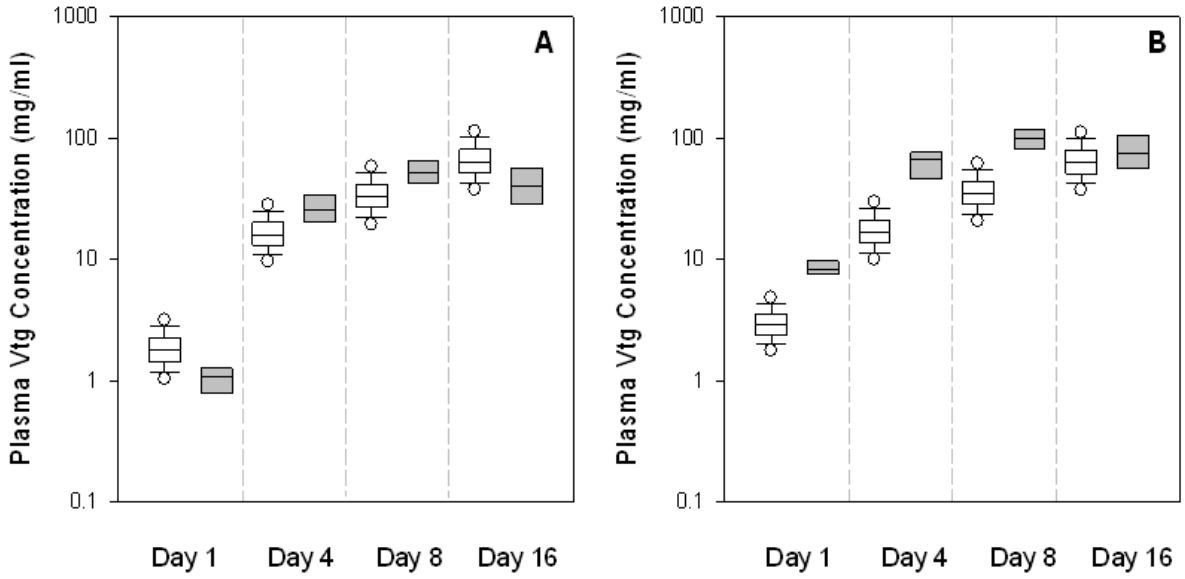

Figure 2.3: Plasma vitellogenin concentrations (mg/ml) compared with experimental measurements from Ekman et al. (2008): (A) plasma vitellogenin concentrations in male fathead minnows exposed to 10 ng/L 17α-ethinylestradiol for eight days; (B) plasma vitellogenin concentrations in male fathead minnows exposed to 100 ng/L 17α-ethinylestradiol for eight days. White boxes correspond to model predictions (n = 32,000 simulations); gray boxes correspond to experimental measurements (n = 8). The middle line of the box marks the median; the boundary of the box closest to zero indicates the 25th percentile; the boundary of the box farthest from zero indicates the 75th percentile; whisker (error bar) closest to zero marks the 10th percentile; the whisker (error bar) farthest from zero marks the 90th percentile; the circle closest to zero marks the 5th percentile; and the circle farthest from zero marks the 95th percentile.

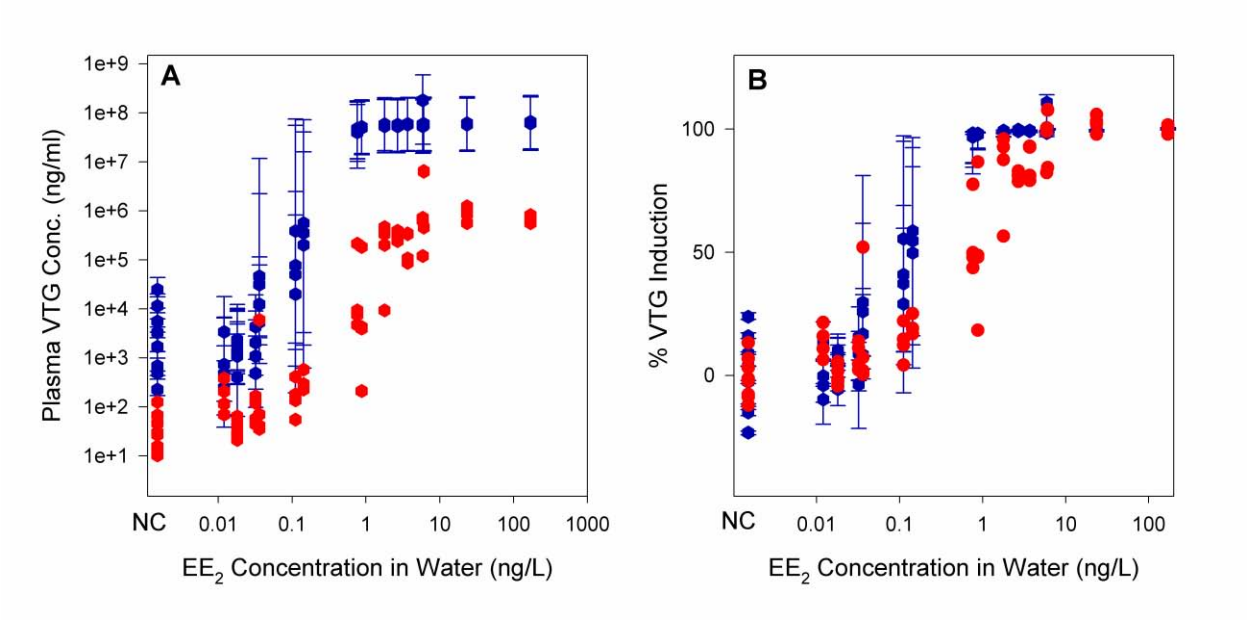

Figure 2.4: Plasma vitellogenin concentrations and percentages of VTG induction compared with experimental data from Brian et al. (2005b): (A) plasma vitellogenin concentrations in male fathead minnows exposed to 17α-ethinylestradiol (EE_2) for 14 days; (B) percentages of VTG induction in male fathead minnows exposed to EE_2 for 14 days. Blue dots correspond to median model predictions (n = 4,000 simulations); the blue bar closest to zero marks the minimum model prediction; the blue bar farthest to zero marks the maximum model prediction; the red dots correspond to measured data. One dot represents one mode output or one measurement.

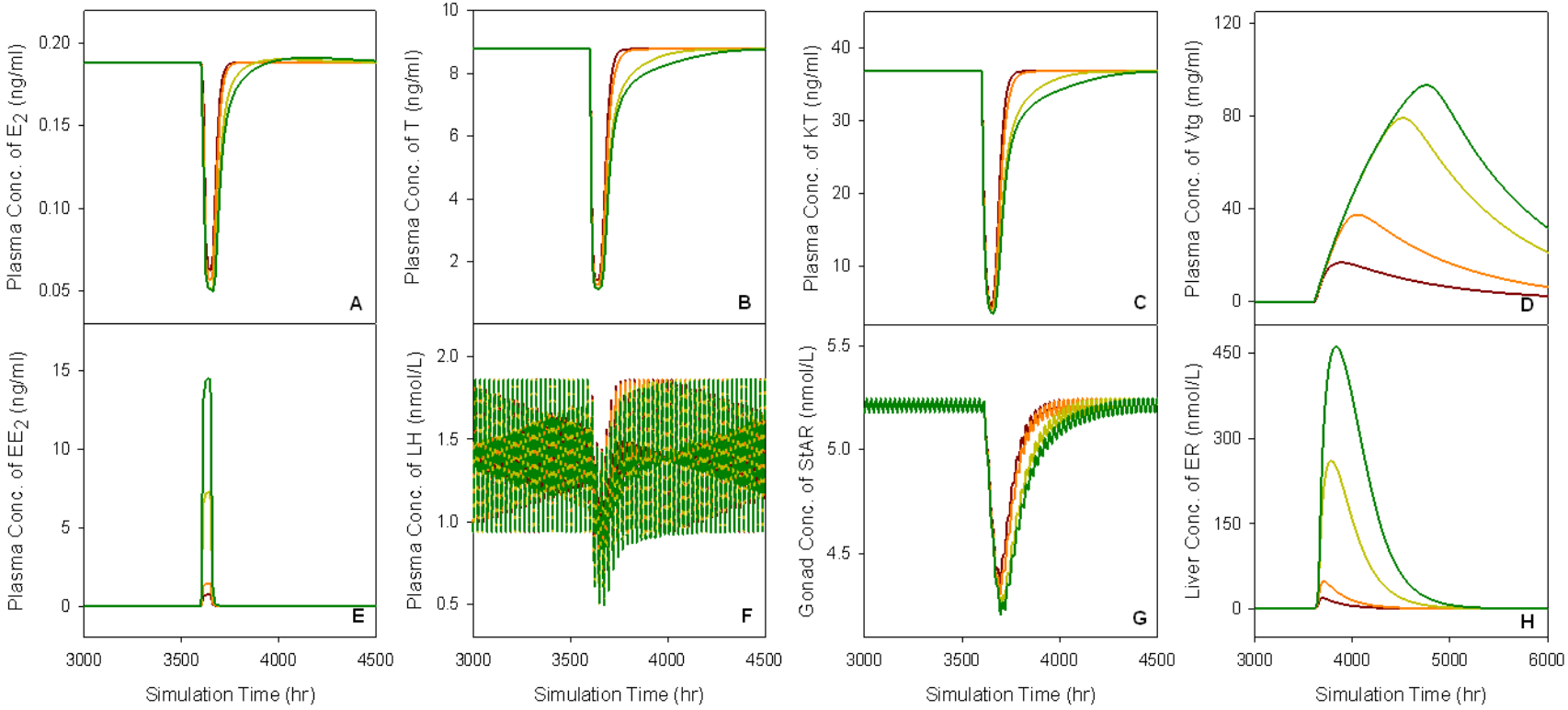

Figure 2.5: Time course simulation of endpoints in male FHMs exposed to 17α-ethinylestradiol (EE_2) 48 hrs (exposure time = 3600 to 3648 hrs): (A) plasma 17β-estradiol (E_2) concentration; (B) plasma testosterone (T) concentration; (C) plasma 11-ketotestosterone (KT) concentration; (D) plasma vitellogenin (VTG) concentration; (E) plasma EE_2 concentration; (F) plasma luteinizing hormone (LH) concentration; (G) steroidogenic acute regulatory protein (StAR) concentration in the gonad; (H) estrogen receptor (ER) concentration in the liver.

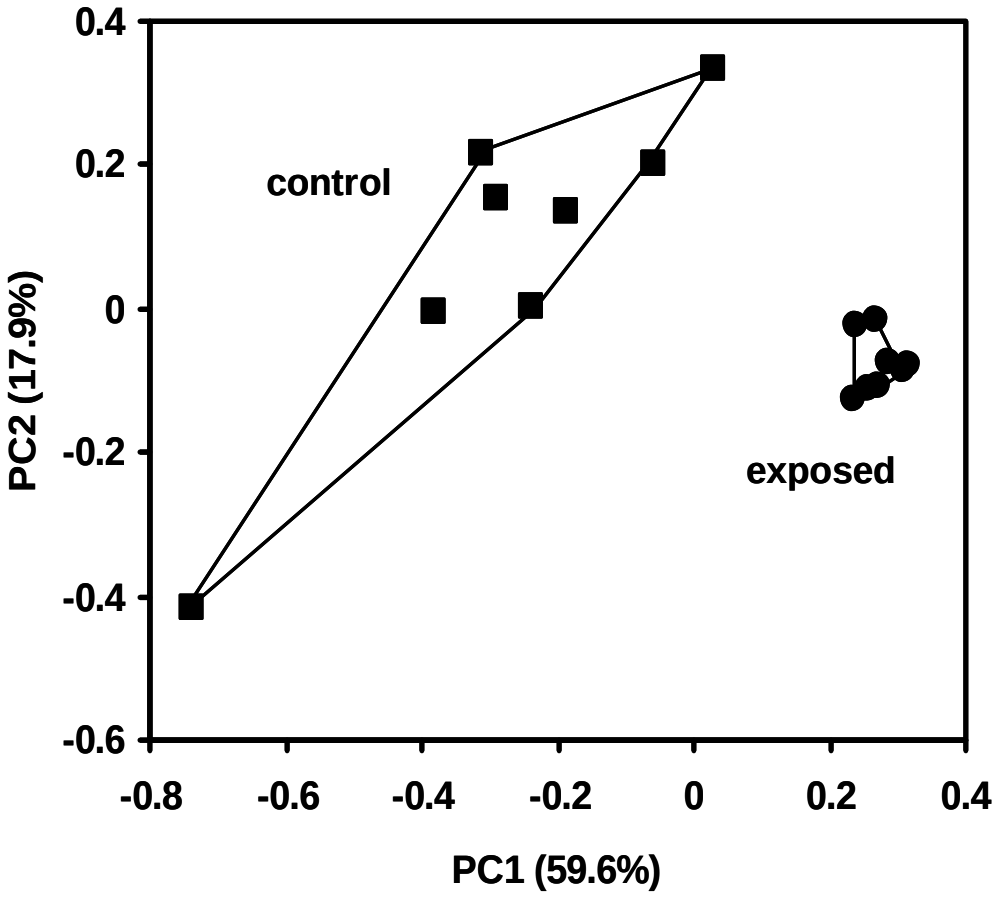

Figure 2.6: Principal components analysis (PCA) scores plot of plasma lipid metabolites from male FHM measured by ^{1}H nuclear magnetic resonance (NMR) spectroscopy. PC1 = principal component 1; PC2 = principal component 2.

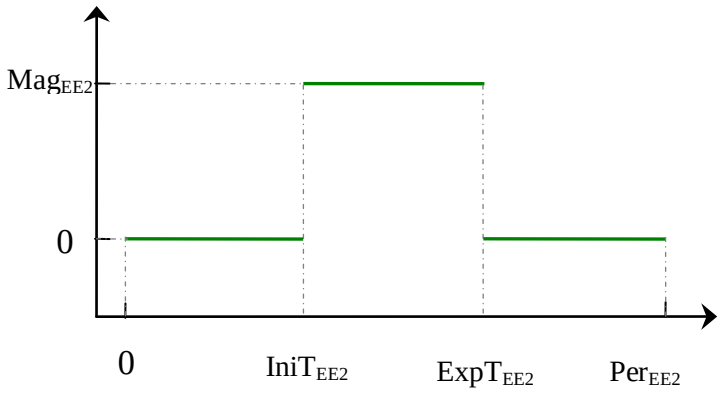

Figure 2.7: An illustration for MCSim's PerDose function used for EE_2 water exposure. Mag_{EE2} (nmol/L) is the EE_2 concentration in aquarium water; Per_{EE2} (hr) represents the period for a repeated dose. For a continuous exposure, Per_{EE2} is set to the total simulation time; $IniT_{EE2}$ (hr) is the time when EE_2 exposure starts (e.g. 3600 hrs); and $ExpT_{EE2}$ (hr) represents the exposure duration

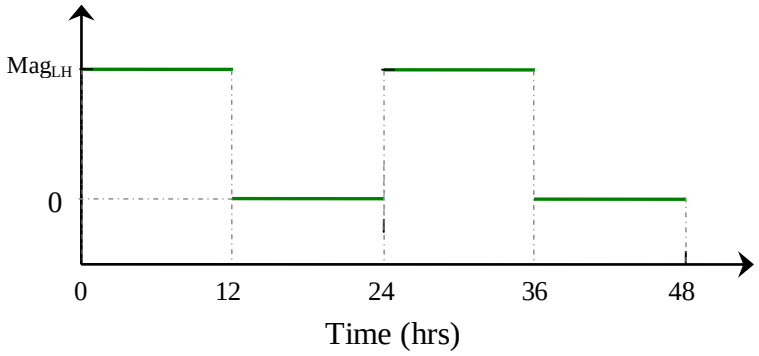

Figure 2.8: An illustration for MCSim's PerDose function used for LH input in the Brain compartment. Mag_{LH} (nmol/hr) is the input magnitude of LH; Per_{LH} (hr) is the period of one cycle of LH production (set as 24 hrs); $IniT_{LH}$ (hr) is the time when LH production starts in one cycle (set as 0 hr); and $ExpT_{LH}$ (hr) is the duration of LH production in one cycle (set as 12 hrs).

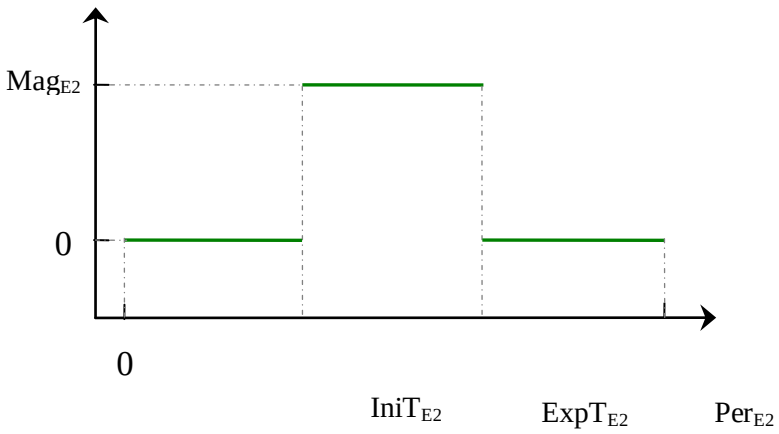

Figure 2.9: An illustration for MCSim's PerDose function used for E_2 injection in the Other compartment. Mag_{E2}(nmol/hr) is the injection magnitude of E_2; Per_{E2} (hr) is the whole period of one E_2 injection experiment; $IniT_{E2}$ (hr) is the time when E_2 injection starts in one experiment; and $ExpT_{E2}$ (hr) is the E_2 injection time in one experiment (set as 2 seconds).

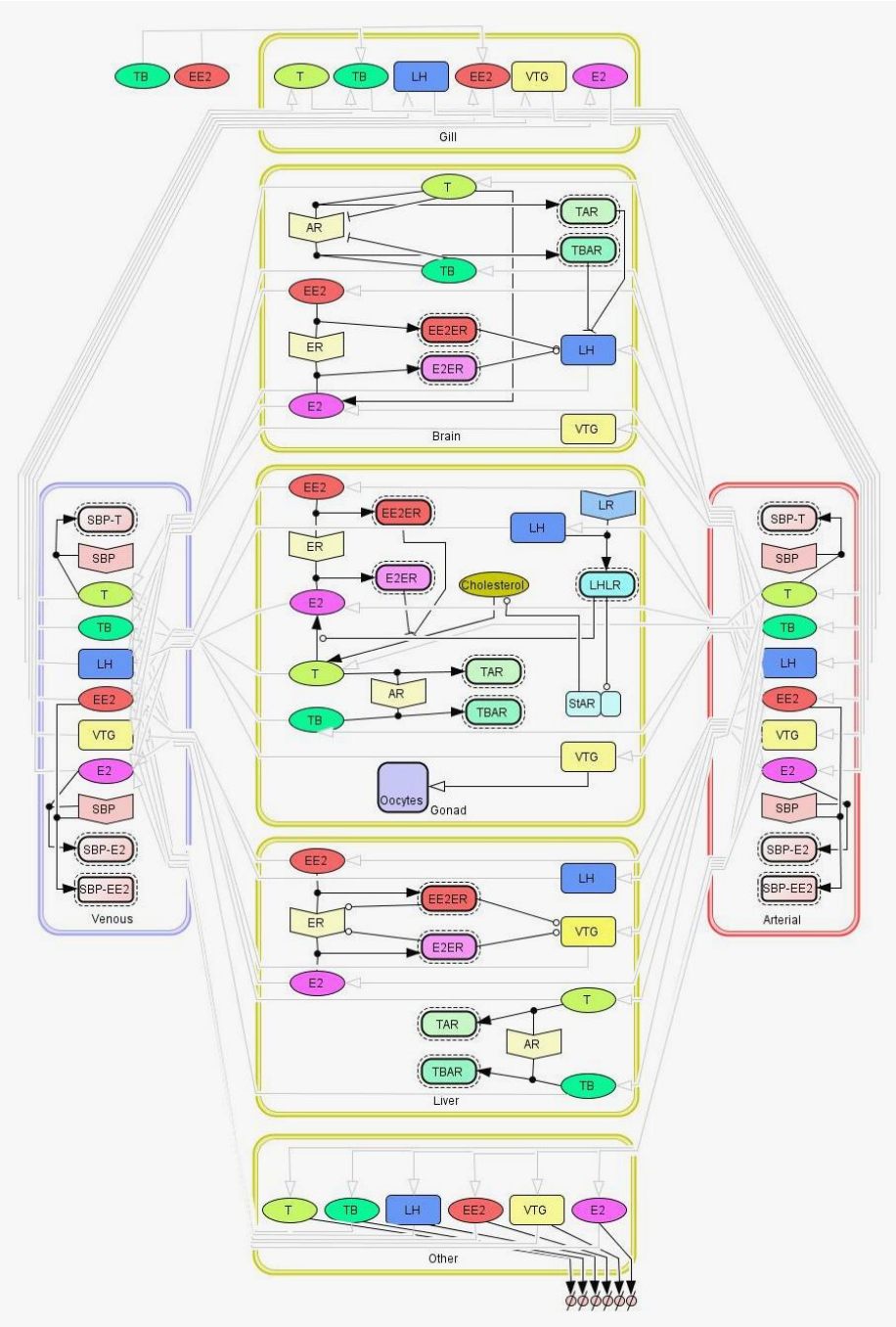

Figure 3.1: Schema of physiologically based model in adult female FHM. Tissues in female FHM are categorized into six compartments: gill, brain, gonad, liver, venous blood, and 'Other'. Each compartment is defined by volume, blood flow, and partition coefficient, and performs multiple physiological functions.

Figure 3.1 (continued)

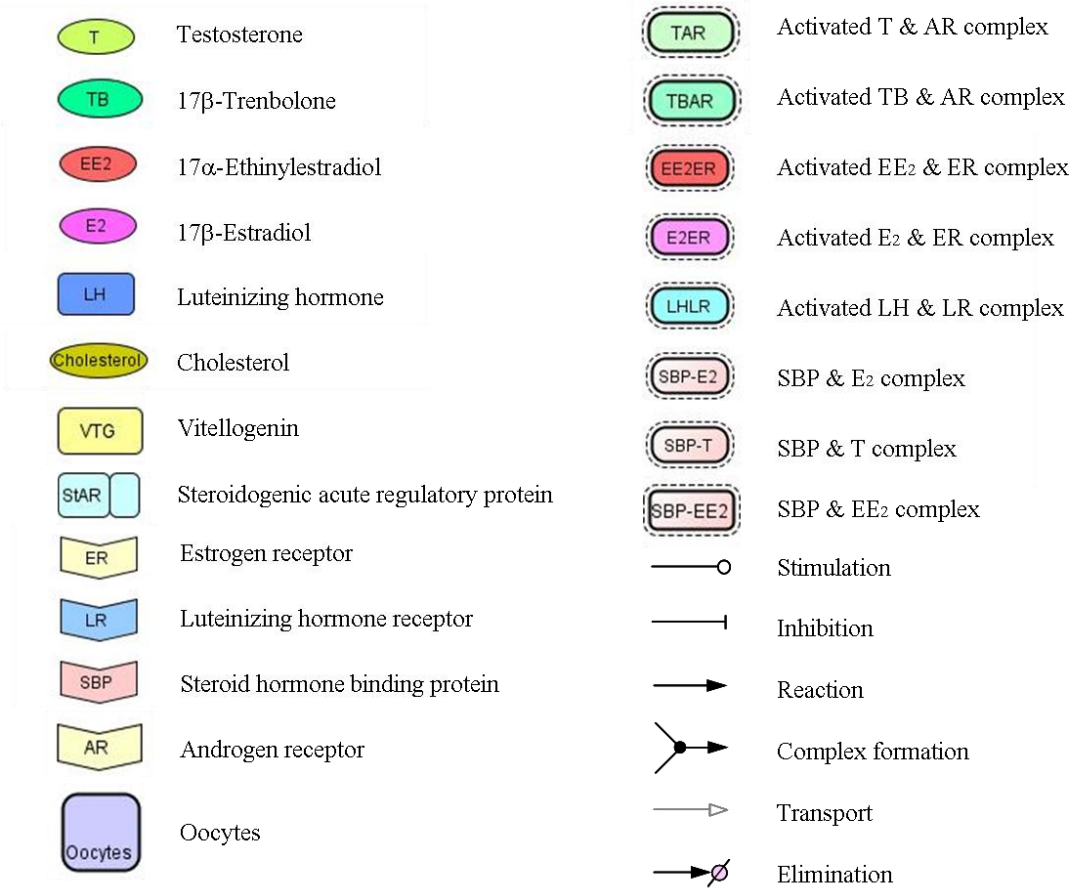

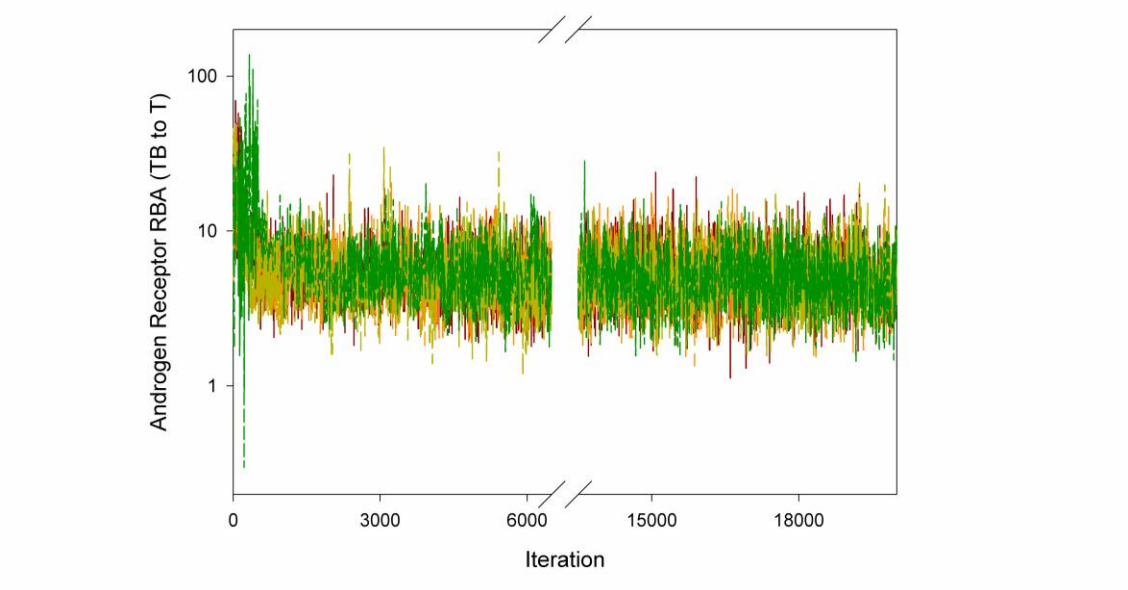

Figure 3.2 Trajectories of the four Markov chains. Relative binding affinity of TB to T (RBATB_T), one of the 26 calibrated model parameters, shows well-mixed trajectories.

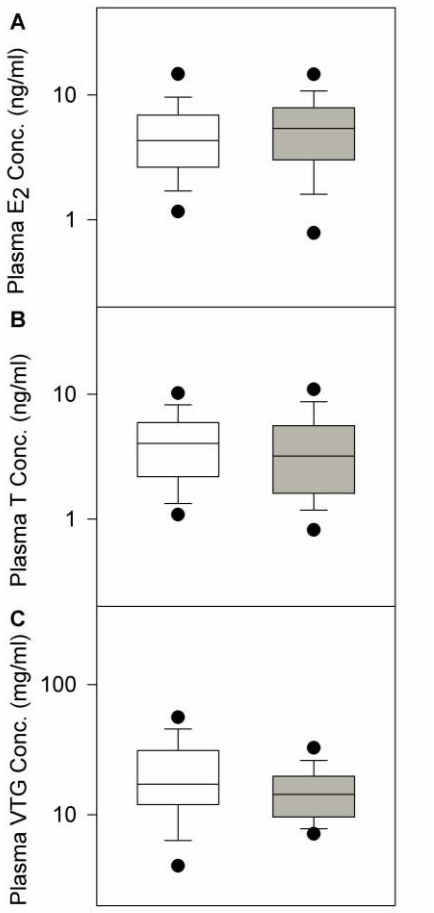

Figure 3.3 Comparison of model predictions with measured data in unexposed female FHMs. *n* = 95. White boxes represent model predictions, and grey boxes represent measured data (Watanabe et al., 2007). The solid line within the box marks the median; the boundary of the box farthest from zero indicates the 75th percentile; the boundary of the box closest to zero indicates the 25th percentile; the whisker (error bar) farthest from zero marks the 90th percentile; whisker (error bar) closest to zero marks the 10th percentile; the circle farthest from zero marks the 95th percentile; and the circle closest to zero marks the 5th percentile.

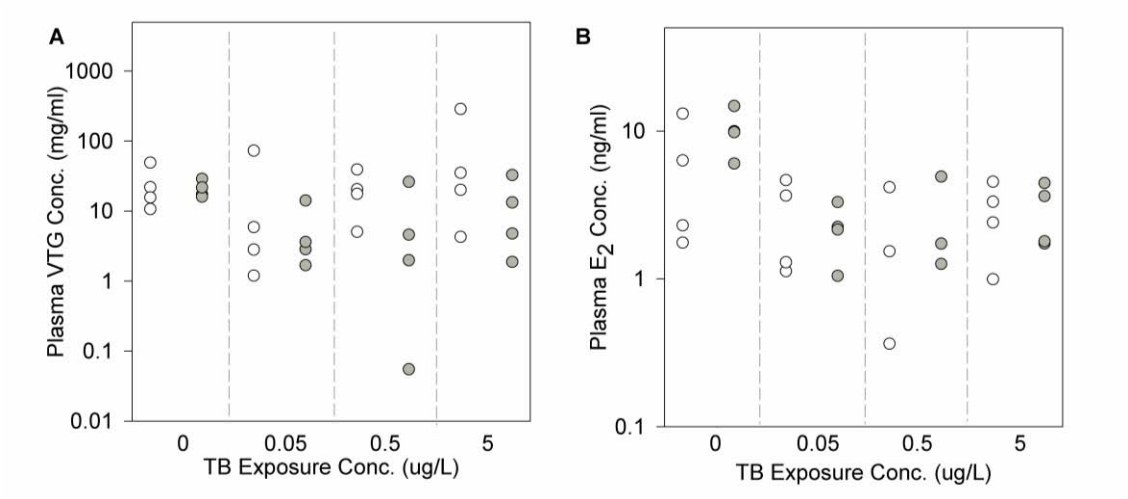

Figure 3.4 Comparison of model predictions with measured data in female FHMs exposed to TB for 48 hours. White dots represent model predictions, and grey dots represent measured data (Garcia-Reyero et al., 2009). Each dot represents one measurement in one fish. (A) plasma VTG concentrations, and (B) plasma E_2 concentrations. The x-axis represents TB concentrations in µg/L.

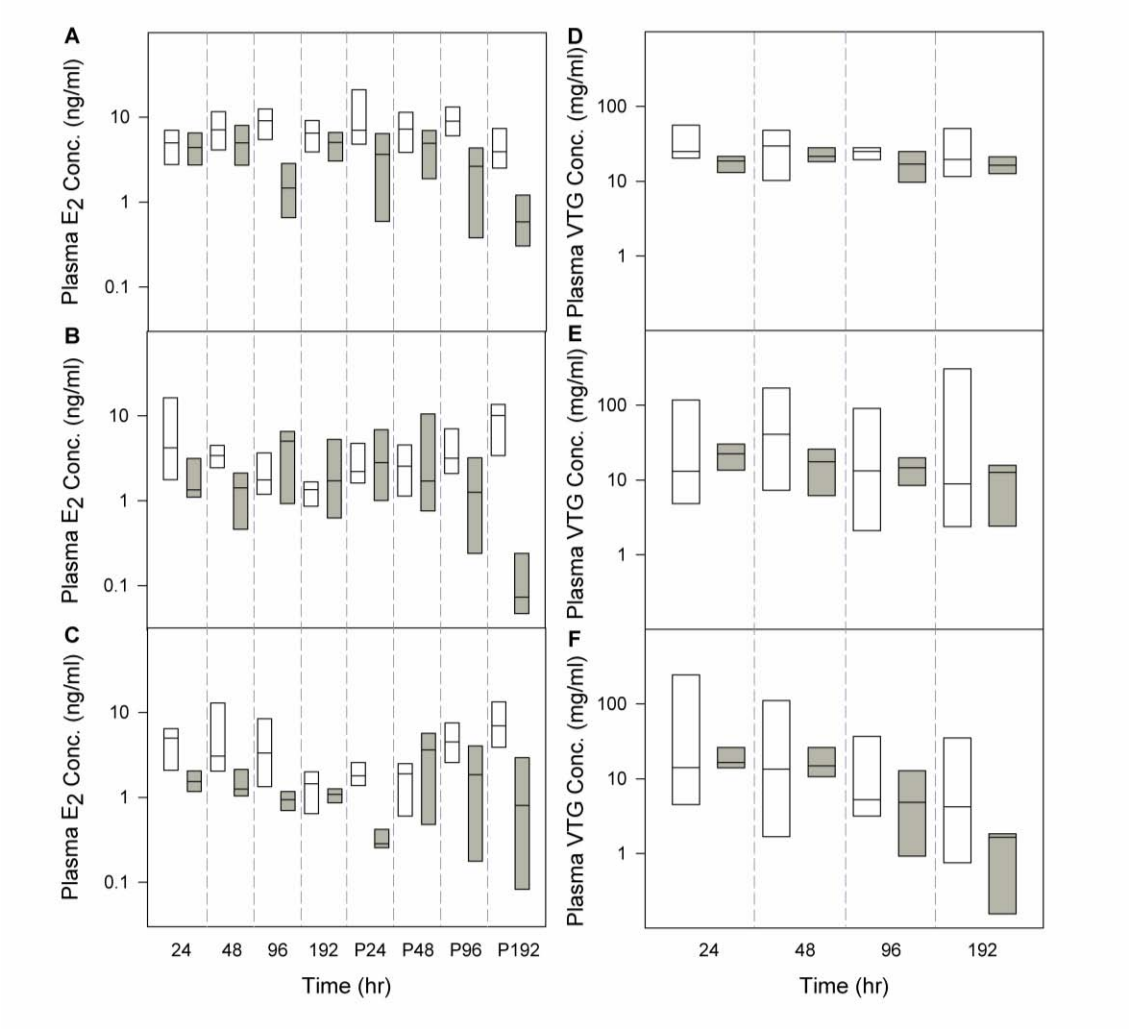

Figure 3.5 Comparison of model predictions with measured data in female FHMs exposed to TB for eight days followed by an eight-day depuration. *n*=8 at each sampling time. White boxes represent model predictions, and grey boxes represent measured data (Ekman et al., in review). The solid line within the box marks the median; the boundary of the box farthest from zero indicates the 75th percentile; the boundary of the box closest to zero indicates the 25th percentile. Because of the small data size (*n*=8), the plots only show the 50% confidence intervals. (A) plasma E_2 concentrations in control FHMs, (B) plasma E_2 concentrations in FHMs exposed to 0.05 µg TB/L, (C) plasma E_2 concentrations in FHMs exposed to 0.5 µg TB/L, (D) plasma VTG concentrations in control FHMs, (E) plasma VTG concentrations in FHMs exposed to 0.05 µg TB/L, (F) plasma VTG concentrations in FHMs exposed to 0.5 µg TB/L. The x-axis represents time in hours. P24, P48, P96, and P192 represent 24, 48, 96, and 192 hours post exposure, respectively.

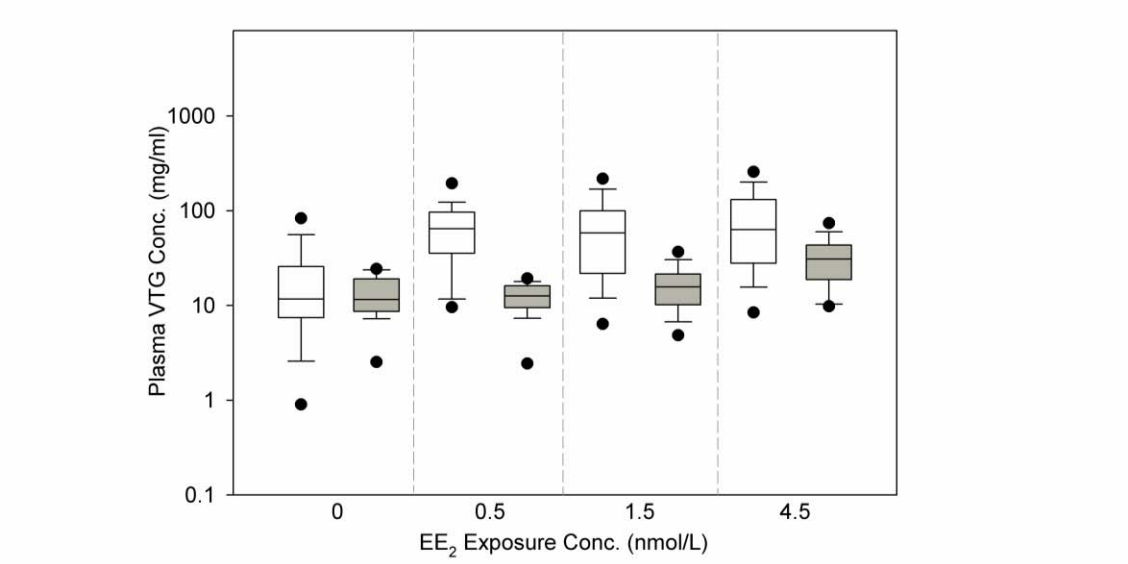

Figure 3.6 Comparison of model predictions with measured data in female FHMs exposed to EE_2. n = 28 at each sampling time. White boxes represent model predictions, and grey boxes represent measured data (Lazorchak et al., manuscript in preparation). The x-axis represents EE_2 concentrations in ng/L. The solid line within the box marks the median; the boundary of the box farthest from zero indicates the 75th percentile; the boundary of the box closest to zero indicates the 25th percentile; the whisker (error bar) farthest from zero marks the 90th percentile; whisker (error bar) closest to zero marks the 10th percentile; the circle farthest from zero marks the 95th percentile; and the circle closest to zero marks the 5th percentile.

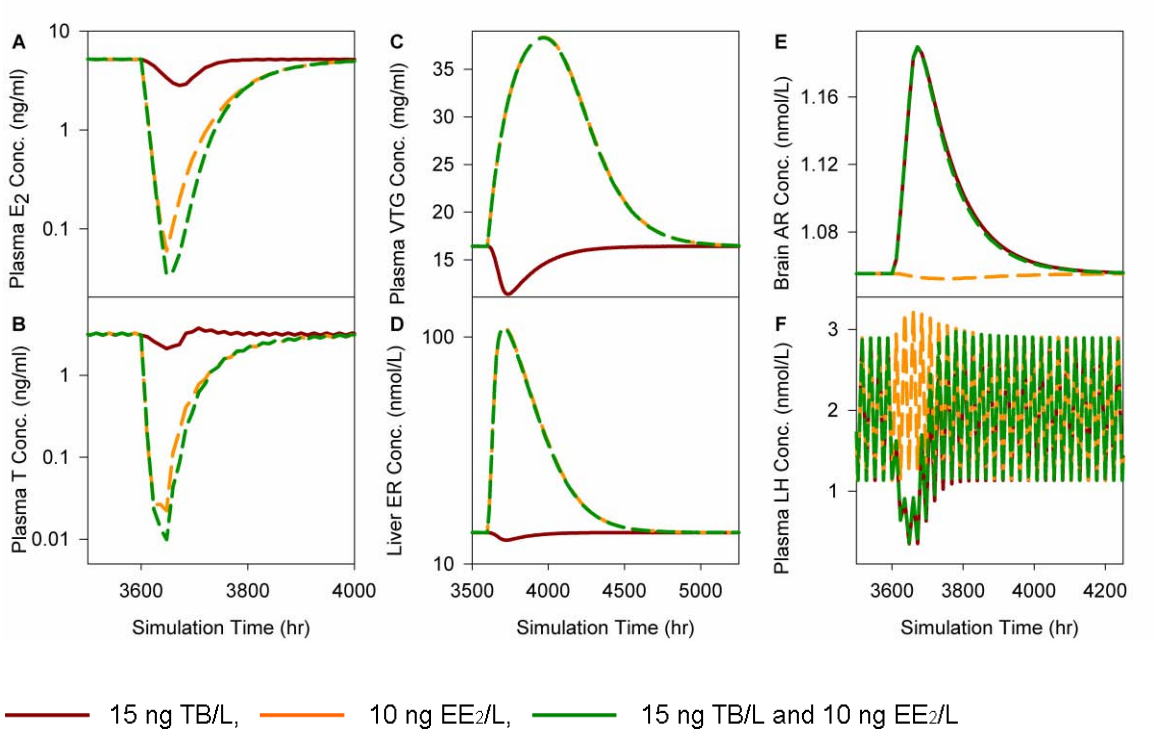

Figure 3.7 Model predictions for unmeasured reproductive endpoints in female FHMs. The predictions are for female FHMs exposed to 15 ng/L TB, 10 ng/L EE_2, or a mixture of 15 ng/L TB and 10 ng/L EE_2 for 48 hours respectively: (A) plasma E_2 concentration, (B) plasma T concentration, (C) plasma VTG concentration, (D) liver ER concentration, (E) brain AR concentration, and (F) plasma LH concentration.

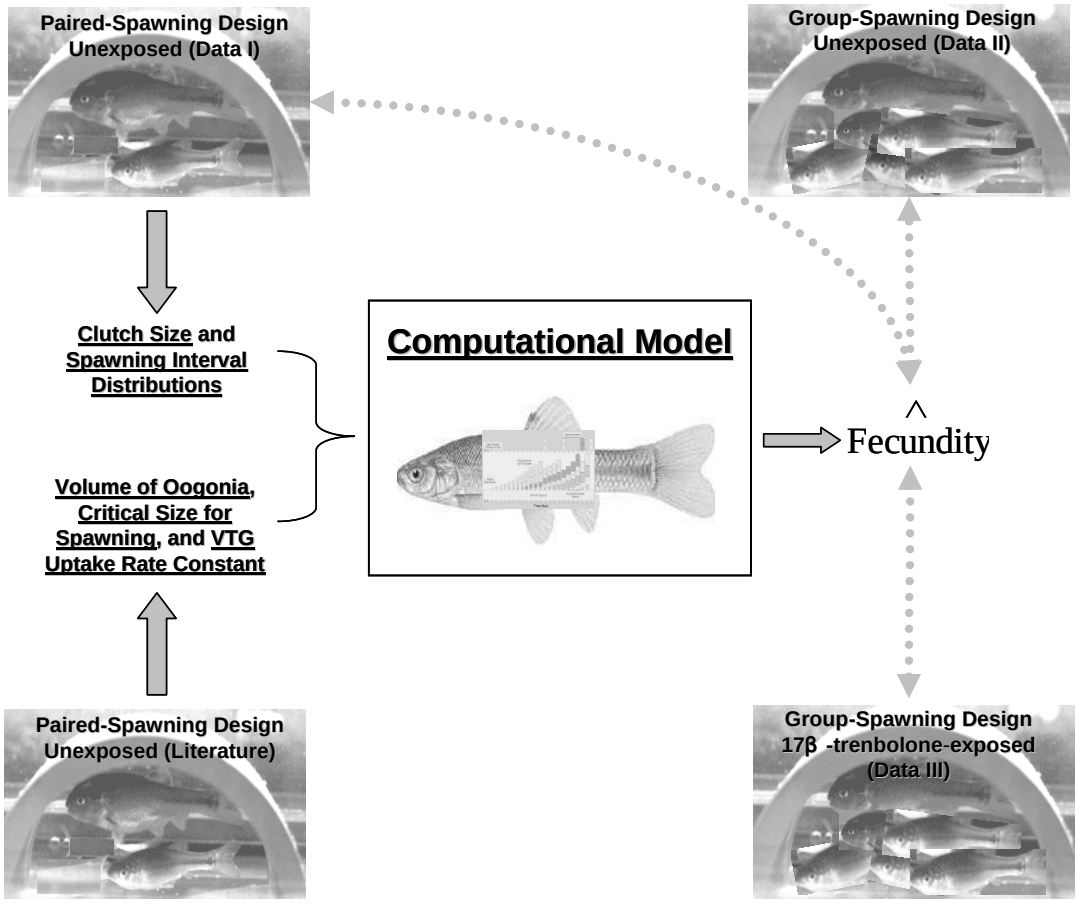

Figure 4.1 A schema for data usage in model parameterization and evaluation. The solid arrows represent parameter generation and model output. The dash arrows represent comparisons between model predictions and experimental data.

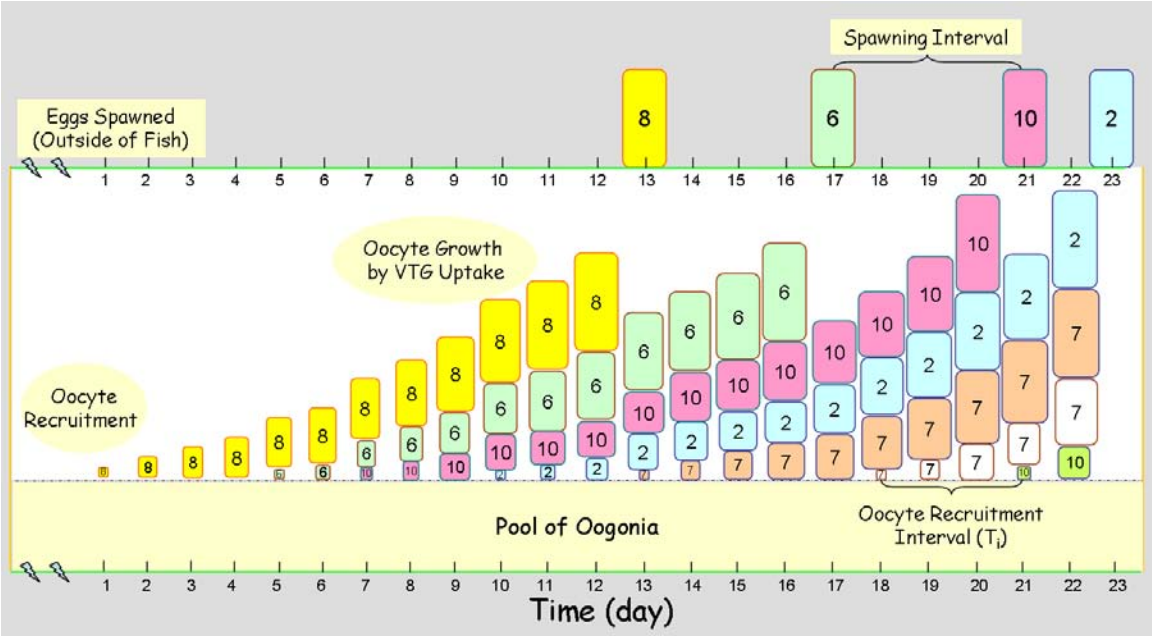

Figure 4.2 A conceptual model of oocyte growth dynamics in asynchronous spawning fish. The x-axis represents time in days. The yellow rectangle at the bottom represents a pool of oogonia. The colored squares in the middle represent different batches of oocytes. The colored squares at the top represent oocytes spawned on a specific day. The number in each square represents the number of oocytes in the batch.

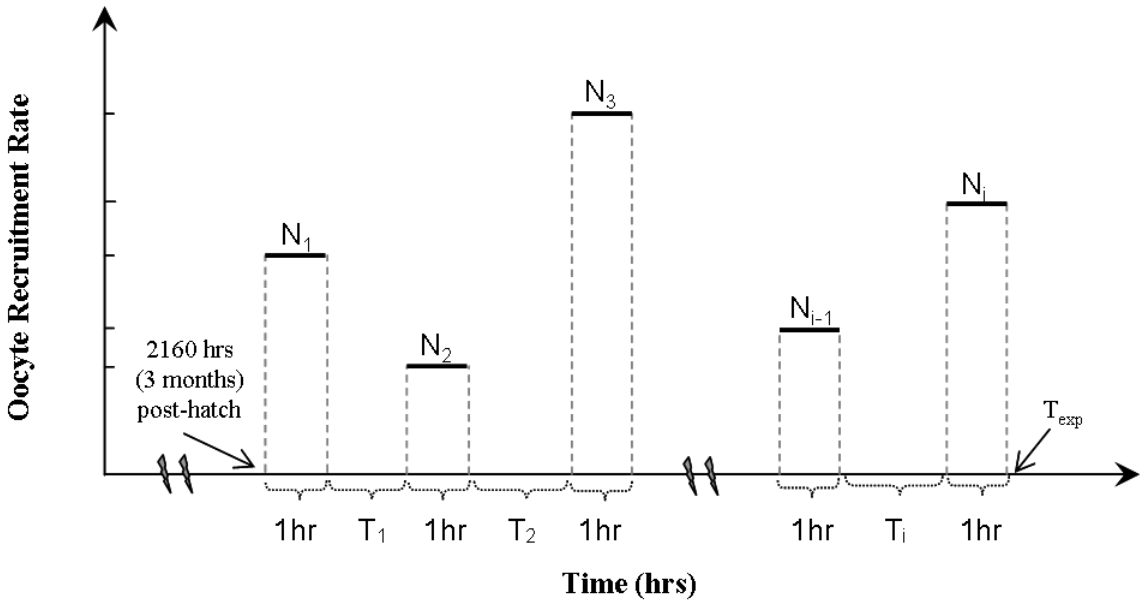

Figure 4.3 A schema for MCSim's PerDose function and its application in model formulation. N_1, N_2, N_3, N_{i-1}, and N_i represent number of oocytes recruited for the 1^{st}, 2^{nd}, 3^{rd}, $(i-1)^{th}$, and i^{th} batch, respectively. Oocyte recruitment is completed within 1 hr. T_1, T_2, and T_i represent spawning intervals between two successive oocyte recruitments.

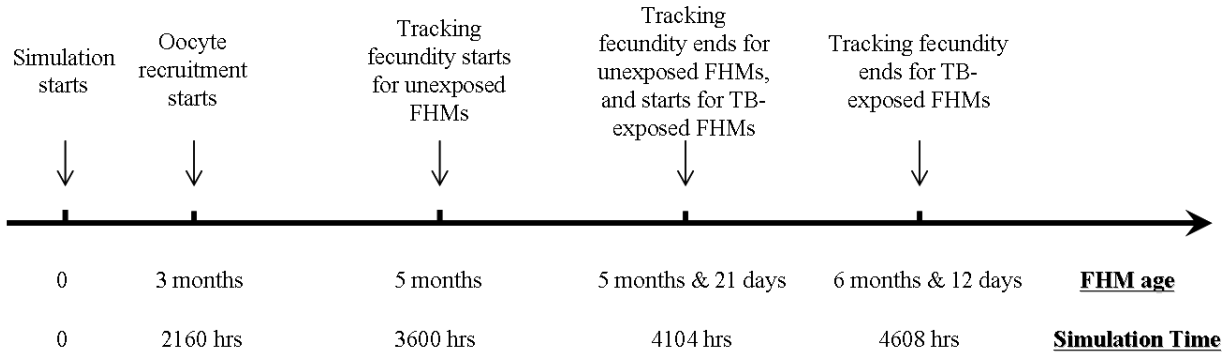

Figure 4.4 A timeline for model simulations. The x-axis represents the age of FHMs in months and days, and model simulation time in hrs.

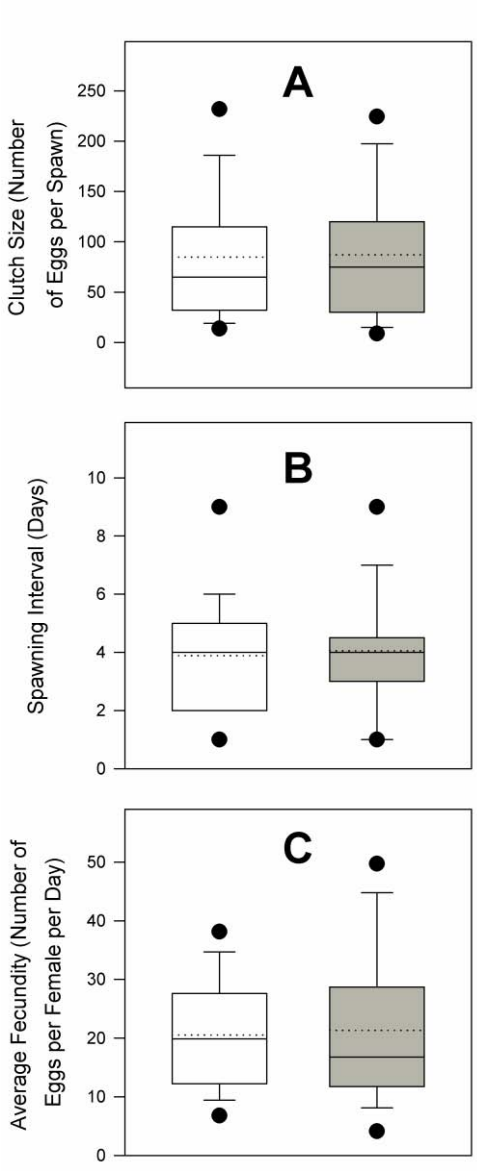

Figure 4.5 Model-predicted reproductive endpoints compared to experimental data from 50 unexposed (control) female FHMs with a paired-spawning experimental design: (A) clutch size, (B) spawning interval, and (C) average fecundity. White boxes represent model predictions; grey boxes represent measured data. The solid line within the box marks the median; the dashed line within the box marks the mean; the boundary of the box farthest from zero indicates the 75th percentile; the boundary of the box closest to zero indicates the 25th percentile; the whisker (error bar) farthest from zero marks the 90th percentile; whisker (error bar) closest to zero marks the 10th percentile; the circle farthest from zero marks the 95th percentile; and the circle closest to zero marks the 5th percentile.

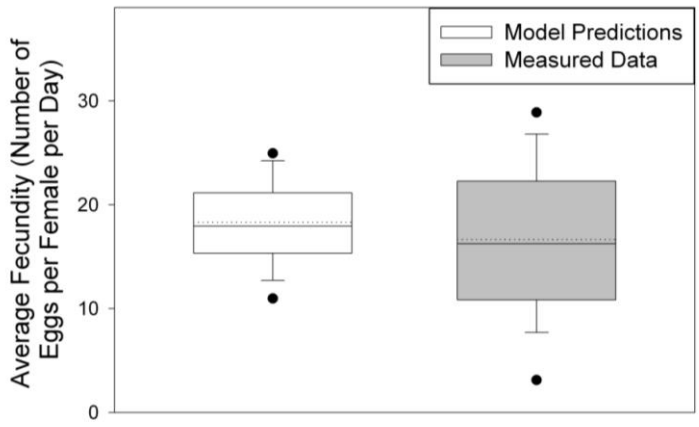

Figure 4.6 Model-predicted average fecundity compared to experimental data from 77 unexposed female FHMs with a group-spawning experimental design. White boxes represent model predictions; grey boxes represent measured data. The solid line within the box marks the median; the dashed line within the box marks the mean; the boundary of the box farthest from zero indicates the 75th percentile; the boundary of the box closest to zero indicates the 25th percentile; the whisker (error bar) farthest from zero marks the 90th percentile; whisker (error bar) closest to zero marks the 10th percentile; the circle farthest from zero marks the 95th percentile; and the circle closest to zero marks the 5th percentile.

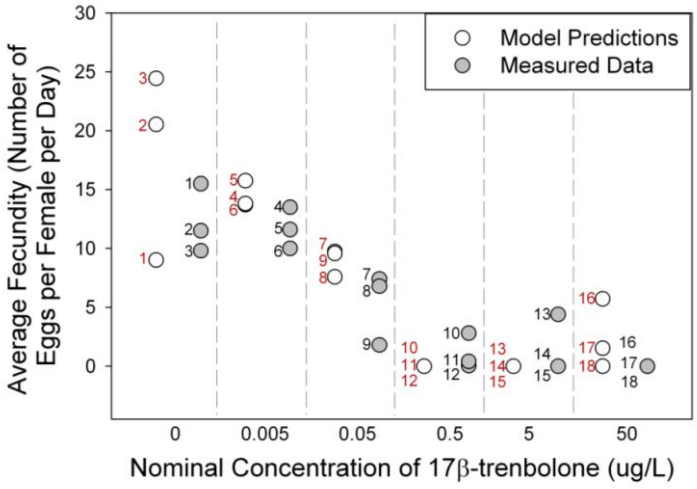

Figure 4.7 Model-predicted average fecundity compared to experimental data from 71 female FHMs exposed to TB for 21 days with a group-spawning experimental design. White circles correspond to model predictions; grey circles correspond to measured data. Group numbers are shown next to each marker: red for model predictions; and black for experimental data.